Cancer Cell

Article

Neutrophil-activating therapy for the treatment of cancer

Graphical abstract

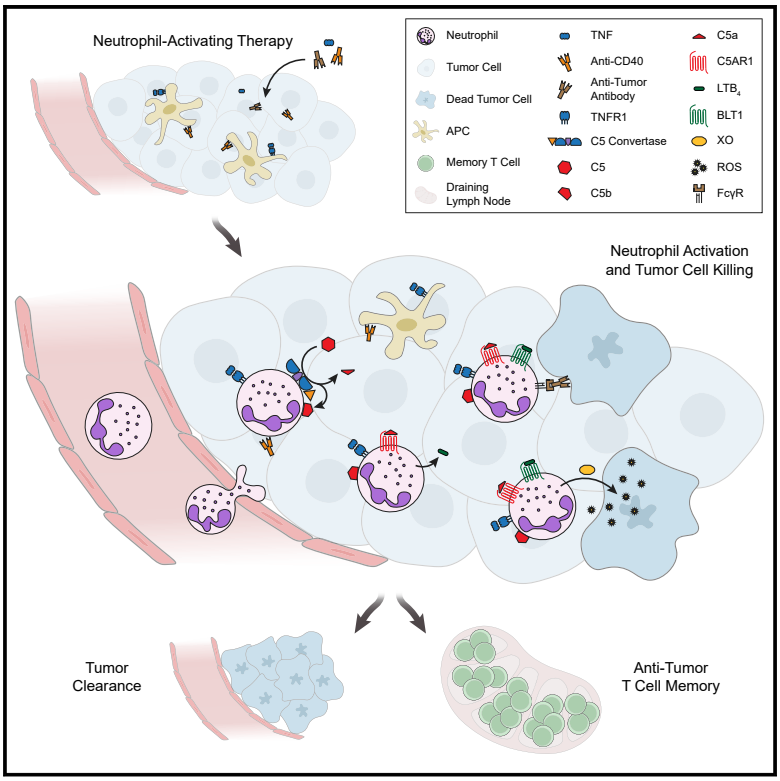

Highlights

- Therapeutically activated neutrophils infiltrate and eradicate multiple tumor types
- Intratumoral TNF + anti-CD40 + anti-tumor antibodies induce an inflammatory cascade
- Neutrophil C5AR1 signaling stimulates LTB_4 release, driving ROS production via XO
- Neutrophil-mediated oxidative damage drives T cell-independent tumor clearance

Authors

Ian L. Linde, Tyler R. Prestwood, Jingtao Qiu, ..., Lorna L. Tolentino, Wen-Chao Song, Edgar G. Engleman

Correspondence

edengleman@stanford.edu

In brief

Linde et al. describe a cancer therapy that activates neutrophils to infiltrate and eradicate tumors and reduce metastatic seeding. The authors elucidate the responsible mechanism, which involves complement component C5a, leukotriene B_4, and reactive oxygen species, and demonstrate the potential of harnessing neutrophils through inflammatory activation to drive tumor clearance.

Linde et al., 2023, Cancer Cell *41*, 356–372
February 13, 2023
https://doi.org/10.1016/j.ccell.2023.01.002

CellPress

CellPress

Cancer Cell

Article

Neutrophil-activating therapy for the treatment of cancer

Ian L. Linde,[1,2] Tyler R. Prestwood,[2] Jingtao Qiu,[2] Genay Pilarowski,[2] Miles H. Linde,[1] Xiangyue Zhang,[2] Lei Shen,[2] Nathan E. Reticker-Flynn,[2] David Kung-Chun Chiu,[2] Lauren Y. Sheu,[2] Simon Van Deursen,[2] Lorna L. Tolentino,[2] Wen-Chao Song,[3] and Edgar G. Engleman[1,2,4,*]

[1]Program in Immunology, Stanford University, Stanford, CA 94305, USA
[2]Department of Pathology, Stanford University, Stanford, CA 94305, USA
[3]Department of Systems Pharmacology and Translational Therapeutics, Perelman School of Medicine, University of Pennsylvania, Philadelphia, PA 19104, USA
[4]Lead contact
*Correspondence: edengleman@stanford.edu
https://doi.org/10.1016/j.ccell.2023.01.002

SUMMARY

Despite their cytotoxic capacity, neutrophils are often co-opted by cancers to promote immunosuppression, tumor growth, and metastasis. Consequently, these cells have received little attention as potential cancer immunotherapeutic agents. Here, we demonstrate in mouse models that neutrophils can be harnessed to induce eradication of tumors and reduce metastatic seeding through the combined actions of tumor necrosis factor, CD40 agonist, and tumor-binding antibody. The same combination activates human neutrophils *in vitro*, enabling their lysis of human tumor cells. Mechanistically, this therapy induces rapid mobilization and tumor infiltration of neutrophils along with complement activation in tumors. Complement component C5a activates neutrophils to produce leukotriene B_4, which stimulates reactive oxygen species production via xanthine oxidase, resulting in oxidative damage and T cell-independent clearance of multiple tumor types. These data establish neutrophils as potent anti-tumor immune mediators and define an inflammatory pathway that can be harnessed to drive neutrophil-mediated eradication of cancer.

INTRODUCTION

Although initially appreciated for their role in defense against microbial pathogens, neutrophils are now recognized to promote the growth and spread of many cancers.[1–3] Cancers are frequently accompanied by neutrophil recruitment to the tumor and expansion in the blood, which is associated with poor prognosis in most cases.[1,2,4,5] Studies of neutrophils from cancer patients and mouse models have established that neutrophils promote tumor growth,[6] angiogenesis,[7,8] and metastasis[9–11] and inhibit anti-cancer T cell responses.[9,12,13] Furthermore, myeloid-derived suppressor cells (MDSCs), a heterogeneous group of cells that overlap phenotypically with neutrophils,[1,2,14] are well appreciated to induce T cell suppression and promote tumor growth and metastasis.[2,14–16]

Nonetheless, neutrophils have the potential to exert anti-tumor activity. Early studies demonstrated the ability of neutrophils to kill tumor cells *in vitro*,[17] and although neutrophils exert pro-tumor activity in most settings,[1,2] a growing number of studies support the potential for neutrophils to perform anti-tumor functions in certain contexts. Neutrophils naturally can inhibit some tumors during the early stages of tumor development[18–21] or early metastasis,[22,23] and they are capable of promoting anti-tumor responses by other immune cells, including natural killer (NK) cells and multiple subsets of T cells.[19–21,24–26] The apparently contradictory roles of neutrophils in cancer are likely the result of differences in the tumor milieu affecting neutrophil maturation, activation, and functional states.[2,24,27]

Despite the natural capacity of neutrophils to inhibit cancer in certain contexts, little effort has been made to harness neutrophils as anti-tumor effector cells. Neutrophil-targeted treatments have generally focused on depleting MDSCs or blocking the recruitment of neutrophils and MDSCs to the tumor.[2,14,28,29] Recently, targeted inhibition of receptors on neutrophils has been shown to slow tumor growth by inhibiting pro-tumor functions of neutrophils such as the promotion of angiogenesis[30] and T cell suppression.[25] Additionally, inhibition of certain suppressive signals can enhance killing of tumor cells by neutrophils *ex vivo*,[24] induce modest reductions in tumor growth,[31] and promote activation of $CD8^+$ T cells[24] or NK cells[26] to inhibit tumor growth. Neutrophils can also kill antibody-bound tumor cells[32] and mediate the effects of monoclonal antibody (mAb) therapy initiated concurrently with tumor engraftment.[33] Despite these promising results, it is still not clear whether neutrophils can be harnessed therapeutically to drive regression of established tumors.

We set out to determine whether neutrophils in a tumor-bearing host could be mobilized and activated to attack tumors.

Using intratumoral injection of neutrophil stimuli and tumor-binding antibodies, we show that manipulation of the tumor milieu can result in the infiltration and activation of tumor-killing neutrophils that drive T cell-independent tumor clearance. We further reveal the mechanistic steps underlying this response, demonstrating the ability of neutrophil-mediated inflammation to generate a tumor-eradicating immune response and identifying multiple promising targets for therapeutic intervention.

RESULTS

Neutrophil-activating therapy recruits activated neutrophils to the tumor

To determine if neutrophils might be harnessed therapeutically, we investigated how the tumor microenvironment could be modulated to optimally recruit neutrophils and activate their cytotoxic function. When we assessed the impact of various cytokines injected intratumorally in B16 melanoma, tumor necrosis factor (TNF) notably induced robust recruitment of neutrophils (Figures S1A and S1B) and upregulated neutrophil surface molecules consistent with activation[34–36] (Figures S1C and S1D) in a dose-dependent manner (Figures S1E–S1G). However, TNF monotherapy failed to clear tumors in most mice (Figure S1H).

Given the promising neutrophil infiltration and activation induced by TNF but the failure to clear tumors, we sought complementary agents capable of enabling neutrophil-mediated tumor clearance in combination with TNF. As cluster of differentiation 40 (CD40) agonists can activate neutrophils and promote neutrophil cytotoxicity,[37] we evaluated the effect of an agonistic anti-CD40 monoclonal antibody. As neutrophils are also potent mediators of antibody-dependent cellular cytotoxicity (ADCC) through ligation of their Fc receptors,[2,32] we also tested a mAb targeting the melanoma-associated antigen gp75. Strikingly, intratumoral treatment of tumors with two doses of 1 μg TNF + 100 μg anti-CD40 + 100 μg anti-gp75 two days apart induced durable clearance of B16 melanoma tumors (Figure 1A). In contrast, treatment with only one or two of these components failed to achieve the same frequency of tumor clearance (Figures S1I and S1J). Mice treated with TNF + anti-CD40 + anti-gp75 transiently lost a small amount of weight but rapidly recovered within two days of the second treatment (Figure S1K). Additionally, blood chemistry analysis one week after treatment completion and 60 days post-treatment revealed essentially normal liver and renal function (Figure S1L).

Mice treated with the full three-component therapy consisting of TNF, anti-CD40, and tumor-binding antibody, hereafter referred to as neutrophil-activating therapy, exhibited rapid recruitment of neutrophils to tumors (Figures 1B and 1C), and neutrophils expanded in the blood with similar kinetics (Figure 1D). Treated neutrophils infiltrated throughout B16 tumors and were not merely confined to the periphery (Figure 1E). Evaluation of the impact of individual treatment components revealed that neutrophil recruitment to tumors was primarily induced by TNF (Figure 1F). Although TNF induced a transient increase in neutrophil frequency in the blood (Figure 1G), anti-CD40 induced a large and sustained expansion of neutrophils in the blood (Figure 1H).

Flow cytometry analysis to identify hematopoietic stem cells (HSCs) and progenitors (Figures S1M and S1N)[38–40] in the bone marrow 24 h after neutrophil-activating therapy revealed an increase in the frequencies of HSCs and multipotent progenitors (MPPs) (Figure 1I). Although the full neutrophil-activating therapy had a minimal effect on the frequency of common lymphoid progenitors (CLPs), it induced a drastic reduction in common myeloid progenitors (CMPs), granulocyte-monocyte progenitors (GMPs), megakaryocyte-erythrocyte progenitors (MEPs), and common monocyte progenitors (cMoPs), whereas committed neutrophil progenitors (proNeu1s and proNeu2s) were not significantly altered (Figures 1I and S1O). These data indicate the induction of granulopoiesis. In addition, although the frequency in the bone marrow of late neutrophil precursors (preNeus) decreased with therapy, $Ly6G^{lo}$ immature neutrophils increased, and $Ly6G^{hi}$ mature neutrophils decreased (Figure 1I), consistent with an increased differentiation of neutrophils in the bone marrow and a mobilization of mature neutrophils into the blood. Furthermore, the spleen displayed an expansion of neutrophils and similar alterations in the frequencies of HSCs and progenitors (Figure S1P), indicating extramedullary granulopoiesis.

In mice lacking TNF receptors (TNFR knockout [KO] mice), treatment with neutrophil-activating therapy failed to recruit or activate neutrophils (Figures S2A–S2C). Although treatment induced cell death throughout tumors in wild-type (WT) mice, TNFR KO mice had reduced levels of cell death (Figures S2D and S2E) and failed to clear their tumors following treatment (Figure S2F). Tumor clearance was mediated through TNF receptor 1 (TNFR1) (Figure S2G) and was independent of TNFR1 expression on tumor cells (Figures S2H and S2I). These data demonstrate that TNF signaling in non-tumor cells is essential for neutrophil recruitment, tumor cell killing, and tumor clearance.

Neutrophil-activating therapy induced multiple alterations in the surface phenotype of tumor-infiltrating neutrophils, primarily in response to TNF (Figure 1J). These neutrophils upregulated CD11b and intercellular adhesion molecule (ICAM)-1, indicating activation or priming,[34–36] and increased expression of CD177, which has been associated with anti-tumor neutrophils in colon cancer.[41] Therapeutically activated neutrophils also had lower levels of signal regulatory protein-α (SIRPα), a myeloid checkpoint that inhibits neutrophil ADCC,[2,32] suggesting the capacity for enhanced tumor cell killing. Neutrophil-activating therapy did not alter the expression of Siglec F, a marker associated with pro-tumor neutrophils,[42] which remained low in all treatment conditions (Figure S2J). In contrast, treated neutrophils downregulated, but did not lose, expression of CD101 (Figure S2K). CD101-negative neutrophils are more immature and have been reported to correlate with tumor burden.[38] Neutrophils in tumors treated with neutrophil-activating therapy also upregulated CD14 and programmed cell death-ligand 1 (PD-L1), which have been reported to identify neutrophils with increased suppressive and reduced tumoricidal activity.[2,43,44] Neutrophils in the blood exhibited a very similar, but less extreme, pattern of changes in expression of these markers following neutrophil-activating therapy (Figure S2L). These alterations in neutrophil phenotype were transient, as neutrophils in both the tumor and blood increasingly reverted toward the phenotype of neutrophils in mock treated mice over the first week post-treatment (Figures 1K and S2M). Neutrophil-activating therapy of other tumors, including Sparkl.4640, a colon

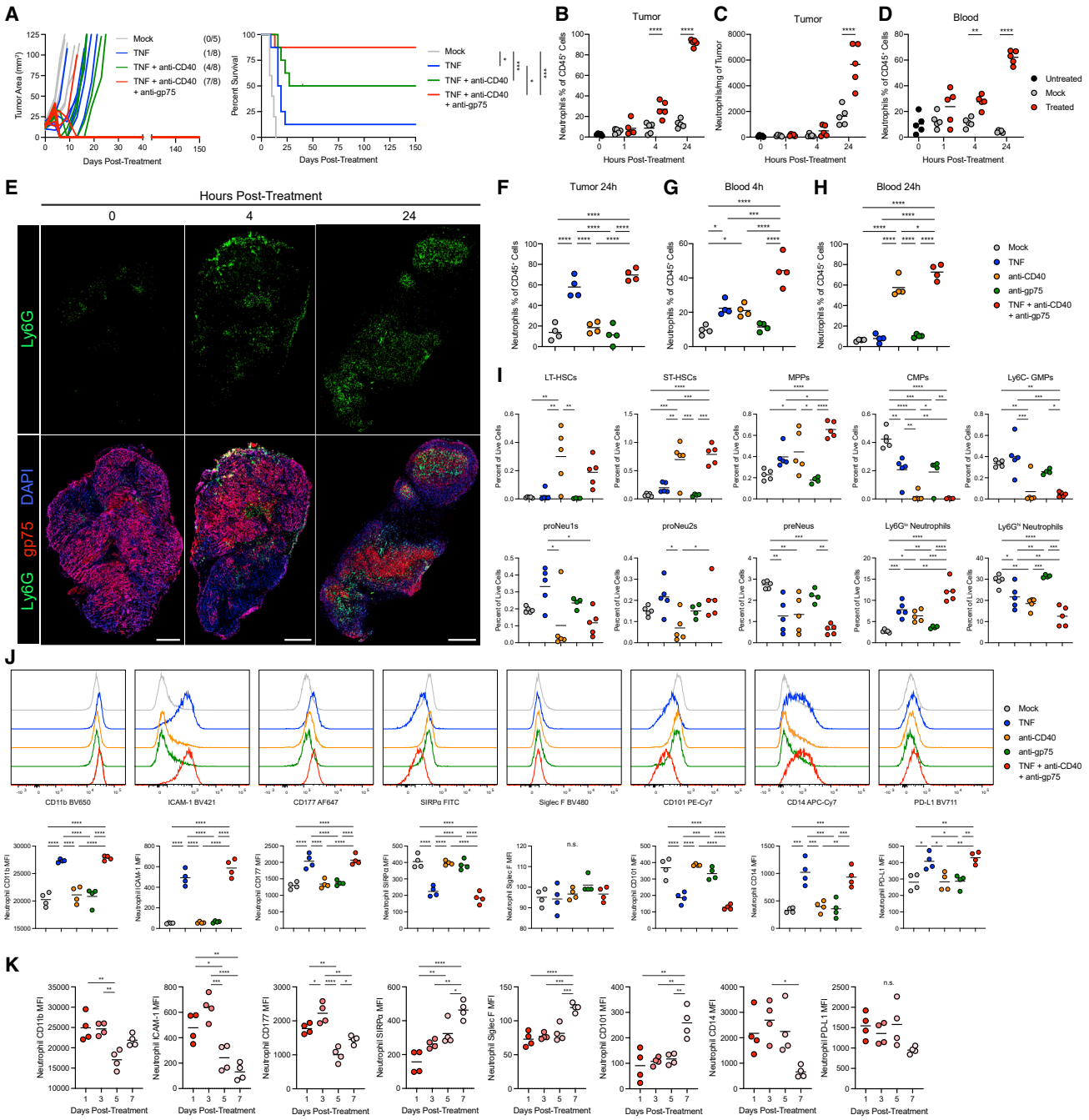

Figure 1. Neutrophil-activating therapy recruits activated neutrophils to the tumor

(A) Left: tumor growth in B16-bearing mice following treatment with the indicated components, indicating mice with undetectable tumors at the conclusion of the study in parentheses. Right: survival of the mice shown in the left panel. Mice were euthanized when tumors exceeded 100 mm^2.

(B and C) Neutrophil frequency (B) and numbers (C) in B16 tumors following treatment with TNF + anti-CD40 + anti-gp75 (n = 5).

(D) Neutrophil frequency in peripheral blood following treatment with this neutrophil-activating therapy (n = 5).

(E) Immunofluorescence of neutrophil infiltration in B16 tumors following treatment with neutrophil-activating therapy. Scale bars, 500 μm.

(F–H) Neutrophil frequency in the tumor (F) and blood (G and H) 4 h (G) or 24 h (F and H) after treatment with the indicated components (n = 4).

(I) Frequencies of HSCs and progenitors in the bone marrow 24 h after treatment with neutrophil-activating therapy (anti-gp75, n = 4; other groups, n = 5).

(J) Representative histograms (top) and median fluorescence intensity (MFI) (bottom) of surface markers on neutrophils infiltrating B16 tumors 4 h after treatment with the indicated components (n = 4).

(K) Surface marker expression on B16 tumor-infiltrating neutrophils following treatment with the full neutrophil-activating therapy (n = 4).

Statistics: log rank test with Bonferroni correction (A), one-way ANOVA with Tukey's multiple-comparisons test (B–D and F–K). For all dot plots, the line indicates the mean. Data are representative of 2 (B–E) or 3 (F–H) independent experiments or pooled from 2 experiments (A). See also Figures S1 and S2.

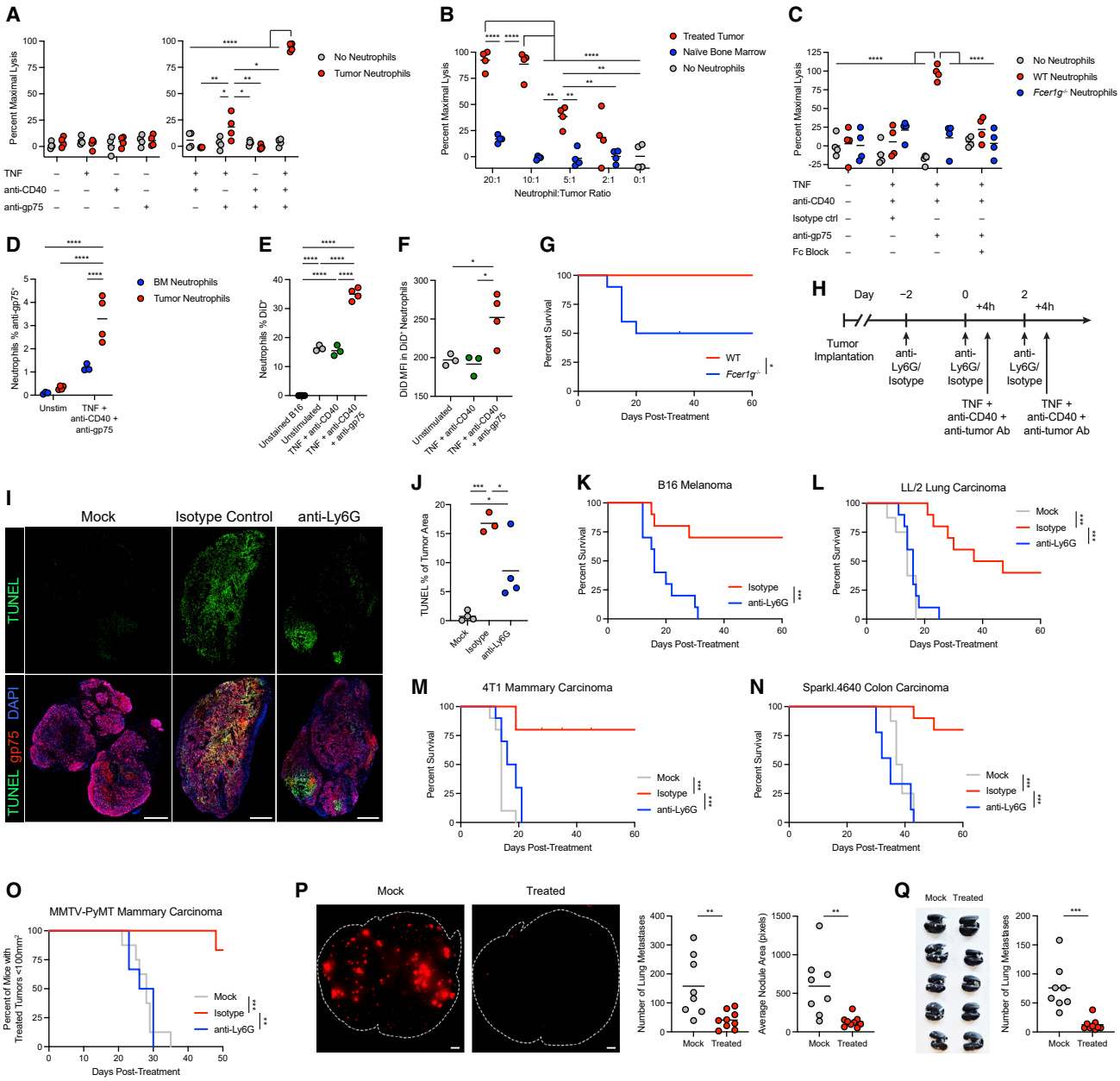

Figure 2. Therapeutically activated neutrophils eradicate multiple tumor types and reduce metastatic seeding

(A) Lysis of B16 cells co-cultured with neutrophils isolated from treated tumors and stimulated *in vitro* with the indicated components (n = 4).

(B) Lysis of B16 cells co-cultured with neutrophils isolated from treated tumors or tumor-naive bone marrow (BM), stimulated *in vitro* with TNF + anti-CD40 + anti-gp75 (n = 4).

(C) Lysis of B16 cells co-cultured with neutrophils isolated from treated tumors in WT or *Fcer1g*$^{-/-}$ mice, stimulated *in vitro* with TNF + anti-CD40 + anti-gp75 or isotype control, with or without anti-CD16/CD32 to block FcγRs (n = 4).

(D) Signal from anti-gp75-Alexa Fluor 647 in neutrophils isolated from treated tumors or naive bone marrow and cultured *in vitro* with B16 cells together with TNF + anti-CD40 + anti-gp75-Alexa Fluor 647 or no stimulation (BM, n = 3; tumor, n = 4).

(E and F) Percentage DiD^{+} neutrophils (E) and DiD MFI in DiD^{+} neutrophils (F) following co-culture of treated tumor neutrophils with DiD-labeled B16 and stimulation *in vitro* with the indicated components (unstained/triple, n = 4; unstimulated/double, n = 3).

(G) Survival of B16-bearing WT or *Fcer1g*$^{-/-}$ mice following treatment with neutrophil-activating therapy (n = 10).

(H) Regimen for neutrophil depletion and therapy. Treatment was performed 4 h after administration of anti-Ly6G or isotype control on days 0 and 2.

(I and J) Representative TUNEL immunofluorescence (I) and quantification (J) in B16 tumors 24 h after treatment with neutrophil-activating therapy, following neutrophil depletion with anti-Ly6G or isotype control. Scale bars, 500 μm. (isotype, n = 3; others, n = 4).

(K) Survival of B16-bearing mice administered anti-Ly6G or isotype control prior to neutrophil-activating therapy (n = 10).

(L–N) Survival of mice bearing LL/2 (L) (mock, n = 8; others, n = 10), 4T1 (M) (n = 10), and Sparkl.4640 (N) (mock, n = 8; isotype, n = 10; anti-Ly6G, n = 9) tumors administered anti-Ly6G or isotype control prior to neutrophil-activating therapy.

(legend continued on next page)

carcinoma cell line isolated from a genetically engineered mouse model (Figures S2N and S2O), and 4T1 mammary carcinoma (Figures S2P and S2Q) induced similar neutrophil expansion, recruitment, and activation.

Furthermore, treated tumor-infiltrating neutrophils possessed a mature morphology with hypersegmented nuclei (Figure S2R). Consistent with their activated status, they exhibited enhanced production of reactive oxygen species (ROS) (Figures S2S–S2U). Although activated neutrophils can extrude neutrophil extracellular traps (NETs), neutrophils in the tumor and blood of treated mice exhibited no detectable increase in NETotic neutrophils[45] (Figures S2V and S2W). Altogether, these data indicate that neutrophil-activating therapy induces an acute activation of tumor-infiltrating and circulating neutrophils, which exhibit a unique surface phenotype including markers associated with both anti-tumor and pro-tumor function.

Therapeutically activated neutrophils eradicate multiple tumor types and reduce metastatic seeding

To directly evaluate the anti-tumor activity of neutrophils following neutrophil-activating therapy, neutrophils were isolated from treated B16 tumors and co-cultured with B16 tumor cells *ex vivo*. Following stimulation *ex vivo* with neutrophil-activating therapy, these neutrophils mediated potent tumor cell killing (Figure 2A). In contrast, neutrophils isolated from the bone marrow of naive mice failed to mediate significant tumor cell killing, even after *ex vivo* stimulation with neutrophil-activating therapy (Figure 2B). Notably, stimulation with all three components of the therapy was required for maximal cytotoxic function (Figure 2A). Tumor-infiltrating neutrophils required both anti-gp75 and Fc gamma receptors (FcγRs) to kill B16 tumor cells *ex vivo* (Figure 2C), and tumor-infiltrating neutrophils stimulated with neutrophil-activating therapy demonstrated enhanced uptake of anti-gp75 mAb (Figure 2D) and B16 cell membrane (Figures 2E and 2F), suggesting that antibody-mediated trogocytosis[32] may mediate ADCC by these activated neutrophils. Mice lacking functional activating FcγRs (*Fcer1g*$^{-/-}$) exhibited reduced tumor clearance *in vivo* (Figures 2G and S3A), while neutrophil recruitment and CD11b upregulation were still maintained (Figures S3B–S3D). B16 tumors that recurred following therapy exhibited reduced levels of the antibody target antigen gp75, suggesting that ADCC may exert a selection pressure against the antibody target antigen (Figure S3E). Treatment of mice bearing B16 tumors with heterogeneous expression of cell-surface enhanced green fluorescent protein (EGFP) with TNF + anti-CD40 + anti-EGFP induced tumor clearance at a comparable rate as tumors with homogeneous EGFP expression (Figure S3F). Altogether, these data suggest that tumor-binding antibody-FcγR interactions enhance *in vivo* neutrophil killing of tumors through ADCC, but this is not absolutely required for tumor clearance.

To determine the role of therapeutically activated neutrophils in tumor clearance *in vivo*, neutrophils were depleted using anti-Ly6G antibodies (Figure 2H). Although neutrophil depletion with anti-Ly6G did not completely remove neutrophils, this protocol blocked treatment-induced neutrophil tumor infiltration and reduced neutrophil expansion in the blood (Figures S3G–S3L). Similar results were obtained across multiple tumor models (Figures S3M–S3R).

Depletion of neutrophils with anti-Ly6G mAb prior to treatment markedly reduced cell death within tumors (Figures 2I and 2J). Although neutrophil depletion did not alter tumor growth in untreated mice (Figure S3S), it completely prevented tumor clearance in response to neutrophil-activating therapy (Figures 2K and S3T), demonstrating a crucial role for neutrophils in tumor eradication. Treatment with neutrophil-activating therapy enabled neutrophils to clear multiple additional tumor types, including LL/2 lung carcinoma, 4T1 mammary carcinoma, and Sparkl.4640 colon carcinoma (Figures 2L–2N and S3U–S3W). We next tested neutrophil-activating therapy in the MMTV-PyMT model of mammary carcinoma, in which tumors spontaneously develop in multiple breasts nearly simultaneously. Treatment of one tumor per mouse resulted in neutrophil-dependent regression of the treated tumors (Figures 2O and S3X), whereas tumors in untreated breasts did not regress. Tumors later grew out in treated breasts, which could represent either recurrences of the treated tumor or development of additional tumors in the same breast.

To determine whether neutrophil-activating therapy could restrict the growth of distant tumors in the context of metastasis, we injected B16 expressing tdTomato into the tail vein one week after subcutaneous implantation of B16. Treatment of the subcutaneous tumor ten hours after this seeding of the lungs resulted in a substantial reduction in the number and size of lung metastases (Figure 2P). Furthermore, treatment of orthotopically implanted 4T1 mammary carcinoma with neutrophil-activating therapy reduced the number of spontaneous lung metastases (Figure 2Q). These data indicate that neutrophil-activating therapy can reduce metastatic seeding, restrict metastatic growth, and/or eliminate metastases.

Therapy activates antigen-presenting cells and primes T cell memory

Neutrophil infiltration following treatment was accompanied by a TNF-dependent decrease in multiple other immune cell populations within the tumor (Figures 3A and S4A–S4C). Additionally,

(O) Percentage of MMTV-PyMT mice with treated tumors below the threshold of 100 mm^2 following treatment of one tumor per mouse in the context of anti-Ly6G or isotype control (mock, n = 8; others, n = 6).

(P) Representative images of B16-tdTomato fluorescence in the lung (left) and quantification of the number and average area of tdTomato$^+$ lung metastases (right) in mice bearing subcutaneous (s.c.) B16 tumors that were injected intravenously through the tail vein with B16-tdTomato one week after tumor implantation. Ten hours after tail vein injection, s.c. tumors were treated with mock or neutrophil-activating therapy, and the lungs were harvested and imaged 9 days after the tail vein injection. Lung borders are outlined in white. Scale bars, 1 mm (mock, n = 8; treated, n = 9).

(Q) Representative image of India ink-stained lungs (left) and number of lung metastases (right) 30 days after orthotopic implantation of 4T1, in mice receiving neutrophil-activating therapy or mock treatment (mock, n = 8; treated, n = 9).

Statistics: two-way ANOVA with Tukey's multiple-comparisons test (A–D), one-way ANOVA with Tukey's multiple-comparisons test (E, F, and J), log rank test (F and K), log rank test with Bonferroni correction (L–O), unpaired two-tailed t test (P and Q). For all dot plots, the line indicates the mean. Data are representative of 2 (A–J and P) or 3 (K) independent experiments or pooled from 2 (Q), 3 (L–N), or 6 (O) experiments. See also Figure S3.

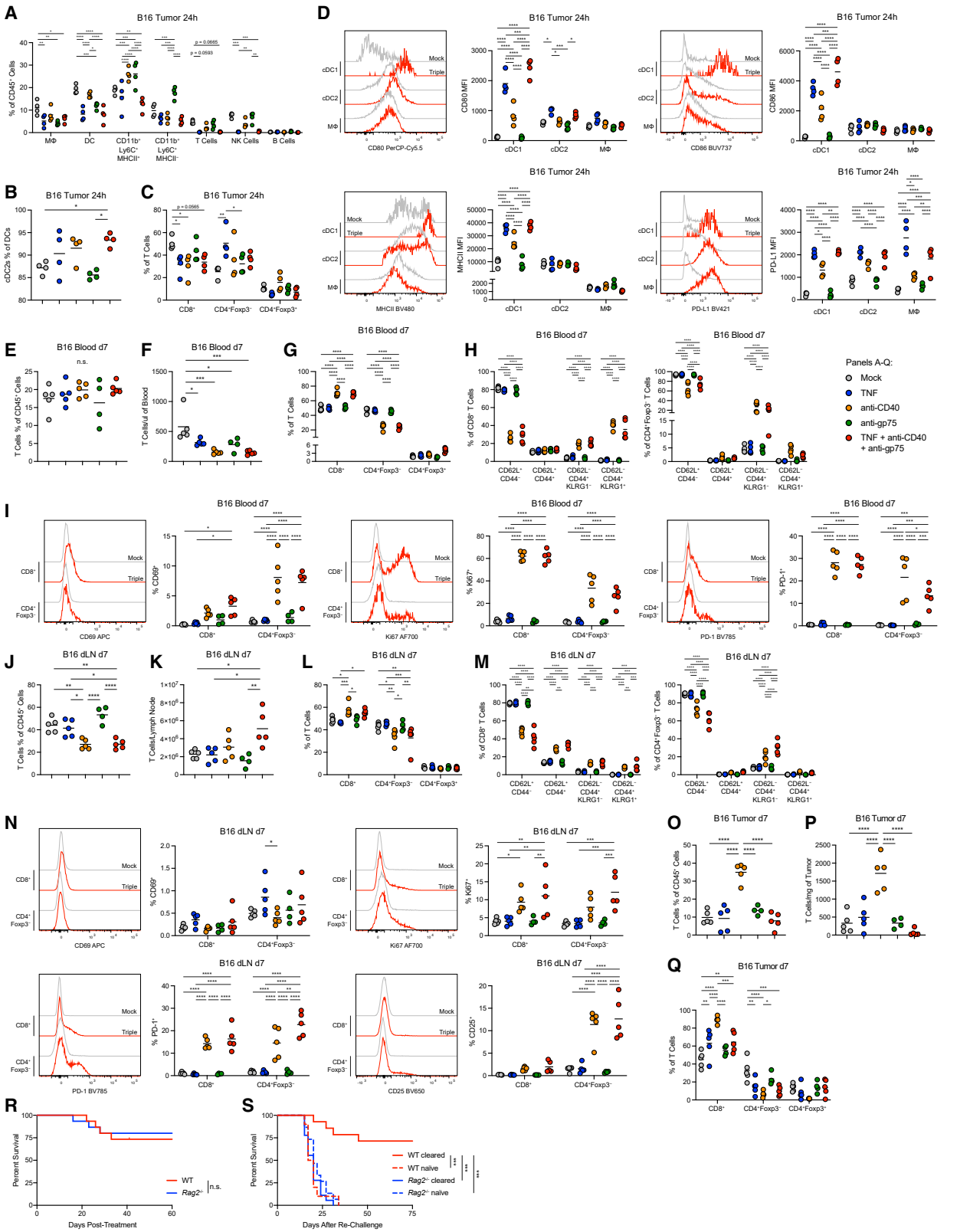

Figure 3. Therapy activates antigen-presenting cells and primes T cell memory

(A) Frequency of immune cell subsets in B16 tumors 24 h after treatment (n = 4).

(B) Percentage of cDC2s out of total DCs in B16 tumors 24 h after treatment (n = 4).

(legend continued on next page)

conventional dendritic cell (cDC) populations were skewed further toward cDC2s (Figure 3B), and the relative frequency of $CD8^+$ T cells decreased slightly after treatment (Figure 3C). Treatment of TNFR KO mice with neutrophil-activating therapy did not induce the large alterations to immune cell populations seen in treated WT mice (Figures S4D and S4E). In contrast, treated *Fcer1g*$^{-/-}$ mice had alterations in immune subsets closely resembling treated WT mice (Figures S4F and S4G). The anti-CD40-dependent expansion of neutrophils in the blood (Figure 1H) was counterbalanced by a decrease in blood B cell frequency, and anti-CD40 increased the proportion of circulating $CD4^+$ Forkhead box $P3^-$ ($Foxp3^-$) T cells at the expense of $CD8^+$ T cells (Figures S4H–S4J). Treatment of 4T1 and Sparkl.4640 tumors with neutrophil-activating therapy elicited similar changes in immune cell populations (Figures S4K–S4Q).

TNF and CD40 agonists are capable of activating antigen-presenting cells (APCs); indeed, both agents induced upregulation of major histocompatibility complex class II (MHCII), CD80, and CD86 on cDC1s in B16 tumors (Figure 3D), indicating activation. In contrast, there were minimal changes in activation markers in the more abundant cDC2s and macrophages, other than CD80 upregulation in cDC2s (Figure 3D). Opposing this activation, all three APC subsets upregulated PD-L1 with treatment (Figure 3D). Macrophage polarization, assessed by the ratio of $CD206^{hi}$ to $MHCII^{hi}$ macrophages, did not change significantly following therapy (Figure S5A). Sparkl.4640 and 4T1 tumors treated with neutrophil-activating therapy exhibited mostly similar patterns of APC activation (Figures S5B–S5E). Altogether, these data indicate that neutrophil-activating therapy induces activation of APCs in the tumor, although this activation is mainly confined to the relatively rare cDC1 subset.

To determine the effects of neutrophil-activating therapy on T cells, we examined blood, tumor-draining lymph nodes (dLNs), and tumors one week after treatment of B16 tumors. Although T cells in the blood did not expand (Figures 3E and 3F), there was an anti-CD40-dependent increase in the proportion of $CD8^+$ T cells (Figure 3G), as well as a large shift in both $CD8^+$ T cells and $CD4^+Foxp3^-$ T cells from a naive $CD62L^+CD44^-$ phenotype to a $CD62L^-CD44^+$ Killer cell lectin-like receptor $G1^-$ ($KLRG1^-$) effector memory/memory precursor effector phenotype and a $CD62L^-CD44^+KLRG1^+$ phenotype that could encompass both short-lived effectors and future memory cells[46] (Figure 3H). In addition, treatment activated $CD8^+$ and $CD4^+Foxp3^-$ T cells, indicated by expression of CD69, programmed cell death protein-1 (PD-1), and the proliferation marker Ki67 (Figure 3I). In the dLN, treatment induced an expansion of T cells and a similar bias toward $CD8^+$ T cells (Figures 3J–3L), in addition to increased memory differentiation (Figure 3M) and T cell activation (Figure 3N). The full neutrophil-activating therapy did not increase the numbers of tumor T cells, although the proportion of $CD8^+$ T cells increased (Figures 3O–3Q). Examination of T cells in the 4T1 model revealed a more blunted response, although certain commonalities were preserved, including T cell proliferation in the blood and dLN, activation and memory differentiation in the dLN, and elevated proportions of $CD8^+$ T cells in the tumor (Figures S5F–S5Q).

To investigate the role of adaptive immunity in tumor clearance, we treated *Rag2*$^{-/-}$ mice, which lack mature T cells and B cells. Neutrophil-activating therapy cleared B16 tumors in both WT and *Rag2*$^{-/-}$ mice (Figures 3R and S5R–S5T). Nonetheless, WT mice that had previously cleared B16 were protected from re-challenge with the same tumor, in contrast to *Rag2*$^{-/-}$ mice or naive WT mice (Figures 3S and S5U), indicating that neutrophil-activating therapy is capable of priming anti-tumor adaptive immune memory, even though this is not required for initial tumor clearance. These data are consistent with the low number of T cells in the tumor and the large-scale T cell activation, proliferation, and memory differentiation in the blood and dLN observed post-treatment.

Complement activates tumor-infiltrating neutrophils through C5AR1

To identify the mechanism by which neutrophil-activating therapy stimulates neutrophils, we investigated the complement system, which generates products that are well known to stimulate neutrophil activation and recruitment.[47] Within four hours of treatment, complement component C3 was deposited on the surface of tumor-infiltrating neutrophils (Figure 4A) and throughout the tumor (Figures 4B and 4C), indicating local complement activation. Complement deposition throughout the tumor was dependent on TNF signaling (Figure S6A) with potential contributions from anti-CD40 and anti-gp75 (Figures S6B–S6D). Neutrophil depletion did not alter complement deposition

(C) Percentage of T cell subsets out of total T cells in B16 tumors 24 h after treatment (n = 4).
(D) Representative histograms and MFIs for markers expressed on APC populations in B16 tumors 24 h after treatment (n = 4).
(E and F) Frequencies (E) and numbers (F) of T cells in the blood 7 days after treatment of B16 (anti-gp75, n = 4; others, n = 5).
(G) Percentage of T cell subsets out of total T cells in the blood 7 days after treatment of B16 (anti-gp75, n = 4; others, n = 5).
(H) Memory and effector phenotypes of T cell subsets in the blood 7 days after treatment of B16 (anti-gp75, n = 4; others, n = 5).
(I) Representative histograms and MFIs for markers expressed on T cell subsets in the blood 7 days after treatment (anti-gp75, n = 4; others, n = 5).
(J and K) Frequencies (J) and numbers (K) of T cells in the dLN 7 days after treatment of B16 (anti-gp75, n = 4; others, n = 5).
(L) Percentage of T cell subsets out of total T cells in the dLN 7 days after treatment of B16 (anti-gp75, n = 4; others, n = 5).
(M) Memory and effector phenotypes of T cell subsets in the dLN 7 days after treatment of B16 (anti-gp75, n = 4; others, n = 5).
(N) Representative histograms and MFIs for markers expressed on T cell subsets in the dLN 7 days after treatment (anti-gp75, n = 4; others, n = 5).
(O and P) Frequencies (O) and numbers (P) of T cells in the tumor 7 days after treatment of B16 (anti-gp75, n = 4; others, n = 5).
(Q) Percentage of T cell subsets out of total T cells in the tumor 7 days after treatment of B16 (anti-gp75, n = 4; others, n = 5).
(R) Survival of B16-bearing WT or *Rag2*$^{-/-}$ mice treated with neutrophil-activating therapy (n = 15).
(S) Survival of WT or *Rag2*$^{-/-}$ mice following implantation of B16 in tumor-naive or B16-cleared mice 50 days after initial treatment with neutrophil-activating therapy (WT cleared, n = 14; *Rag2*$^{-/-}$ cleared, n = 18; WT naive, n = 10; *Rag2*$^{-/-}$ naive, n = 15).
Statistics: two-way ANOVA with Tukey's multiple-comparisons test (A, E–I, L–N, and Q), one-way ANOVA with Tukey's multiple-comparisons test (B–D, J, K, O, and P), log rank test (R), log rank test with Bonferroni correction (S). For all dot plots, the line indicates the mean. Data are representative of 2 (A–Q and S) or 3 (R) independent experiments. See also Figures S4 and S5.

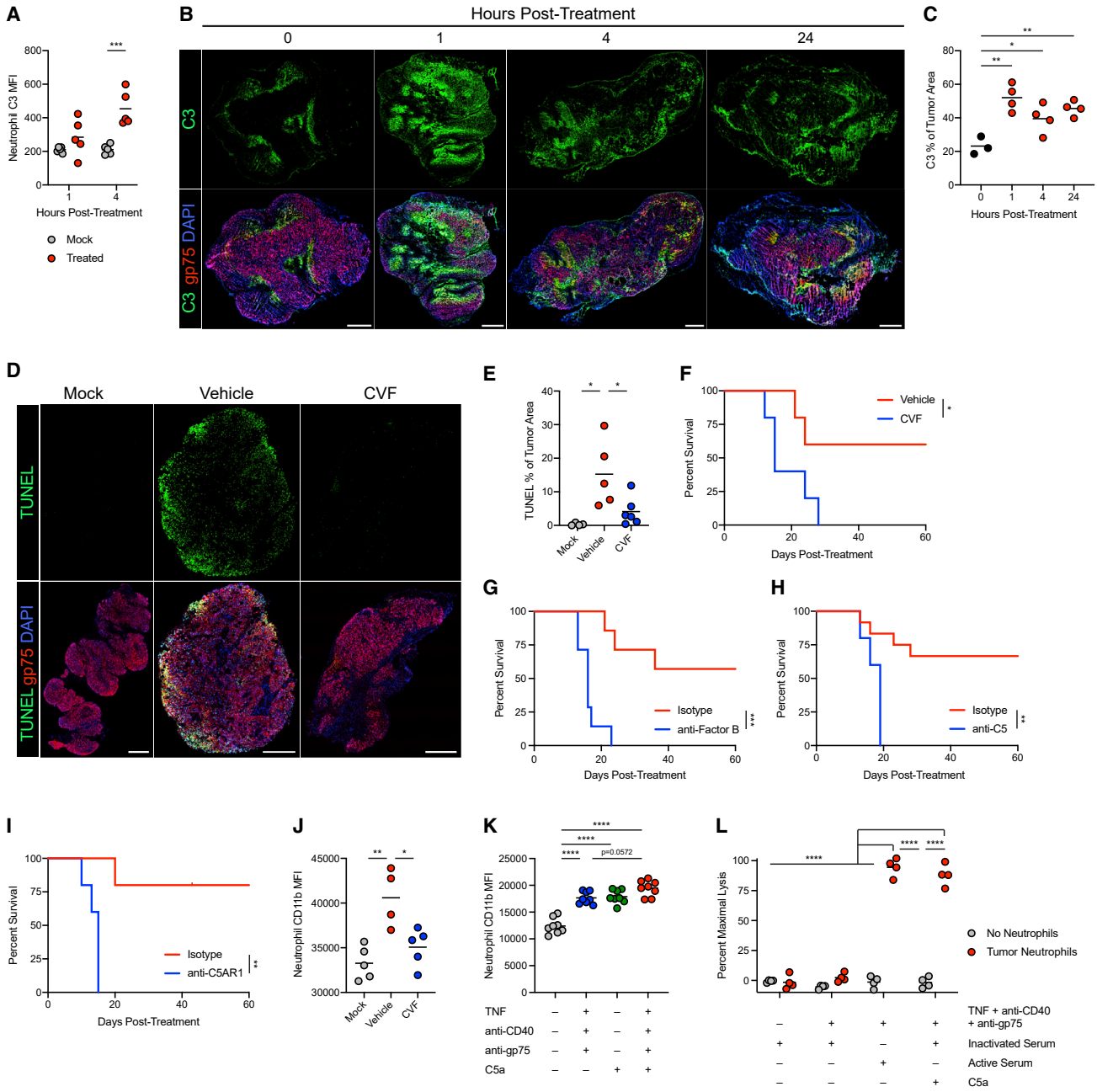

Figure 4. Complement activates tumor-infiltrating neutrophils through C5AR1

(A) Deposition of C3 on B16 tumor-infiltrating neutrophils following treatment with neutrophil-activating therapy (n = 5).

(B and C) Representative immunofluorescence (B) and quantification (C) of C3 staining in B16 tumors after treatment. Scale bars, 500 μm (0 h, n = 3; others, n = 4).

(D and E) Representative immunofluorescence (D) and quantification (E) of TUNEL staining in B16 tumors 24 h after treatment of mice that had received CVF or vehicle prior to treatment. Scale bars, 500 μm (mock, n = 4; vehicle, n = 5; CVF, n = 6).

(F) Survival of B16-bearing mice administered CVF prior to treatment with neutrophil-activating therapy (n = 5).

(G–I) Survival of B16-bearing mice administered anti-Factor B (G) (n = 7), anti-C5 (H) (isotype, n = 12; anti-C5, n = 5), and anti-C5AR1 (I) (n = 5) blocking antibodies prior to treatment.

(J) Expression of CD11b on B16 tumor-infiltrating neutrophils 4 h after treatment following CVF or vehicle administration (vehicle, n = 4; others, n = 5).

(K) Expression of CD11b on naive neutrophils following stimulation *in vitro* with the indicated factors (n = 8).

(L) Lysis of B16 cells co-cultured with neutrophils isolated from treated tumors and stimulated *in vitro* with the indicated factors (n = 4).

Statistics: two-way ANOVA with Tukey's multiple-comparisons test (A and L), one-way ANOVA with Tukey's multiple-comparisons test (C, E, J, and K), log rank test (F–I). For all dot plots, the line indicates the mean. Data are representative of 2 (A–C, F, G, and I–L) or 3 (D and E) independent experiments or pooled from 2 experiments (H). See also Figures S6 and S7.

(Figures S6E–S6G), suggesting that complement activation occurs upstream of neutrophil recruitment and activation.

Administration of cobra venom factor (CVF) to deplete complement prior to treatment prevented complement activation throughout tumors (Figures S6H and S6I), which mirrored the results seen in *C3*$^{-/-}$ mice (Figure S6J). CVF administration or C3 deficiency reduced tumor cell death following treatment (Figures 4D, 4E, S7A, and S7B) and prevented tumor eradication (Figures 4F, S7C, and S7D). Depletion of Factor B, which is required for complement activation through the alternative pathway (AP), as well as depletion or deficiency of the AP positive regulator properdin, blocked tumor clearance (Figures 4G and S7E–S7G), implicating AP complement activation as a crucial mediator of the treatment response.

The effect of complement activation was mediated through complement component C5, as C5-depleted mice failed to clear tumors (Figures 4H and S7H). Although cleavage of C5 both generates the anaphylatoxin C5a and catalyzes the formation of the membrane attack complex (MAC) through C5b,[47] *C6*$^{-/-}$ mice, which are incapable of forming the MAC, showed no deficit in tumor clearance (Figure S7I). In contrast, blocking complement C5a receptor 1 (C5AR1) prevented tumor eradication (Figures 4I and S7J), implicating C5a as the relevant complement effector. Although complement deficiency did not induce a major deficit in neutrophil recruitment (Figures S7K and S7L), it reduced neutrophil activation in response to treatment (Figures 4J and S7M). In contrast, complement depletion did not reduce activation of other myeloid populations in the tumor (Figure S7N), suggesting that neutrophils are the main cell type activated by complement. Additionally, recombinant C5a activated neutrophils *in vitro* (Figure 4K), and neutrophils isolated from treated tumors required C5a or serum containing functional complement to lyse tumor cells (Figures 4L and S7O). Altogether, these data demonstrate that neutrophil-activating therapy induces complement activation through the AP, which in turn activates neutrophils through C5a-C5AR1 signaling to kill tumors.

Secretion of leukotriene B_4 by C5a-activated neutrophils drives tumor clearance

To identify neutrophil-derived mediators that might contribute to tumor clearance, we considered the potent pro-inflammatory lipid mediator leukotriene B_4 (LTB_4).[48] Neutrophil-activating therapy induced a neutrophil-dependent increase in LTB_4 in the tumor (Figures 5A and S8A), with neutrophils responsible for the majority of LTB_4 production (Figure 5B). Furthermore, LTB_4 production was dependent on TNF signaling and complement (Figures 5C, S8B, and S8C), and stimulation of neutrophils with C5a *in vitro* induced LTB_4 (Figure 5D). Inhibition of LTB_4 production through the leukotriene A_4 hydrolase (LTA_4H) inhibitor SC57461A prevented treatment-induced tumor cell death (Figures 5E and S8D) and tumor clearance (Figures 5F and S8E). The effects of LTB_4 were mediated through LTB_4 receptor 1 (BLT1), as the BLT1 antagonist CP-105696 also prevented tumor clearance (Figures 5G and S8F), and SC57461A and CP-105696 both prevented *ex vivo* killing of tumor cells by neutrophils (Figure 5H). These data demonstrate that C5a-activated neutrophils mediate tumor eradication through LTB_4 in response to neutrophil-activating therapy.

LTB_4-dependent induction of xanthine oxidase induces oxidative damage and tumor clearance

As LTB_4[48] and C5a[49] can induce production of ROS by neutrophils, and as ROS are potent effectors of neutrophil-mediated cytotoxicity, we investigated the role of ROS in tumor clearance. Neutrophil-activating therapy induced neutrophil-dependent oxidative damage, as evidenced by oxidation of nucleic acids (Figures 6A and 6B) and endogenous glutathione (Figure 6C) within the tumor. This oxidation was dependent on TNF signaling, complement, and LTB_4 (Figures 6D, 6E, and S8G), suggesting that production of LTB_4 by C5a-activated neutrophils drives the production of ROS and resulting oxidative damage in the tumor. Scavenging of ROS with reduced glutathione (GSH) or neutralization of hydrogen peroxide with catalase blocked *ex vivo* killing of tumor cells by tumor-infiltrating neutrophils (Figure 6F), demonstrating that ROS mediate neutrophil killing of tumor cells. Administration of GSH decreased tumor cell death *in vivo* (Figures S8H and S8I) and prevented tumor clearance (Figure S8J) following treatment. Furthermore, administration of catalase blocked tumor eradication in treated mice (Figures 6G and S8K). These data demonstrate a critical role for ROS, and specifically hydrogen peroxide, in neutrophil-dependent tumor clearance following neutrophil-activating therapy.

Despite the requirement for neutrophils and ROS, *Ncf1*$^{-/-}$ mice, which lack the p47 subunit of the phagocyte nicotinamide adenine dinucleotide phosphate oxidase complex (NOX) and fail to produce ROS through phagocyte NOX, were still able to clear tumors, albeit less efficiently than WT mice (Figure S8L). Given these results, we sought an additional source of ROS in the context of this treatment. Xanthine oxidoreductase is a bidirectional enzyme capable of both xanthine dehydrogenase (XDH) and xanthine oxidase (XO) activities, and XO can produce superoxide, serving as a source of ROS.[50] Neutrophil-activating therapy induced a neutrophil-dependent elevation in XO activity within the tumor (Figure 6H), and depletion of complement and inhibition of LTB_4 prevented this increase in XO activity (Figures 6I and 6J). XO inhibition with topiroxostat did not prevent neutrophil infiltration or LTB_4 production (Figures S8M and S8N), indicating that XO activation occurs downstream of neutrophil LTB_4 production. Importantly, inhibition of XO by topiroxostat prevented oxidation in tumors (Figure 6K), demonstrating XO to be responsible for the ROS-mediated damage of the tumor induced by treatment. Inhibition of XO also reduced cell death (Figures 6L and S8O), prevented tumor clearance (Figures 6M and S8P), and inhibited *ex vivo* tumor cell killing (Figure 6N). Thus, following neutrophil-activating therapy, LTB_4 production by complement-activated neutrophils induces ROS production through XO, leading to oxidative damage of tumor cells and subsequent tumor clearance.

Neutrophil-activating therapy activates human neutrophils to kill tumor cells

To determine whether neutrophils could clear human tumors, we treated *Rag2*$^{-/-}$ *Il2rg*$^{-/-}$ mice bearing A549 human lung carcinoma or orthotopic MDA-MB-231 human mammary carcinoma with neutrophil-activating therapy. Whereas neutrophil-sufficient mice cleared the tumors, neutrophil-depleted mice were uniformly unable to do so (Figures 7A and 7B). We next examined

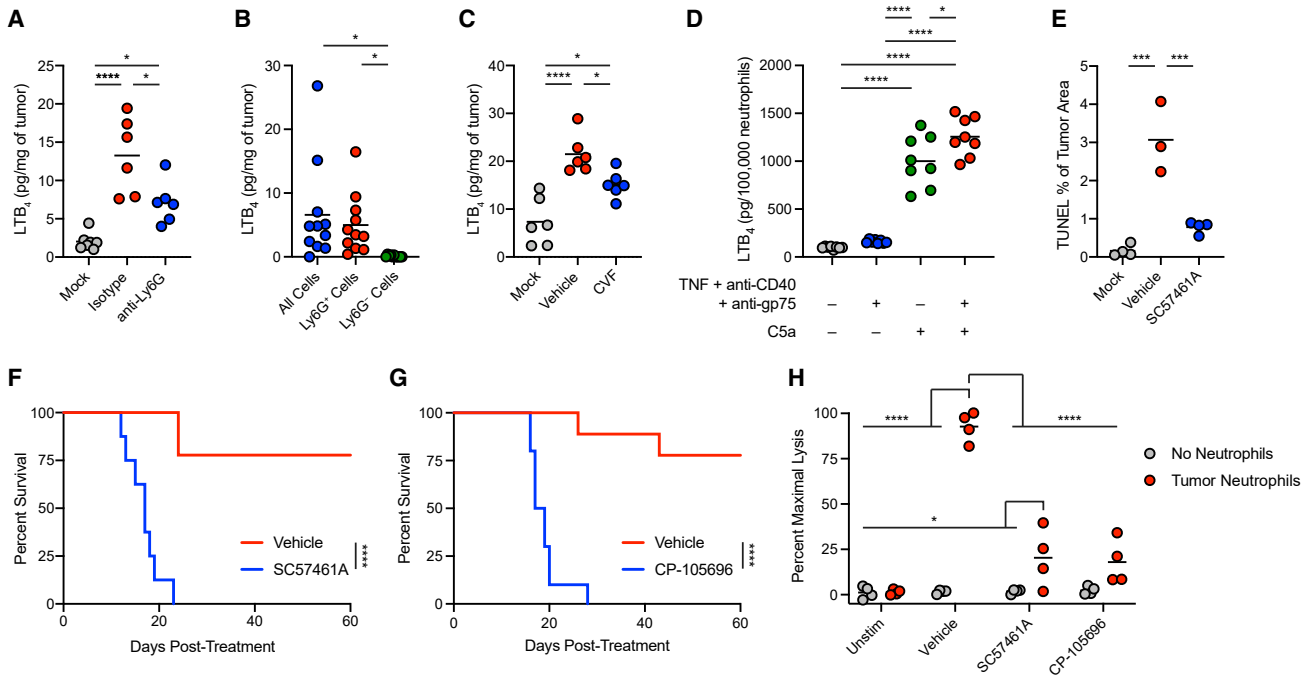

Figure 5. Secretion of leukotriene B_4 by C5a-activated neutrophils drives tumor clearance

(A) LTB_4 levels in B16 tumors 24 h after treatment with neutrophil-activating therapy following neutrophil depletion by anti-Ly6G (mock, n = 7; others, n = 6).

(B) LTB_4 produced *ex vivo* by cells harvested from B16 tumors 12 h after treatment (n = 11).

(C) LTB_4 levels in B16 tumors 24 h after treatment following administration of CVF (n = 6).

(D) LTB_4 production by naive neutrophils following stimulation *in vitro* with the indicated factors (n = 8).

(E) Quantification of TUNEL staining in B16 tumors 24 h after treatment with neutrophil-activating therapy following administration of SC57461A (vehicle, n = 3; others, n = 4).

(F and G) Survival of B16-bearing mice after treatment following administration of SC57461A (F) (vehicle, n = 9; SC57461A, n = 8) or CP-105696 (G) (vehicle, n = 9; CP-105696, n = 10).

(H) Lysis of B16 cells co-cultured with neutrophils isolated from treated tumors and stimulated *in vitro* with neutrophil-activating therapy together with the indicated inhibitors (n = 4).

Statistics: one-way ANOVA with Tukey's multiple-comparisons test (A and C–E), repeated-measures one-way ANOVA with Tukey's multiple-comparisons test (B), log rank test (F and G), two way ANOVA with Tukey's multiple-comparisons test (H). For all dot plots, the line indicates the mean. Data are representative of 2 (A, C, D, and H) or 1 (E) independent experiment or pooled from 2 experiments (B, F, and G). See also Figure S8.

whether human neutrophils could be activated *in vitro* using human versions of our neutrophil-activating therapy components. Stimulation of neutrophils isolated from the peripheral blood of healthy human donors with TNF + anti-CD40 + anti-EGFR mAb induced the upregulation of multiple activation markers, including CD11b and ICAM-1, which were also upregulated in mouse neutrophils (Figure 7C). The FcγR CD32 was upregulated, while CD16 was downregulated, consistent with reports that it can be cleaved from the surface upon neutrophil activation.[51] In addition, CD66b and CD63 were both upregulated on the cell surface, indicating degranulation, while increased DHR-123 staining indicated ROS production by the stimulated neutrophils. Consistent with our findings in mice, C5a induced upregulation of some activation markers and downregulation of C5AR1, while the combined effect of C5a together with neutrophil-activating therapy enhanced expression of CD63. To determine whether these activated neutrophils could kill human tumor cells, we co-cultured neutrophils from healthy donors with A549 human lung carcinoma cells. Stimulation with neutrophil-activating therapy induced high levels of tumor cell lysis, albeit at higher neutrophil-to-tumor ratios than were necessary with mouse neutrophils isolated from treated tumors (Figure 7D). In agreement with our findings with mouse neutrophils, all three components of neutrophil-activating therapy were required to achieve efficient lysis of tumor cells (Figure 7E). These data suggest that human neutrophils can be activated to kill tumor cells in the same manner we described for mouse neutrophils.

DISCUSSION

On the basis of the findings reported here, we propose a multistep mechanism by which neutrophils can be harnessed to eradicate multiple types of tumors (Figure 8). TNF signals through TNFR1 to induce neutrophil recruitment and activation in the tumor. Anti-CD40 promotes neutrophil cytotoxicity and granulopoiesis, and tumor-binding antibody enhances tumor clearance through FcγR-mediated ADCC, potentially by trogocytosis. These treatment components combine to activate complement through the AP, inducing production of C5a. C5a signaling through C5AR1 activates neutrophils to produce LTB_4, which drives XO activity in the tumor microenvironment. ROS produced by XO induce oxidative damage and death of

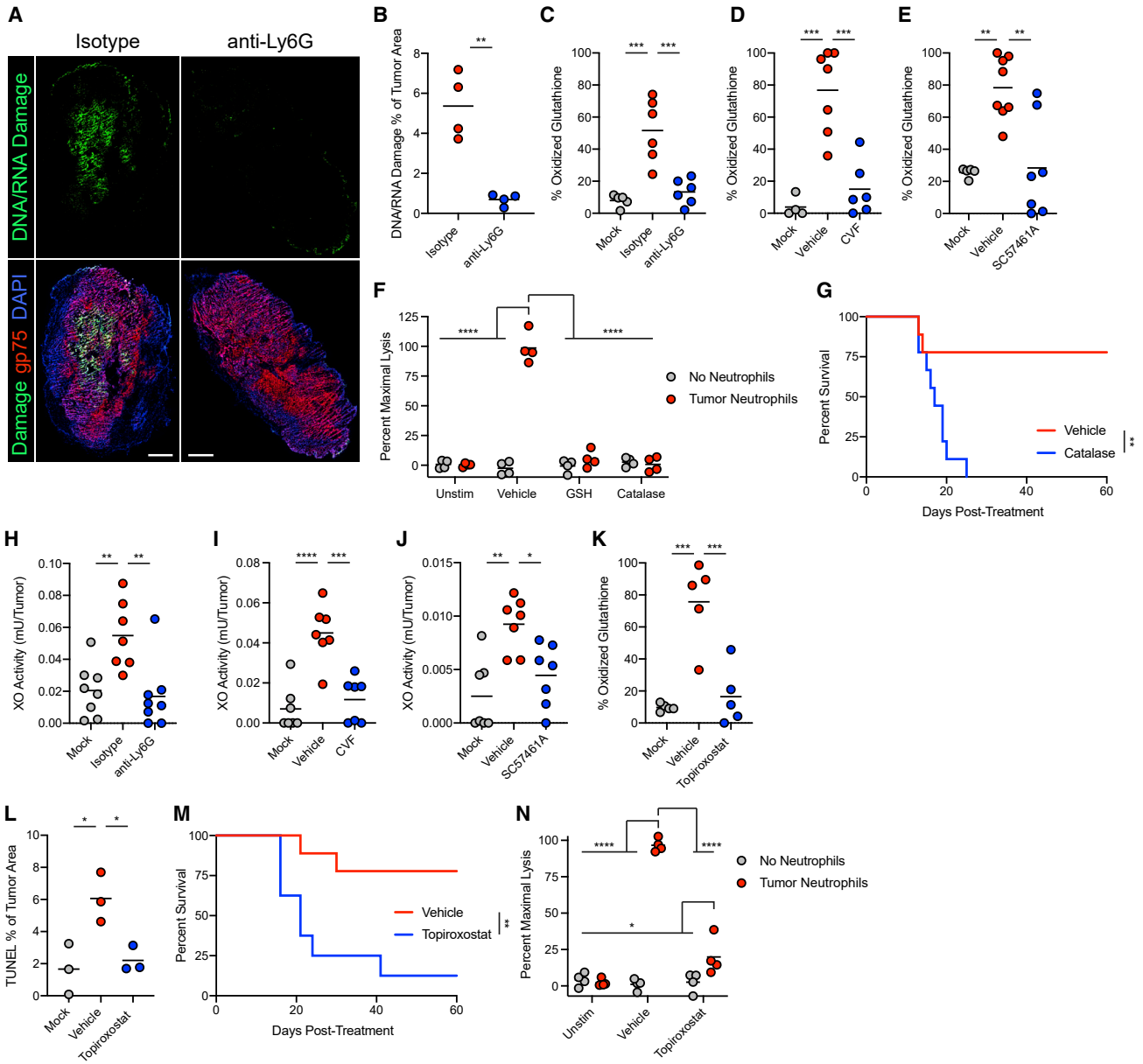

Figure 6. LTB_4-dependent induction of xanthine oxidase induces oxidative damage and tumor clearance

(A and B) Representative immunofluorescence (A) and quantification (B) of DNA/RNA oxidative damage in B16 tumors 24 h post-treatment with neutrophil-activating therapy. Scale bars, 500 μm (n = 4).

(C–E) Percentage of oxidized glutathione in B16 lysates 24 h after treatment with neutrophil-activating therapy following administration of anti-Ly6G (C) (mock, n = 5; others, n = 6), CVF (D) (mock, n = 4; vehicle, n = 7; CVF, n = 6), or SC57461A (E) (mock, n = 5; vehicle, n = 8; SC57461A, n = 7).

(F) Lysis of B16 cells co-cultured with neutrophils isolated from treated tumors and stimulated *in vitro* with neutrophil-activating therapy together with the indicated inhibitors (n = 4).

(G) Survival of B16-bearing mice treated with neutrophil-activating therapy following administration of catalase (n = 9).

(H–J) XO activity in the tumor 24 h after treatment of B16 with neutrophil-activating therapy following administration of anti-Ly6G (H) (isotype, n = 7; others, n = 8), CVF (I) (n = 7), or SC57461A (J) (n = 7).

(K) Percentage of oxidized glutathione in B16 lysates 24 h after treatment following administration of topiroxostat (n = 5).

(L) Quantification of TUNEL staining in B16 tumors 24 h after treatment with neutrophil-activating therapy following administration of topiroxostat (n = 3).

(M) Survival of B16-bearing mice treated with neutrophil-activating therapy following administration of topiroxostat (vehicle, n = 9; topiroxostat, n = 8).

(N) Lysis of B16 cells co-cultured with neutrophils isolated from treated tumors and stimulated *in vitro* with neutrophil-activating therapy in the presence of topiroxostat (n = 4).

Statistics: one-way ANOVA with Tukey's multiple-comparisons test (B–E and H–L), two-way ANOVA with Tukey's multiple-comparisons test (F and N), log rank test (G and M). For all dot plots, the line indicates the mean. Data are representative of 2 (F, I–K, M, and N) or 1 (A, B, and L) independent experiment or pooled from 2 experiments (C–E, G, and H). See also Figure S8.

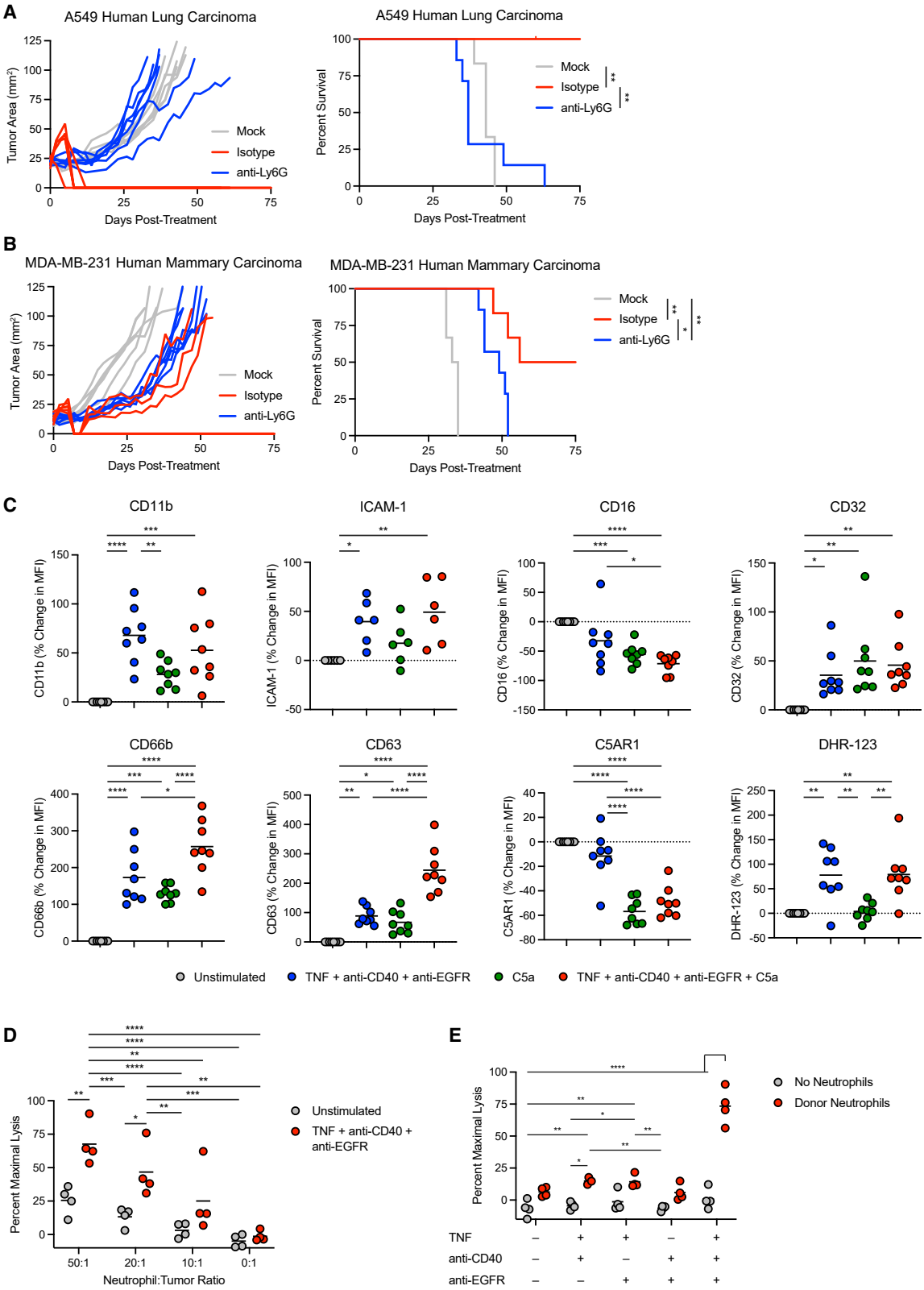

Figure 7. Neutrophil-activating therapy activates human neutrophils to kill tumors

(A and B) Survival of *Rag2*$^{-/-}$ *Il2rg*$^{-/-}$ mice bearing subcutaneous A549 (A) (anti-Ly6G, n = 7; others, n = 6) or orthotopic MDA-MB-231 (B) (anti-Ly6G, n = 7; others, n = 6) treated with neutrophil-activating therapy following anti-Ly6G administration.

(legend continued on next page)

tumor cells, ultimately leading to tumor clearance. In contrast to most previous reports of neutrophil anti-tumor activity,[1,2] this mechanism relies on activation of neutrophils rather than inhibition of their suppressive effects. Moreover, it is capable of inducing eradication of multiple tumor types in immunocompetent mice, it is effective when therapy is initiated after tumors are already established, and it can reduce metastasis. Importantly, the same combination of therapeutic components that eradicates tumors in mice activates human neutrophils to kill tumors *in vitro*, suggesting that the therapy has the potential to prove effective in patients.

The identification of C5a and LTB_4 as crucial mediators of tumor clearance in this mechanism is noteworthy, as previous studies have shown that these molecules generally promote cancer. Signaling through the C5a-C5AR1 axis recruits granulocytes and MDSCs to the tumor, stimulates secretion of immunosuppressive factors by these and other tumor-resident myeloid cells, and results in inhibition of T cell responses.[49,52–56] Similarly, LTB_4 can promote tumor growth by recruiting suppressive neutrophils and MDSCs to the tumor,[57–59] and neutrophil-derived leukotrienes can support metastasis.[10]

However, in non-cancer contexts, C5a and LTB_4 are potent inflammatory mediators that can induce neutrophil activation and ROS-mediated tissue damage. AP activation on the neutrophil surface can produce high local concentrations of C5a, inducing neutrophil activation and extravasation into inflamed tissue.[60,61] LTB_4 promotes neutrophil ''swarming'' in the tissue and vasculature, amplifying neutrophil activation, inflammation, and tissue damage.[62–64] Elements of the mechanism we describe, such as AP-mediated complement activation, C5a-induced LTB_4 production by neutrophils, and C5a-dependent production of ROS by neutrophils and XO, can contribute to tissue damage in pathologies as diverse as inflammatory arthritis,[60,65–67] fungal sepsis,[63] and acute lung injury.[68]

The immunotherapeutic strategy used in this study likely taps into the neutrophil's capacity for potent cytotoxic activation that results in tissue damage in the context of these inflammatory pathologies. Although dysregulated inflammation in the tumor can induce pathological activation of neutrophils through chronic exposure to factors such as C5a and LTB_4, our work demonstrates that these inflammatory mediators have the capacity to drive tumor-eradicating neutrophil responses if applied with the appropriate threshold and context. Although inhibitors of C5AR1, LTB_4 production, and BLT1 have been evaluated as cancer treatments,[49,59] our work here suggests an alternative approach by which these pathways can be exploited to direct neutrophil cytotoxic responses against the tumor.

Even though this mechanism of neutrophil-mediated tumor clearance is not dependent on adaptive immunity, it can still prime immune memory. Neutrophil-activating therapy induced activation of DC populations, and we have shown previously that treatment with tumor-binding antibody in an immunostimulatory context induces tumor antigen uptake by APCs and priming of T cells.[69,70] We observed activation, proliferation, and memory differentiation of T cells in the blood and dLN following neutrophil-activating therapy, and mice were protected from rechallenge with the same tumor. As such, combination with T cell-targeted treatments such as immune checkpoint blockade represents an attractive avenue for future study with the potential to further enhance therapeutic efficacy. Moreover, the ability of our neutrophil-activating approach to induce an inflammatory cascade resulting in large-scale neutrophil infiltration and cytotoxicity within the tumor may help overcome barriers to the efficacy of immune checkpoint blockade, such as ''cold'' tumors with poor T cell infiltration.[71] Additionally, although tumors could downregulate the antibody target antigen in response to therapy, as ADCC contributes to, but is not required for, tumor clearance, neutrophil-activating therapy is likely to be robust against acquired resistance that can limit the efficacy of other monoclonal antibody therapies.

This study lays the groundwork for a neutrophil-activating approach to cancer therapy with the potential to both reverse neutrophil-mediated immunosuppression and activate anti-cancer immunity. As neutrophils are numerous, plastic, and can amplify their own activation and recruitment, strategies to harness their potential to function as anti-cancer effector cells are an attractive option, and attempts to deplete or inhibit suppressive neutrophil populations may squander this powerful anti-cancer capacity. The present study defines therapeutic conditions and an *in vivo* mechanism by which neutrophils can be exploited to induce potent tumor eradication. Future work can build upon the data presented here to rationally design cancer therapies beyond the combination of agents used in this study.

Limitations of the study

This study raises some questions that should be addressed prior to potential clinical translation. First, the metastasis models were treated at time points shortly after the initiation of metastatic seeding,[72] so future work will be necessary to determine whether neutrophil-activating therapy can eliminate established metastases or whether inhibition of metastatic seeding is the primary anti-metastatic effect. Additionally, although blood chemistries and body weight were normal one week and 60 days following completion of treatment in mice, we did not perform a thorough analysis of the safety and tolerability of our therapy, which will be necessary prior to clinical translation. In this regard, systemically infused TNF has a history of toxicity in cancer patients,[73] although we used an intratumoral treatment approach that should reduce systemic exposure to the injected agents. On the other hand, although the intratumoral treatment approach was highly effective, it limits the use of this therapy to accessible

(C) Cell surface markers on neutrophils from the peripheral blood of healthy human donors following stimulation with the indicated components for 30 min (ICAM-1, n = 6; others, n = 8).

(D and E) Lysis of A549 cells co-cultured with neutrophils isolated from healthy donor peripheral blood and stimulated *in vitro* with the indicated components (n = 4).

Statistics: log-rank test with Bonferroni correction (A and B), one-way ANOVA with Tukey's multiple-comparisons test (C), two-way ANOVA with Tukey's multiple-comparisons test (D and E). For all dot plots, the line indicates the mean. Data are representative of 2 independent experiments (D and E) or pooled from 2 (B and C) or 3 (A) experiments.

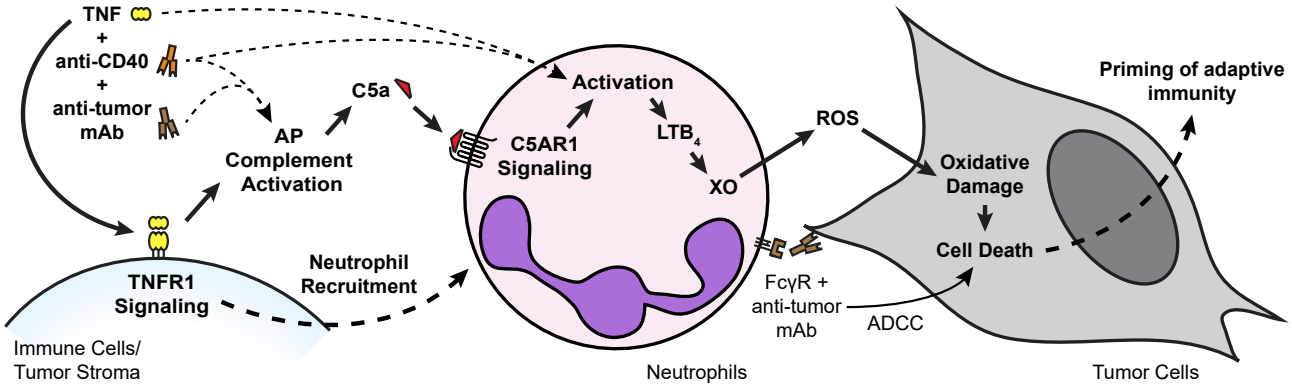

Figure 8. Proposed mechanism of neutrophil-dependent tumor eradication

Treatment with neutrophil-activating therapy recruits neutrophils to the tumor through TNFR1 signaling and activates the complement AP, generating C5a. C5a signals through C5AR1 in neutrophils and induces neutrophil activation and production of LTB_4, which drives XO activity in the tumor environment. ROS produced by XO induce oxidative damage and death in tumor cells, driving tumor clearance. Tumor-binding antibody contributes to neutrophil killing of tumor cells by inducing ADCC, possibly involving trogocytosis. Although not dependent on adaptive immunity, this process is capable of priming protective immune memory.

tumors. Future work to develop systemic tumor-targeted delivery methods such as antibody conjugates and nanoparticles may broaden the applicability and utility of neutrophil-activating therapy.

STAR★METHODS

Detailed methods are provided in the online version of this paper and include the following:

- KEY RESOURCES TABLE
- RESOURCE AVAILABILITY
  - Lead contact
  - Material availability
  - Data code and availability
- EXPERIMENTAL MODEL AND SUBJECT DETAILS
  - Animals
  - Cell lines and culture
  - Human blood
- METHOD DETAILS
  - Tumor implantation, treatment, and survival
  - Blood chemistry
  - Mouse *in vitro* cytotoxicity studies
  - Depletion and inhibition studies
  - Metastasis studies
  - Knockout of TNFR1 in B16 using CRISPR-Cas9
  - B16-EGFP
  - Flow cytometry
  - May-Grünwald-Giemsa staining
  - Immunofluorescence
  - LTB_4 ELISA
  - *Ex vivo* neutrophil LTB_4 assay
  - Mouse *in vitro* neutrophil stimulations
  - Determination of oxidized glutathione content
  - XO assay
  - ROS assays
  - Human neutrophil studies
- QUANTIFICATION AND STATISTICAL ANALYSIS
  - Statistics

SUPPLEMENTAL INFORMATION

Supplemental information can be found online at https://doi.org/10.1016/j.ccell.2023.01.002.

ACKNOWLEDGEMENTS

We thank Hannah Wastyk, Raghav Kumar, and Tyler Zhang for experimental assistance; Okmi Choi and Nancy Wu for expert technical support; Sameera Kongara for critical evaluation of the manuscript; and all members of the Engleman lab for helpful discussions. This work was supported by NIH grants U54 CA209971 (E.G.E.), R01 CA222969 (E.G.E.), R01 CA233958 (E.G.E.), P01 CA244114 (E.G.E.), R01 AI085596 (W.-C.S.), R01 AI117410 (W.-C.S.), R01 AI146162 (W.-C.S.), F31 CA196029 (I.L.L.), F30 CA196145 (T.R.P.), T32 HL120824 (G.P.), and F32 CA189408 (N.E.R.-F.).

AUTHOR CONTRIBUTIONS

Conceptualization, I.L.L. and T.R.P.; Methodology, I.L.L. and T.R.P.; Investigation, I.L.L., T.R.P., J.Q., G.P., M.H.L., X.Z., L.S., N.E.R.-F., D.K.-C.C., L.Y.S., and S.V.D.; Resources, L.L.T. and W.-C.S.; Writing – Original Draft, I.L.L.; Writing – Review & Editing, I.L.L., T.R.P., J.Q., G.P., N.E.R.-F., M.H.L., W.-C.S., and E.G.E.; Funding Acquisition, E.G.E.; Supervision, E.G.E.

DECLARATION OF INTERESTS

I.L.L., T.R.P., and E.G.E. are co-inventors on a patent application filed by Stanford University related to this work. W.-C.S. owns equity in, receives a consultant fee and research grant from, and is an inventor of patents licensed to Kira Pharmaceuticals and Aevitas Therapeutics. The other authors declare no competing interests.

Received: December 1, 2021
Revised: November 2, 2022
Accepted: January 5, 2023
Published: January 26, 2023

REFERENCES

1. Coffelt, S.B., Wellenstein, M.D., and de Visser, K.E. (2016). Neutrophils in cancer: neutral no more. Nat. Rev. Cancer *16*, 431–446. https://doi.org/10.1038/nrc.2016.52.
2. Jaillon, S., Ponzetta, A., Di Mitri, D., Santoni, A., Bonecchi, R., and Mantovani, A. (2020). Neutrophil diversity and plasticity in tumour progression and therapy. Nat. Rev. Cancer *20*, 485–503. https://doi.org/10.1038/s41568-020-0281-y.

3. Mantovani, A., Cassatella, M.A., Costantini, C., and Jaillon, S. (2011). Neutrophils in the activation and regulation of innate and adaptive immunity. Nat. Rev. Immunol. *11*, 519–531. https://doi.org/10.1038/nri3024.

4. Gentles, A.J., Newman, A.M., Liu, C.L., Bratman, S.V., Feng, W., Kim, D., Nair, V.S., Xu, Y., Khuong, A., Hoang, C.D., et al. (2015). The prognostic landscape of genes and infiltrating immune cells across human cancers. Nat. Med. *21*, 938–945. https://doi.org/10.1038/nm.3909.

5. Shaul, M.E., and Fridlender, Z.G. (2019). Tumour-associated neutrophils in patients with cancer. Nat. Rev. Clin. Oncol. *16*, 601–620. https://doi.org/10.1038/s41571-019-0222-4.

6. Pekarek, L.A., Starr, B.A., Toledano, A.Y., and Schreiber, H. (1995). Inhibition of tumor growth by elimination of granulocytes. J. Exp. Med. *181*, 435–440. https://doi.org/10.1084/jem.181.1.435.

7. Jablonska, J., Leschner, S., Westphal, K., Lienenklaus, S., and Weiss, S. (2010). Neutrophils responsive to endogenous IFN-β regulate tumor angiogenesis and growth in a mouse tumor model. J. Clin. Invest. *120*, 1151–1164. https://doi.org/10.1172/JCI37223.

8. Nozawa, H., Chiu, C., and Hanahan, D. (2006). Infiltrating neutrophils mediate the initial angiogenic switch in a mouse model of multistage carcinogenesis. Proc. Natl. Acad. Sci. USA *103*, 12493–12498. https://doi.org/10.1073/pnas.0601807103.

9. Coffelt, S.B., Kersten, K., Doornebal, C.W., Weiden, J., Vrijland, K., Hau, C.-S., Verstegen, N.J.M., Ciampricotti, M., Hawinkels, L.J.A.C., Jonkers, J., and de Visser, K.E. (2015). IL-17-producing γδ T cells and neutrophils conspire to promote breast cancer metastasis. Nature *522*, 345–348. https://doi.org/10.1038/nature14282.

10. Wculek, S.K., and Malanchi, I. (2015). Neutrophils support lung colonization of metastasis-initiating breast cancer cells. Nature *528*, 413–417. https://doi.org/10.1038/nature16140.

11. Szczerba, B.M., Castro-Giner, F., Vetter, M., Krol, I., Gkountela, S., Landin, J., Scheidmann, M.C., Donato, C., Scherrer, R., Singer, J., et al. (2019). Neutrophils escort circulating tumour cells to enable cell cycle progression. Nature *566*, 553–557. https://doi.org/10.1038/s41586-019-0915-y.

12. Schmielau, J., and Finn, O.J. (2001). Activated granulocytes and granulocyte-derived hydrogen peroxide are the underlying mechanism of suppression of t-cell function in advanced cancer patients. Cancer Res. *61*, 4756–4760.

13. Mishalian, I., Bayuh, R., Eruslanov, E., Michaeli, J., Levy, L., Zolotarov, L., Singhal, S., Albelda, S.M., Granot, Z., and Fridlender, Z.G. (2014). Neutrophils recruit regulatory T-cells into tumors via secretion of CCL17—a new mechanism of impaired antitumor immunity. Int. J. Cancer *135*, 1178–1186. https://doi.org/10.1002/ijc.28770.

14. Veglia, F., Sanseviero, E., and Gabrilovich, D.I. (2021). Myeloid-derived suppressor cells in the era of increasing myeloid cell diversity. Nat. Rev. Immunol. *21*, 485–498. https://doi.org/10.1038/s41577-020-00490-y.

15. Kusmartsev, S., Nefedova, Y., Yoder, D., and Gabrilovich, D.I. (2004). Antigen-specific inhibition of $CD8^+$ T cell response by immature myeloid cells in cancer is mediated by reactive oxygen species. J. Immunol. *172*, 989–999. https://doi.org/10.4049/jimmunol.172.2.989.

16. Youn, J.-I., Nagaraj, S., Collazo, M., and Gabrilovich, D.I. (2008). Subsets of myeloid-derived suppressor cells in tumor-bearing mice. J. Immunol. *181*, 5791–5802. https://doi.org/10.4049/jimmunol.181.8.5791.

17. Clark, R.A., and Klebanoff, S.J. (1975). Neutrophil-mediated tumor cell cytotoxicity: role of the peroxidase system. J. Exp. Med. *141*, 1442–1447. https://doi.org/10.1084/jem.141.6.1442.

18. Blaisdell, A., Crequer, A., Columbus, D., Daikoku, T., Mittal, K., Dey, S.K., and Erlebacher, A. (2015). Neutrophils oppose uterine epithelial carcinogenesis via debridement of hypoxic tumor cells. Cancer Cell *28*, 785–799. https://doi.org/10.1016/j.ccell.2015.11.005.

19. Eruslanov, E.B., Bhojnagarwala, P.S., Quatromoni, J.G., Stephen, T.L., Ranganathan, A., Deshpande, C., Akimova, T., Vachani, A., Litzky, L., Hancock, W.W., et al. (2014). Tumor-associated neutrophils stimulate T cell responses in early-stage human lung cancer. J. Clin. Invest. *124*, 5466–5480. https://doi.org/10.1172/jci77053.

20. Singhal, S., Bhojnagarwala, P.S., O'Brien, S., Moon, E.K., Garfall, A.L., Rao, A.S., Quatromoni, J.G., Stephen, T.L., Litzky, L., Deshpande, C., et al. (2016). Origin and role of a subset of tumor-associated neutrophils with antigen-presenting cell features in early-stage human lung cancer. Cancer Cell *30*, 120–135. https://doi.org/10.1016/j.ccell.2016.06.001.

21. Ponzetta, A., Carriero, R., Carnevale, S., Barbagallo, M., Molgora, M., Perucchini, C., Magrini, E., Gianni, F., Kunderfranco, P., Polentarutti, N., et al. (2019). Neutrophils driving unconventional T cells mediate resistance against murine sarcomas and selected human tumors. Cell *178*, 346–360.e24. https://doi.org/10.1016/j.cell.2019.05.047.

22. Costanzo-Garvey, D.L., Keeley, T., Case, A.J., Watson, G.F., Alsamraae, M., Yu, Y., Su, K., Heim, C.E., Kielian, T., Morrissey, C., et al. (2020). Neutrophils are mediators of metastatic prostate cancer progression in bone. Cancer immunology, immunotherapy. Cancer Immunol. Immunother. *69*, 1113–1130. https://doi.org/10.1007/s00262-020-02527-6.

23. Granot, Z., Henke, E., Comen, E.A., King, T.A., Norton, L., and Benezra, R. (2011). Tumor entrained neutrophils inhibit seeding in the premetastatic lung. Cancer Cell *20*, 300–314. https://doi.org/10.1016/j.ccr.2011.08.012.

24. Fridlender, Z.G., Sun, J., Kim, S., Kapoor, V., Cheng, G., Ling, L., Worthen, G.S., and Albelda, S.M. (2009). Polarization of tumor-associated neutrophil phenotype by TGF-beta: "N1" versus "N2" TAN. Cancer Cell *16*, 183–194. https://doi.org/10.1016/j.ccr.2009.06.017.

25. Veglia, F., Tyurin, V.A., Blasi, M., De Leo, A., Kossenkov, A.V., Donthireddy, L., To, T.K.J., Schug, Z., Basu, S., Wang, F., et al. (2019). Fatty acid transport protein 2 reprograms neutrophils in cancer. Nature *569*, 73–78. https://doi.org/10.1038/s41586-019-1118-2.

26. Yang, J., Kumar, A., Vilgelm, A.E., Chen, S.-C., Ayers, G.D., Novitskiy, S.V., Joyce, S., and Richmond, A. (2018). Loss of CXCR4 in myeloid cells enhances antitumor immunity and reduces melanoma growth through NK cell and FASL mechanisms. Cancer Immunol. Res. *6*, 1186–1198. https://doi.org/10.1158/2326-6066.Cir-18-0045.

27. Sagiv, J.Y., Michaeli, J., Assi, S., Mishalian, I., Kisos, H., Levy, L., Damti, P., Lumbroso, D., Polyansky, L., Sionov, R.V., et al. (2015). Phenotypic diversity and plasticity in circulating neutrophil subpopulations in cancer. Cell Rep. *10*, 562–573. https://doi.org/10.1016/j.celrep.2014.12.039.

28. Steele, C.W., Karim, S.A., Leach, J.D.G., Bailey, P., Upstill-Goddard, R., Rishi, L., Foth, M., Bryson, S., McDaid, K., Wilson, Z., et al. (2016). CXCR2 inhibition profoundly suppresses metastases and augments immunotherapy in pancreatic ductal adenocarcinoma. Cancer Cell *29*, 832–845. https://doi.org/10.1016/j.ccell.2016.04.014.

29. Acharyya, S., Oskarsson, T., Vanharanta, S., Malladi, S., Kim, J., Morris, P.G., Manova-Todorova, K., Leversha, M., Hogg, N., Seshan, V.E., et al. (2012). A CXCL1 paracrine network links cancer chemoresistance and metastasis. Cell *150*, 165–178. https://doi.org/10.1016/j.cell.2012.04.042.

30. Pylaeva, E., Harati, M.D., Spyra, I., Bordbari, S., Strachan, S., Thakur, B.K., Höing, B., Franklin, C., Skokowa, J., Welte, K., et al. (2019). NAMPT signaling is critical for the proangiogenic activity of tumor-associated neutrophils. Int. J. Cancer *144*, 136–149. https://doi.org/10.1002/ijc.31808.

31. Shrestha, S., Noh, J.M., Kim, S.-Y., Ham, H.-Y., Kim, Y.-J., Yun, Y.-J., Kim, M.-J., Kwon, M.-S., Song, D.-K., and Hong, C.-W. (2016). Angiotensin converting enzyme inhibitors and angiotensin II receptor antagonist attenuate tumor growth via polarization of neutrophils toward an antitumor phenotype. Oncoimmunology *5*, e1067744. https://doi.org/10.1080/2162402X.2015.1067744.

32. Matlung, H.L., Babes, L., Zhao, X.W., van Houdt, M., Treffers, L.W., van Rees, D.J., Franke, K., Schornagel, K., Verkuijlen, P., Janssen, H., et al. (2018). Neutrophils kill antibody-opsonized cancer cells by trogoptosis. Cell Rep. *23*, 3946–3959.e6. https://doi.org/10.1016/j.celrep.2018.05.082.

33. Albanesi, M., Mancardi, D.A., Jönsson, F., Iannascoli, B., Fiette, L., Di Santo, J.P., Lowell, C.A., and Bruhns, P. (2013). Neutrophils mediate antibody-induced antitumor effects in mice. Blood *122*, 3160–3164. https://doi.org/10.1182/blood-2013-04-497446.

34. Miralda, I., Uriarte, S.M., and McLeish, K.R. (2017). Multiple phenotypic changes define neutrophil priming. Front. Cell. Infect. Microbiol. *7*, 217. https://doi.org/10.3389/fcimb.2017.00217.

35. Woodfin, A., Beyrau, M., Voisin, M.-B., Ma, B., Whiteford, J.R., Hordijk, P.L., Hogg, N., and Nourshargh, S. (2016). ICAM-1-expressing neutrophils exhibit enhanced effector functions in murine models of endotoxemia. Blood *127*, 898–907. https://doi.org/10.1182/blood-2015-08-664995.

36. Condliffe, A.M., Chilvers, E.R., Haslett, C., and Dransfield, I. (1996). Priming differentially regulates neutrophil adhesion molecule expression/function. Immunology *89*, 105–111. https://doi.org/10.1046/j.1365-2567.1996.d01-711.x.

37. Khan, S.Y., Kelher, M.R., Heal, J.M., Blumberg, N., Boshkov, L.K., Phipps, R., Gettings, K.F., McLaughlin, N.J., and Silliman, C.C. (2006). Soluble CD40 ligand accumulates in stored blood components, primes neutrophils through CD40, and is a potential cofactor in the development of transfusion-related acute lung injury. Blood *108*, 2455–2462. https://doi.org/10.1182/blood-2006-04-017251.

38. Evrard, M., Kwok, I.W.H., Chong, S.Z., Teng, K.W.W., Becht, E., Chen, J., Sieow, J.L., Penny, H.L., Ching, G.C., Devi, S., et al. (2018). Developmental analysis of bone marrow neutrophils reveals populations specialized in expansion, trafficking, and effector functions. Immunity *48*, 364–379.e8. https://doi.org/10.1016/j.immuni.2018.02.002.

39. Kwok, I., Becht, E., Xia, Y., Ng, M., Teh, Y.C., Tan, L., Evrard, M., Li, J.L.Y., Tran, H.T.N., Tan, Y., et al. (2020). Combinatorial single-cell analyses of granulocyte-monocyte progenitor heterogeneity reveals an early uni-potent neutrophil progenitor. Immunity *53*, 303–318.e5. https://doi.org/10.1016/j.immuni.2020.06.005.

40. Challen, G.A., Boles, N., Lin, K.K.Y., and Goodell, M.A. (2009). Mouse hematopoietic stem cell identification and analysis. Cytometry A. *75*, 14–24. https://doi.org/10.1002/cyto.a.20674.

41. Zhou, G., Peng, K., Song, Y., Yang, W., Shu, W., Yu, T., Yu, L., Lin, M., Wei, Q., Chen, C., et al. (2018). CD177+ neutrophils suppress epithelial cell tumourigenesis in colitis-associated cancer and predict good prognosis in colorectal cancer. Carcinogenesis *39*, 272–282. https://doi.org/10.1093/carcin/bgx142.

42. Engblom, C., Pfirschke, C., Zilionis, R., Da Silva Martins, J., Bos, S.A., Courties, G., Rickelt, S., Severe, N., Baryawno, N., Faget, J., et al. (2017). Osteoblasts remotely supply lung tumors with cancer-promoting SiglecF(high) neutrophils. Science *358*, eaal5081. https://doi.org/10.1126/science.aal5081.

43. Veglia, F., Hashimoto, A., Dweep, H., Sanseviero, E., De Leo, A., Tcyganov, E., Kossenkov, A., Mulligan, C., Nam, B., Masters, G., et al. (2021). Analysis of classical neutrophils and polymorphonuclear myeloid-derived suppressor cells in cancer patients and tumor-bearing mice. J. Exp. Med. *218*, e20201803. https://doi.org/10.1084/jem.20201803.

44. Yajuk, O., Baron, M., Toker, S., Zelter, T., Fainsod-Levi, T., and Granot, Z. (2021). The PD-L1/PD-1 Axis blocks neutrophil cytotoxicity in cancer. Cells *10*, 1510.

45. Gavillet, M., Martinod, K., Renella, R., Harris, C., Shapiro, N.I., Wagner, D.D., and Williams, D.A. (2015). Flow cytometric assay for direct quantification of neutrophil extracellular traps in blood samples. Am. J. Hematol. *90*, 1155–1158. https://doi.org/10.1002/ajh.24185.

46. Herndler-Brandstetter, D., Ishigame, H., Shinnakasu, R., Plajer, V., Stecher, C., Zhao, J., Lietzenmayer, M., Kroehling, L., Takumi, A., Kometani, K., et al. (2018). KLRG1+ effector CD8+ T cells lose KLRG1, differentiate into all memory T cell lineages, and convey enhanced protective immunity. Immunity *48*, 716–729.e8. https://doi.org/10.1016/j.immuni.2018.03.015.

47. Dunkelberger, J.R., and Song, W.C. (2010). Complement and its role in innate and adaptive immune responses. Cell Res. *20*, 34–50. https://doi.org/10.1038/cr.2009.139.

48. Brandt, S.L., and Serezani, C.H. (2017). Too much of a good thing: how modulating LTB(4) actions restore host defense in homeostasis or disease. Semin. Immunol. *33*, 37–43. https://doi.org/10.1016/j.smim.2017.08.006.

49. Roumenina, L.T., Daugan, M.V., Petitprez, F., Sautès-Fridman, C., and Fridman, W.H. (2019). Context-dependent roles of complement in cancer. Nat. Rev. Cancer *19*, 698–715. https://doi.org/10.1038/s41568-019-0210-0.

50. Battelli, M.G., Polito, L., Bortolotti, M., and Bolognesi, A. (2016). Xanthine oxidoreductase in cancer: more than a differentiation marker. Cancer Med. *5*, 546–557. https://doi.org/10.1002/cam4.601.

51. Wang, Y., Wu, J., Newton, R., Bahaie, N.S., Long, C., and Walcheck, B. (2013). ADAM17 cleaves CD16b (FcγRIIIb) in human neutrophils. Biochim. Biophys. Acta *1833*, 680–685. https://doi.org/10.1016/j.bbamcr.2012.11.027.

52. Ajona, D., Ortiz-Espinosa, S., Moreno, H., Lozano, T., Pajares, M.J., Agorreta, J., Bértolo, C., Lasarte, J.J., Vicent, S., Hoehlig, K., et al. (2017). A combined PD-1/C5a blockade synergistically protects against lung cancer growth and metastasis. Cancer Discov. *7*, 694–703. https://doi.org/10.1158/2159-8290.Cd-16-1184.

53. Corrales, L., Ajona, D., Rafail, S., Lasarte, J.J., Riezu-Boj, J.I., Lambris, J.D., Rouzaut, A., Pajares, M.J., Montuenga, L.M., and Pio, R. (2012). Anaphylatoxin C5a creates a favorable microenvironment for lung cancer progression. J. Immunol. *189*, 4674–4683. https://doi.org/10.4049/jimmunol.1201654.

54. Vadrevu, S.K., Chintala, N.K., Sharma, S.K., Sharma, P., Cleveland, C., Riediger, L., Manne, S., Fairlie, D.P., Gorczyca, W., Almanza, O., et al. (2014). Complement c5a receptor facilitates cancer metastasis by altering T-cell responses in the metastatic niche. Cancer Res. *74*, 3454–3465. https://doi.org/10.1158/0008-5472.Can-14-0157.

55. Piao, C., Cai, L., Qiu, S., Jia, L., Song, W., and Du, J. (2015). Complement 5a enhances hepatic metastases of colon cancer via monocyte chemoattractant protein-1-mediated inflammatory cell infiltration. J. Biol. Chem. *290*, 10667–10676. https://doi.org/10.1074/jbc.M114.612622.

56. Markiewski, M.M., DeAngelis, R.A., Benencia, F., Ricklin-Lichtsteiner, S.K., Koutoulaki, A., Gerard, C., Coukos, G., and Lambris, J.D. (2008). Modulation of the antitumor immune response by complement. Nat. Immunol. *9*, 1225–1235. https://doi.org/10.1038/ni.1655.

57. Satpathy, S.R., Jala, V.R., Bodduluri, S.R., Krishnan, E., Hegde, B., Hoyle, G.W., Fraig, M., Luster, A.D., and Haribabu, B. (2015). Crystalline silica-induced leukotriene B4-dependent inflammation promotes lung tumour growth. Nat. Commun. *6*, 7064. https://doi.org/10.1038/ncomms8064.

58. Yokota, Y., Inoue, H., Matsumura, Y., Nabeta, H., Narusawa, M., Watanabe, A., Sakamoto, C., Hijikata, Y., Iga-Murahashi, M., Takayama, K., et al. (2012). Absence of LTB4/BLT1 axis facilitates generation of mouse GM-CSF-induced long-lasting antitumor immunologic memory by enhancing innate and adaptive immune systems. Blood *120*, 3444–3454. https://doi.org/10.1182/blood-2011-10-383240.

59. Tian, W., Jiang, X., Kim, D., Guan, T., Nicolls, M.R., and Rockson, S.G. (2020). Leukotrienes in tumor-associated inflammation. Front. Pharmacol. *11*, 1289. https://doi.org/10.3389/fphar.2020.01289.

60. Akk, A., Springer, L.E., Yang, L., Hamilton-Burdess, S., Lambris, J.D., Yan, H., Hu, Y., Wu, X., Hourcade, D.E., Miller, M.J., and Pham, C.T.N. (2019). Complement activation on neutrophils initiates endothelial adhesion and extravasation. Mol. Immunol. *114*, 629–642. https://doi.org/10.1016/j.molimm.2019.09.011.

61. Camous, L., Roumenina, L., Bigot, S., Brachemi, S., Frémeaux-Bacchi, V., Lesavre, P., and Halbwachs-Mecarelli, L. (2011). Complement alternative pathway acts as a positive feedback amplification of neutrophil activation. Blood *117*, 1340–1349. https://doi.org/10.1182/blood-2010-05-283564.

62. Lämmermann, T., Afonso, P.V., Angermann, B.R., Wang, J.M., Kastenmüller, W., Parent, C.A., and Germain, R.N. (2013). Neutrophil swarms require LTB4 and integrins at sites of cell death in vivo. Nature *498*, 371–375. https://doi.org/10.1038/nature12175.

63. Lee, E.K.S., Gillrie, M.R., Li, L., Arnason, J.W., Kim, J.H., Babes, L., Lou, Y., Sanati-Nezhad, A., Kyei, S.K., Kelly, M.M., et al. (2018). Leukotriene B4-mediated neutrophil recruitment causes pulmonary capillaritis during lethal fungal sepsis. Cell Host Microbe *23*, 121–133.e4. https://doi.org/10.1016/j.chom.2017.11.009.

64. Uderhardt, S., Martins, A.J., Tsang, J.S., Lämmermann, T., and Germain, R.N. (2019). Resident macrophages cloak tissue microlesions to prevent neutrophil-driven inflammatory damage. Cell *177*, 541–555.e17. https://doi.org/10.1016/j.cell.2019.02.028.

65. Sadik, C.D., Kim, N.D., Iwakura, Y., and Luster, A.D. (2012). Neutrophils orchestrate their own recruitment in murine arthritis through C5aR and FcγR signaling. Proc. Natl. Acad. Sci. USA *109*, E3177–E3185. https://doi.org/10.1073/pnas.1213797109.

66. Kim, N.D., Chou, R.C., Seung, E., Tager, A.M., and Luster, A.D. (2006). A unique requirement for the leukotriene B4 receptor BLT1 for neutrophil recruitment in inflammatory arthritis. J. Exp. Med. *203*, 829–835. https://doi.org/10.1084/jem.20052349.

67. Kimura, Y., Zhou, L., Miwa, T., and Song, W.-C. (2010). Genetic and therapeutic targeting of properdin in mice prevents complement-mediated tissue injury. J. Clin. Invest. *120*, 3545–3554. https://doi.org/10.1172/JCI41782.

68. Kubo, H., Morgenstern, D., Quinian, W.M., Ward, P.A., Dinauer, M.C., and Doerschuk, C.M. (1996). Preservation of complement-induced lung injury in mice with deficiency of NADPH oxidase. J. Clin. Invest. *97*, 2680–2684. https://doi.org/10.1172/jci118718.

69. Carmi, Y., Spitzer, M.H., Linde, I.L., Burt, B.M., Prestwood, T.R., Perlman, N., Davidson, M.G., Kenkel, J.A., Segal, E., Pusapati, G.V., et al. (2015). Allogeneic IgG combined with dendritic cell stimuli induce antitumour T-cell immunity. Nature *521*, 99–104. https://doi.org/10.1038/nature14424.

70. Spitzer, M.H., Carmi, Y., Reticker-Flynn, N.E., Kwek, S.S., Madhireddy, D., Martins, M.M., Gherardini, P.F., Prestwood, T.R., Chabon, J., Bendall, S.C., et al. (2017). Systemic immunity is required for effective cancer immunotherapy. Cell *168*, 487–502.e15. https://doi.org/10.1016/j.cell.2016.12.022.

71. Bonaventura, P., Shekarian, T., Alcazer, V., Valladeau-Guilemond, J., Valsesia-Wittmann, S., Amigorena, S., Caux, C., and Depil, S. (2019). Cold tumors: a therapeutic challenge for immunotherapy. Front. Immunol. *10*, 168. https://doi.org/10.3389/fimmu.2019.00168.

72. Arroyo-Crespo, J.J., Armiñán, A., Charbonnier, D., Deladriere, C., Palomino-Schätzlein, M., Lamas-Domingo, R., Forteza, J., Pineda-Lucena, A., and Vicent, M.J. (2019). Characterization of triple-negative breast cancer preclinical models provides functional evidence of metastatic progression. Int. J. Cancer *145*, 2267–2281. https://doi.org/10.1002/ijc.32270.

73. Roberts, N.J., Zhou, S., Diaz, L.A., Jr., and Holdhoff, M. (2011). Systemic use of tumor necrosis factor alpha as an anticancer agent. Oncotarget *2*, 739–751. https://doi.org/10.18632/oncotarget.344.

74. Miwa, T., Sato, S., Gullipalli, D., Nangaku, M., and Song, W.-C. (2013). Blocking properdin, the alternative pathway, and anaphylatoxin receptors ameliorates renal ischemia-reperfusion injury in decay-accelerating factor and CD59 double-knockout mice. J. Immunol. *190*, 3552–3559. https://doi.org/10.4049/jimmunol.1202275.

75. Ueda, Y., Miwa, T., Ito, D., Kim, H., Sato, S., Gullipalli, D., Zhou, L., Golla, M., Song, D., Dunaief, J.L., et al. (2019). Differential contribution of C5aR and C5b-9 pathways to renal thrombic microangiopathy and macrovascular thrombosis in mice carrying an atypical hemolytic syndrome-related factor H mutation. Kidney Int. *96*, 67–79. https://doi.org/10.1016/j.kint.2019.01.009.

76. Ran, F.A., Hsu, P.D., Wright, J., Agarwala, V., Scott, D.A., and Zhang, F. (2013). Genome engineering using the CRISPR-Cas9 system. Nat. Protoc. *8*, 2281–2308. https://doi.org/10.1038/nprot.2013.143.

77. Sato, T., Vries, R.G., Snippert, H.J., van de Wetering, M., Barker, N., Stange, D.E., van Es, J.H., Abo, A., Kujala, P., Peters, P.J., and Clevers, H. (2009). Single Lgr5 stem cells build crypt-villus structures in vitro without a mesenchymal niche. Nature *459*, 262–265. https://doi.org/10.1038/nature07935.

78. Sjögren, J., Lood, R., and Nägeli, A. (2020). On enzymatic remodeling of IgG glycosylation; unique tools with broad applications. Glycobiology *30*, 254–267. https://doi.org/10.1093/glycob/cwz085.

79. Van den Berg, C.W., Aerts, P.C., and Van Dijk, H. (1991). In vivo anti-complementary activities of the cobra venom factors from Naja naja and Naja haje. J. Immunol. Methods *136*, 287–294. https://doi.org/10.1016/0022-1759(91)90015-8.

80. Paschall, A.V., and Liu, K. (2016). An orthotopic mouse model of spontaneous breast cancer metastasis. J. Vis. Exp. https://doi.org/10.3791/54040.

81. Doench, J.G., Fusi, N., Sullender, M., Hegde, M., Vaimberg, E.W., Donovan, K.F., Smith, I., Tothova, Z., Wilen, C., Orchard, R., et al. (2016). Optimized sgRNA design to maximize activity and minimize off-target effects of CRISPR-Cas9. Nat. Biotechnol. *34*, 184–191. https://doi.org/10.1038/nbt.3437.

STAR★METHODS

KEY RESOURCES TABLE

REAGENT or RESOURCE	SOURCE	IDENTIFIER
Antibodies		
BUV395 anti-CD45	BD Biosciences	Cat# 564279; RRID: AB_2651134
BV421 anti-ICAM-1	BioLegend	Cat# 116141; RRID: AB_2876428
BV480 anti-MHC II	BD Biosciences	Cat# 566086; RRID: AB_2869739
BV650 anti-CD11b	BioLegend	Cat# 101259; RRID: AB_2566568
PE-Cy7 anti-Ly6G	BioLegend	Cat# 127618; RRID: AB_1877261
PE anti-C3	Novus Biologicals	Cat# NB200-540PE
AF647 anti-C3	Novus Biologicals	Cat# NB200-540AF647
APC-R700 anti-CD11c	BD Biosciences	Cat# 565872; RRID: AB_2744277
APC-Cy7 anti-Ly6C	BioLegend	Cat# 128026; RRID: AB_10640120
Purified anti-CD16/CD32	Bio X Cell	Cat# BE0307; RRID: AB_2736987
FITC anti-CD45	BioLegend	Cat# 103108; RRID: AB_312973
PE anti-Ly6G	BioLegend	Cat# 127608; RRID: AB_1186099
APC-Cy7 anti-CD11b	BioLegend	Cat# 101226; RRID: AB_830642
APC anti-TNFR1	BioLegend	Cat# 113006; RRID: AB_2208779
Purified anti-gp75	Bio X Cell	Cat# BE0151; RRID: AB_10949462
FITC anti-DNA/RNA damage	Abcam	Cat# ab183393
AF488 anti-FITC	ThermoFisher Scientific	Cat# A11096; RRID: AB_221558
APC-Fire 750 anti-CD11b	BioLegend	Cat# 101262; RRID: AB_2572122
FITC anti-ICAM-1	BioLegend	Cat# 353108; RRID: AB_10900254
BV711 anti-CD16	BioLegend	Cat# 302044; RRID: AB_2563802
BV786 anti-CD32	BD Biosciences	Cat# 564840; RRID: AB_2738978
AF647 anti-CD66b	BioLegend	Cat# 305110; RRID: AB_2563171
BV510 anti-CD63	BD Biosciences	Cat# 740182; RRID: AB_2739935
PE anti-C5AR1	BioLegend	Cat# 344304; RRID: AB_2067175
AF647 anti-CD177	BD Biosciences	Cat# 566599; RRID: AB_2869790
FITC anti-SIRPa	BioLegend	Cat# 144006; RRID: AB_11204425
BV480 anti-Siglec F	BD Biosciences	Cat# 746668; RRID: AB_2743940
PE-Cy7 anti-CD101	ThermoFisher Scientific	Cat# 25-1011-82; RRID: AB_2573378
APC-Cy7 anti-CD14	BioLegend	Cat# 123316; RRID: AB_10645329
BV711 anti-PD-L1	BioLegend	Cat# 124319; RRID: AB_2563619
APC anti-XCR1	BioLegend	Cat# 148206; RRID: AB_2563932
APC-Cy7 anti-F4/80	BioLegend	Cat# 123118; RRID: AB_893477
FITC anti-CD206	BioLegend	Cat# 141704; RRID: AB_10901166
PerCP-eF710 anti-CD80	ThermoFisher Scientific	Cat# 46-0801-82; RRID: AB_2573696
BUV737 anti-CD86	BD Biosciences	Cat# 741737; RRID: AB_2871107
BV421 anti-PD-L1	BioLegend	Cat# 124315; RRID: AB_10897097
BUV737 anti-Ly6G	BD Biosciences	Cat# 741813; RRID: AB_2871151
BV785 anti-Ly6C	BioLegend	Cat# 128041; RRID: AB_2565852
BV421 anti-TCRb	BioLegend	Cat# 109230; RRID: AB_2562562
PE-Cy7 anti-NK1.1	BioLegend	Cat# 108714; RRID: AB_389364
PE anti-KLRG1	BioLegend	Cat# 138408; RRID: AB_10574313
BV510 anti-CD8a	BioLegend	Cat# 100752; RRID: AB_2563057
BV711 anti-CD4	BioLegend	Cat# 100557; RRID: AB_2562607
B220 anti-BV711	BioLegend	Cat# 103255; RRID: AB_2563491

(*Continued on next page*)

Continued

REAGENT or RESOURCE	SOURCE	IDENTIFIER
AF488 anti-Foxp3	BD Biosciences	Cat# 560403; RRID: AB_1645192
BV650 anti-CD25	BioLegend	Cat# 102038; RRID: AB_2563060
PerCP-Cy5.5 anti-CD62L	BioLegend	Cat# 104432; RRID: AB_2285839
APC-eF780 anti-CD44	ThermoFisher Scientific	Cat# 47-0441-82; RRID: AB_1272244
BV785 anti-PD-1	BioLegend	Cat# 135225; RRID: AB_2563680
APC anti-CD69	BD Biosciences	Cat# 560689; RRID: AB_1727506
AF700 anti-Ki67	ThermoFisher Scientific	Cat# 56-5698-82; RRID: AB_2637480
eF450 anti-CD34	ThermoFisher Scientific	Cat# 48-0341-82; RRID: AB_2043837
AF700 anti-IL-7Ra	ThermoFisher Scientific	Cat# 56-1271-82; RRID: AB_657611
BV711 anti-Sca-1	BioLegend	Cat# 108131; RRID: AB_2562241
FITC anti-cKit	BD Biosciences	Cat# 553354; RRID: AB_394805
PE anti-CD16/32	BioLegend	Cat# 156606; RRID: AB_2800704
PE-Cy7 anti-CD3e	ThermoFisher Scientific	Cat# 25-0032-82; RRID: AB_2815096
PE-Cy7 anti-CD4	ThermoFisher Scientific	Cat# 25-0041-82; RRID: AB_469576
PE-Cy7 anti-CD8a	ThermoFisher Scientific	Cat# 25-0081-82; RRID: AB_469584
PE-Cy7 anti-CD11b	ThermoFisher Scientific	Cat# 25-0112-82; RRID: AB_469588
PE-Cy7 anti-B220	ThermoFisher Scientific	Cat# 25-0452-82; RRID: AB_469627
APC anti-Flt3	BioLegend	Cat# 135310; RRID: AB_2107050
Pacific Blue anti-CD106	BioLegend	Cat# 105722; RRID: AB_2304290
PE-Cy5 anti-Ly6G	ThermoFisher Scientific	Cat# 15-9668-82; RRID: AB_2811754
PerCP-Cy5.5 anti-CD81	BioLegend	Cat# 104911; RRID: AB_2562994
PE-Cy7 anti-NK1.1	ThermoFisher Scientific	Cat# 25-5941-82; RRID: AB_469665
PE-Cy7 anti-Sca-1	BioLegend	Cat# 122514; RRID: AB_756199
AF700 anti-CD34	ThermoFisher Scientific	Cat# 56-0341-82; RRID: AB_493998
AF647 anti-gp75	Novus Biologicals	Cat# NBP2-34720AF647
PE-Cy7 anti-PD-L1	BioLegend	Cat# 124314; RRID: AB_10643573
PE anti-H-2Kb	BioLegend	Cat# 116508; RRID: AB_313735
APC anti-H-2Db	BioLegend	Cat# 111514; RRID: AB_2565862
FITC anti-MPO	Abcam	Cat# ab90812; RRID: AB_2050025
Purified anti-citrullinated H3	Abcam	Cat# ab5103; RRID: AB_304752
PE Donkey anti-rabbit IgG	BioLegend	Cat# 406421; RRID: AB_2563484
Biotin anti-PE	BioLegend	Cat# 408104; RRID: AB_2168923
Purified anti-CD40	Bio X Cell	Cat# BE0016-2; RRID: AB_1107647
Purified anti-CD44	RayBiotech	Cat# DS-MB-00666; RRID: AB_852542
Purified anti-MHC Class I	Bio X Cell	Cat# BE0180; RRID: AB_10950841
Purified anti-human MHC Class I	Bio X Cell	Cat# BE0079; RRID: AB_1107730
Purified mouse IgG2a isotype control	Bio X Cell	Cat# BE0085; RRID: AB_1107771
Purified anti-Ly6G	Bio X Cell	Cat# BE0075-1; RRID: AB_1107721
Purified rat IgG2a isotype control	Bio X Cell	Cat# BE0089; RRID: AB_1107769
Purified anti-TNFR1	BioLegend	Cat# 112906; RRID: AB_2819826
Purified anti-TNFR2	BioLegend	Cat# 113307; RRID: AB_2832385
Purified Armenian Hamster IgG	Bio X Cell	Cat# BE0091; RRID: AB_1107773
Purified anti-Factor B, produced from ATCC hybridoma	ATCC	Cat# PTA-6230
Purified mouse IgG1 isotype control	Bio X Cell	Cat# BE0083; RRID: AB_1107784
Purified anti-properdin	Produced as in Miwa et al.[74]	N/A
Purified anti-C5	Produced as in Miwa et al.[74]	N/A
Purified anti-C5AR1	BioLegend	Cat# 135816; RRID: AB_2819876
Purified rat IgG2b isotype control	Bio X Cell	Cat# BE0090; RRID: AB_1107780

(*Continued on next page*)

Continued

REAGENT or RESOURCE	SOURCE	IDENTIFIER
Purified anti-CD40	Bio X Cell	Cat# BE0189; RRID: AB_10950314
Purified anti-EGFR	Bio X Cell	Cat# SIM0002; RRID: AB_2894723
Purified anti-GFP	Bio X Cell	Cat# RT0265; RRID: AB_2687789
Biological samples		
De-identified human whole blood	Stanford Blood Center	N/A
Chemicals, peptides, and recombinant proteins		
Recombinant mouse TNF	BioLegend	Cat# 575208
Recombinant mouse GM-CSF	BioLegend	Cat# 576302
Recombinant mouse IFNγ	BioLegend	Cat# 575304
Recombinant mouse IL-1β	BioLegend	Cat# 575102
Recombinant mouse IL-17A	BioLegend	Cat# 576002
Recombinant mouse C5a	R&D Systems	Cat# 2150-C5-025/CF
Recombinant human TNF	BioLegend	Cat# 570104
Recombinant human C5a	R&D Systems	Cat# 2037-C5-025/CF
Cobra venom factor	Millipore Sigma	Cat# 233552-1MG
SC57461A	Cayman Chemical	Cat# 10108
CP-105696	Millipore Sigma	Cat# PZ0363-25MG
Reduced L-glutathione	Millipore Sigma	Cat# G4251-25G
Catalase	Millipore Sigma	Cat# C40-500MG
Topiroxostat	MedChem Express	Cat# HY-14874
Luminol sodium salt	Sigma Aldrich	Cat# A4685
DiD' solid	ThermoFisher Scientific	Cat# D7757
Critical commercial assays		
In Situ Cell Death Detection Kit, TMR Red	Millipore Sigma	Cat# 12156792910
OxyBURST Green H2HFF BSA	ThermoFisher Scientific	Cat# O13291
Leukotriene B4 ELISA Kit	Cayman Chemical	Cat# 520111
GSH/GSSG Ratio Detection Kit II	Abcam	Cat# ab205811
Xanthine oxidase activity kit	Abcam	Cat# ab102522
DELFIA EuTDA cytotoxicity reagents	PerkinElmer	Cat# AD0116
Experimental models: Cell lines		
Mouse: B16F10	ATCC	Cat# CRL-6475
Mouse: LL/2	ATCC	Cat# CRL-1642
Mouse: 4T1	ATCC	Cat# CRL-2539
Human: A549	ATCC	Cat# CRM-CCL-185
Human: MDA-MD-231	ATCC	Cat# CRM-HTB-26
Experimental models: Organisms/strains		
Mouse: C57BL6/J	Jackson Laboratory	Cat# 000664
Mouse: BALB/cJ	Jackson Laboratory	Cat# 000651
Mouse: MMTV-PyMT: FVB/N-Tg(MMTV-PyVT)634Mul/J	Jackson Laboratory	Cat# 002374
Mouse: Rag2-/-: B6(Cg)-Rag2tm1.1Cgn/J	Jackson Laboratory	Cat# 008449
Mouse: TNFR KO: B6.129S-Tnfrsf1atm1Imx Tnfrsf1btm1Imx/J	Jackson Laboratory	Cat# 003243
Mouse: C3-/-: B6.129S4-C3tm1Crr/J	Jackson Laboratory	Cat# 029661
Mouse: Ncf1-/-: B6N.129S2-Ncf1tm1Shl/J	Jackson Laboratory	Cat# 027331
Mouse: Rag2-/- Il2rg-/-: B6(Cg)-Rag2tm1.1Cgn/J crossed with B6.129S4-Il2rgtm1Wjl/J	Jackson Laboratory	Cat# 008449 x Cat# 003174
Mouse: Cfp-/-	Kimura et al.[67]	N/A

(*Continued on next page*)

Continued		
REAGENT or RESOURCE	SOURCE	IDENTIFIER
Mouse: C6-/-	Ueda et al.[75]	N/A
Mouse: Fcer1g-/-: B6.129P2-Fcer1gtm1Rav N12	Taconic	Cat# 583
Oligonucleotides		
See Table S1 for oligonucleotide information	N/A	N/A
Recombinant DNA		
pSpCas9(BB)-2A-GFP (PX458)	Ran et al.[76]	Addgene # 48138; RRID: Addgene_48138
pLVX-EF1a-IRES-Puro	Clontech	Cat# 631988
Software and algorithms		
BD FACSDiva (v8)	BD Biosciences	https://www.bdbiosciences.com/en-us/products/software/instrument-software/bd-facsdiva-software
Zen black edition	Zeiss	https://www.zeiss.com/microscopy/us/products/microscope-software/zen.html
Zen blue edition	Zeiss	https://www.zeiss.com/microscopy/us/products/microscope-software/zen.html
BZ-X800 Viewer	Keyence	https://www.keyence.com/
BZ-X800 Analyzer	Keyence	https://www.keyence.com/
WorkOut 2.5	PerkinElmer	https://www.perkinelmer.com/
FlowJo (v10)	BD Biosciences	https://www.flowjo.com/solutions/flowjo/downloads
SpectroFlo V2.2.0.3	Cytek Biosciences	https://cytekbio.com/blogs/resources/spectroflo-v2-2-0-3-release-notes
Living Image	Caliper Life Sciences	https://www.perkinelmer.com/Product/li-software-for-lumina-1-seat-add-on-128110
ImageJ	Fiji	https://imagej.net/software/fiji/downloads
Photoshop CS6	Adobe	https://www.adobe.com/products/photoshop.html
Excel	Microsoft	https://www.microsoft.com/en-us/microsoft-365/excel
GraphPad Prism (v9)	GraphPad	https://www.graphpad.com/scientific-software/prism/

RESOURCE AVAILABILITY

Lead contact

Further information and requests for resources and reagents should be directed to and will be fulfilled by the lead contact, Edgar Engleman (edengleman@stanford.edu).

Material availability

This study did not generate new unique reagents.

Data code and availability

- All data reported in this paper will be shared by the lead contact upon request.
- This paper does not report original code.
- Any additional information required to reanalyze the data reported in this work is available from the lead contact upon request.

EXPERIMENTAL MODEL AND SUBJECT DETAILS

Animals

C57BL6/J (Jackson 000664), BALB/cJ (Jackson 000651), MMTV-PyMT (FVB/N-Tg(MMTV-PyVT)634Mul/J, Jackson 002374), *Rag2*$^{-/-}$ (B6(Cg)-*Rag2*$^{tm1.1Cgn}$/J, Jackson 008449), TNFR KO (B6.129S-*Tnfrsf1a*^{tm1Imx} *Tnfrsf1b*^{tm1Imx}/J, Jackson 003243), *C3*$^{-/-}$

(B6.129S4-*C3*^{tm1Crr}/J, Jackson 029661), and *Ncf1*$^{-/-}$ (B6N.129S2-*Ncf1*^{tm1Shl}/J, Jackson 027331) mice were purchased from Jackson Laboratory. *Fcer1g*$^{-/-}$ mice (B6.129P2-*Fcer1g*^{tm1Rav} N12, Taconic 583) were purchased from Taconic. *Rag2*$^{-/-}$ *Il2rg*$^{-/-}$ mice were generated by crossing B6(Cg)-*Rag2*$^{tm1.1Cgn}$/J mice (Jackson 008449) with B6.129S4-*Il2rg*^{tm1Wjl}/J mice (Jackson 003174). *Cfp*$^{-/-}$ mice[67,74] and *C6*$^{-/-}$ mice[75] were generated as previously described. 8-12 week old female mice were used, and mice of different experimental groups and genotypes were cohoused during all experiments, with the exception of immunocompromised *Rag2*$^{-/-}$ mice. Mice were randomly assigned to experimental groups. All animal studies were performed in accordance with the Stanford University Institutional Animal Care and Use Committee under protocol APLAC-17466. All mice were housed in an American Association for the Accreditation of Laboratory Animal Care-accredited animal facility and maintained in specific pathogen-free conditions.

Cell lines and culture

The mouse melanoma cell line B16F10, mouse lung carcinoma line LL/2, mouse mammary carcinoma line 4T1, human lung carcinoma line A549, and human mammary carcinoma line MDA-MB-231 were purchased from ATCC. To generate the mouse colon carcinoma line Sparkl.4640 (Syngeneic P53 APC ROSA26-LSL-eYFP Kras Lgr5-CreERT2), crypts were harvested and expanded from the colon of an adult female Lgr5-$^{EGFP\text{-}IRES\text{-}creERT2}$ Trp53$^{fl/fl}$ Apc$^{fl/fl}$ Kras$^{LSL\text{-}G12D/+}$ ROSA26$^{LSL\text{-}eYFP/LSL\text{-}eYFP}$ mouse according to a published protocol.[77] Single Lgr5 stem cells build crypt-villus structures *in vitro* without a mesenchymal niche. Cells were dissociated into a single cell suspension and then cultured in 4-hydroxytamoxifen (Sigma). Cells were washed and allowed to form colonies in Matrigel. After 1 week in culture, roughly 50 fluorescent colonies were collected and separated from non-fluorescent colonies under stereomicroscope with fluorescence attachment (Nikon). Colonies were dissociated and plated onto tissue culture treated plates in RPMI-1640 with 10% FBS. Notably, transformed cells were then able to be passaged in the absence of supplemental growth factors or Matrigel, both of which were required for the culture of crypts prior to treatment with 4-hydroxytamoxifen.

B16, LL/2, and A549 were cultured in DMEM (Gibco) supplemented with 10% FBS, 2 mM L-glutamine, 100 U/ml penicillin, and 100 μg/ml streptomycin (Gibco). Sparkl.4640, 4T1, and MDA-MB-231 were cultured in RPMI-1640 (Gibco) supplemented with 10% FBS, 100 U/ml penicillin, and 100 μg/ml streptomycin. Cells were tested for endotoxins using LAL Chromogenic Endotoxin Quantitation Kit (Pierce) and for mycoplasma using PlasmoTest™ (InvivoGen), according to manufacturer's instructions.

Human blood

For studies involving human neutrophils, whole blood was obtained from de-identified healthy blood donors at Stanford Blood Center. Informed consent was obtained from all donors. Human neutrophils were isolated and used in assays immediately and were not maintained in culture.

METHOD DETAILS

Tumor implantation, treatment, and survival

Cell lines were harvested with trypsin-EDTA (Gibco), washed once, and injected in 50 μl phenol red-free RPMI-1640 (Gibco). B16 ($2.5x10^5$ cells), Sparkl.4640 ($5x10^5$ cells), and LL/2 ($1x10^5$ cells) were injected subcutaneously (s.c.) into the flank of WT or KO mice on a syngeneic C57BL/6J background. 4T1 ($1x10^5$ cells) was injected s.c. into the flank of WT mice on a syngeneic BALB/cJ background. A549 ($5x10^6$ cells) was injected s.c. into the flank of *Rag2*$^{-/-}$ *Il2rg*$^{-/-}$ mice on a C57BL6/J background. MDA-MB-231 ($5x10^6$ cells) was injected orthotopically into the mammary fat pad of *Rag2*$^{-/-}$ *Il2rg*$^{-/-}$ mice on a C57BL6/J background. B16, Sparkl.4640, 4T1, and A549 tumors were allowed to grow for approximately 6 days prior to treatment, LL/2 was allowed to grow for approximately 8 days prior to treatment, and MDA-MB-231 was allowed to grow for approximately 12 days prior to treatment, at which point the tumors were approximately 10-30 mm^2. MMTV-PyMT mice were monitored until palpable tumors developed in the breast, at approximately 8 weeks of age, and treatment was initiated when tumors reached approximately 4-10mm^2.

Except where indicated otherwise, tumors were treated by intratumoral injection of tumor-binding antibody, 100 μg of agonistic anti-CD40 antibody (clone FGK4.5, Bio X Cell, Lebanon, NH), and 1 μg (ED_{50} 0.5-3 pg/ml in L929 cytotoxicity assay) of recombinant mouse TNF (BioLegend) in 50 μl total volume in phosphate buffered saline (PBS), which is referred to in the text as neutrophil-activating therapy. As tumor-binding antibody, B16 received 100 μg anti-gp75 (clone TA99, Bio X Cell), B16-EGFP received 100 μg anti-GFP (clone F56-6A1.2.3, Bio X Cell), Sparkl.4640 and LL/2 received 10 μg anti-CD44 (DS-MB-00666, RayBiotech), 4T1 and MMTV-PyMT received 100 μg anti-MHC Class I (clone 34-1-2S, Bio X Cell), and A549 and MDA-MB-231 received 100 μg anti-human MHC Class I (clone W6/32, Bio X Cell). In all cases, tumor-binding antibodies were confirmed to bind the appropriate tumor cells by flow cytometry. Mock-treated mice received an intratumoral injection of 50 μl PBS (treatment vehicle). Treatment was administered twice, two days apart, designated as days 0 and 2 post-treatment. For MMTV-PyMT mice, treatment was repeated weekly for four cycles, so that mice were treated on days 0, 2, 7, 9, 14, 16, 21, and 23. Although tumors develop in multiple breasts in the MMTV-PyMT model, only one tumor was treated per mouse for the duration of the therapy, with the largest tumor at the time of treatment initiation chosen for treatment. For TNF dose response experiments, mice received doses of 10 ng, 50 ng, or 1 μg of TNF (BioLegend). Where indicated, tumors were injected with one or two of the three treatment components. In some experiments, tumors were injected with 1 μg recombinant mouse GM-CSF (BioLegend), 5 μg recombinant mouse IFNγ (BioLegend), 1 μg recombinant mouse IL-1β (BioLegend), or 1 μg recombinant mouse IL-17A (BioLegend). Tumor areas were measured three times per week, and mice were euthanized when treated tumors exceeded 100 mm^2 or when tumors became ulcerated, with both indicated as a death event on the Kaplan Meier plots. Mice were censored from survival studies when they had to be euthanized for reasons unrelated to tumor

progression, such as dermatitis, and were tumor-free. For re-challenge studies, C57BL/6J WT or *Rag2*$^{-/-}$ mice that had cleared B16 tumors were re-challenged with 5x10^4 B16 cells in the opposite flank 50 days after initial treatment.

Blood chemistry

Blood was collected from mice by retro-orbital bleed and allowed to clot for 30 minutes on ice. It was then centrifuged at 2000 x *g* for 20 minutes at 4°C. Serum was collected from the top of the clot and centrifuged again at 2000 x *g* for 10 minutes at 4°C to remove residual red blood cells. Chemistry analysis was performed on the Siemens Dimension EXL200/LOCI analyzer by the Stanford University Animal Diagnostic Lab.

Mouse *in vitro* cytotoxicity studies

B16 tumors were treated by intratumoral injection of TNF + anti-CD40 + anti-gp75 and harvested 12 hours post-treatment. Tumors were dissected away from any surrounding fat, minced, and digested in 5 mg/ml collagenase IV (Worthington) plus 0.1 mg/ml DNase I (Sigma) with continuous mixing by magnetic stir bars for 20 minutes at 37°C in RPMI-1640 (Gibco) with 2% FBS. Following digestion, tissue was mashed through a 70 μm cell strainer (Falcon) and washed. For some studies, bone marrow was harvested by grinding bones from tumor-naïve untreated mice in a mortar and pestle and mashing through a 70 μm strainer (Falcon). Neutrophils were isolated from tumor and bone marrow samples with the MojoSort Mouse Ly6G Selection Kit (BioLegend), according to the manufacturer's instructions, and used in the cytotoxicity assay.

Cytotoxicity assays were conducted using the EuTDA assay from the DELFIA TRF cytotoxicity kit (PerkinElmer) according to the manufacturer's instructions. Briefly, B16 cells were labeled for 10 minutes with BATDA, and 5x10^3 labeled cells were added per well to a 96 well V-bottom plate in RPMI-1640. Neutrophils were added at a ratio of 10:1 unless otherwise stated. All co-cultures were conducted in the presence of TNF (10 ng/ml), anti-CD40 (1 μg/ml), anti-gp75 (1 μg/ml), and 10% active mouse C57BL/6 complement serum (Innovative Research), except where indicated otherwise. Mouse C57BL/6 complement serum was heat-inactivated for 40 minutes at 57°C where inactivation is specified. In some experiments, mouse IgG2a isotype control (1 μg/ml, isotype control for anti-gp75, clone C1.18.4, Bio X Cell), anti-mouse CD16/CD32 (10 μg/ml, clone 2.4G2, Bio X Cell), recombinant mouse C5a (50 nM, R&D Systems), anti-C5a (25 μg/ml, clone 295108, R&D Systems), rat IgG2a isotype control (25 μg/ml, isotype control for anti-C5a, clone 2A3, Bio X Cell), anti-C5AR1 (5 μg/ml, clone 20/70, BioLegend), rat IgG2b isotype control (5 μg/ml, isotype control for anti-C5AR1, clone LTF-2, Bio X Cell), SC57461A (10 μM, Cayman Chemical), CP-105696 (1 μM, Sigma), topiroxostat (10 μM, MedChem Express), or DMSO (vehicle for SC57461A, CP-105696, and topiroxostat) were added to the wells with the B16 and neutrophils. After 4 hours of co-culture at 37°C, supernatant was taken from the wells, Europium solution was added, and TDA released from lysed B16 cells was detected by TRF on a Victor X4 fluorescence microplate reader (PerkinElmer). Percent maximal lysis was determined by calculating the specific release of TDA using the formula: (experimental release – spontaneous release) / (maximum release – spontaneous release), where spontaneous release was determined by wells containing no neutrophils and maximum release was determined by wells with lysis buffer added.

For trogocytosis studies investigating transfer of tumor-binding antibody, anti-gp75 labeled with AF647 (clone TA99, Novus Biologicals) was used in place of unlabeled anti-gp75. For studies investigating transfer of B16 cell membrane, DiD' Solid (ThermoFisher Scientific) was reconstituted in DMSO at 10 mg/ml and diluted to a working solution of 5 μg/ml in serum-free DMEM. B16 cells were labeled in this solution for 20 minutes at 37°C at 1x10^6 cells/ml. Labeled B16 was washed 3 times in warm media before being added to the co-culture wells with the neutrophils. Following co-culture, flow cytometry was used to identify DiD signal in neutrophils.

Depletion and inhibition studies

In neutrophil depletion experiments, 500 μg anti-Ly6G (clone 1A8, Bio X Cell) or isotype control (clone 2A3, Bio X Cell) was administered intraperitoneally (i.p.) on days –2, 0, and 2 relative to treatment, with administration 4 hours prior to treatment on days 0 and 2. For MMTV-PyMT mice, this administration pattern was continued for four weeks for each of the treatment cycles. For neutrophil depletion studies in untreated mice, anti-Ly6G or isotype control administration began 4 days after tumor inoculation (equivalent to day –2 in treated mice), and administration continued every 2 days until the mice were euthanized. Graphing of survival for these mice began at day 6 post tumor inoculation (equivalent to day 0 in treated mice).

For TNFR blocking experiments, 100 μg of anti-TNFR1 (clone 55R-170, BioLegend), anti-TNFR2 (clone TR75-54.7, BioLegend), or isotype control (Armenian Hamster IgG, Bio X Cell) was administered i.p. once per day on days –1 through 4 relative to treatment, with administration 1 hour prior to treatment on days 0 and 2. Anti-factor B (clone 1379) was produced from a hybridoma (PTA-6230, ATCC) with serum-free CD Hybridoma Medium (Gibco) in a 1L CELLine bioreactor flask, purified with HiTrap Protein G HP columns, and buffer-exchanged to PBS in an Amicon Ultra 100 kDa centrifugal filter (Millipore). Anti-factor B or isotype control (clone MOPC-21, Bio X Cell) was administered i.p. at 1 mg once per day on days –1 through 2 relative to treatment, with administration 1 hour prior to treatment on days 0 and 2. Anti-properdin (clone 14E1) and anti-C5 (clone BB5.1) were produced as previously described[74]. For properdin blocking experiments, 1 mg of anti-properdin or isotype control (clone MOPC-21, Bio X Cell) was administered i.p. on days –1 and 1 relative to treatment. For C5 blocking experiments, 800 μg of anti-C5 or isotype control (clone MOPC-21, Bio X Cell) was administered i.p. once daily on days –1 through 2 relative to treatment, with administration 1 hour prior to treatment on days 0 and 2. For C5AR1 blocking experiments, anti-C5AR1 (clone 20/70, BioLegend) and isotype control (clone LTF-2, Bio X Cell) were deglycosylated with the deGlycIT kit (Genovis) prior to administration in order to abrogate Fc receptor binding and prevent

depletion of anti-C5AR1-bound neutrophils,[78] and 100 μg of anti-C5AR1 or isotype control were administered daily on days –1 through 3 relative to treatment, with administration 1 hour prior to treatment on days 0 and 2.

Reduced L-glutathione (Sigma) was dissolved in PBS and administered i.p. at 500 mg/kg at hours –1, 0, 2, 4, and 8 relative to treatment on days 0 and 2, as well as twice per day on days 1 and 3. Catalase (C40, Sigma) was dissolved in PBS and administered i.p. at 500 mg/kg twice per day on days 0, 1, 2, and 3 relative to treatment, with administrations on days 0 and 2 coming immediately prior and 4 hours after treatment. CVF (from *Naja naja kaouthia*, Millipore), which depletes complement components C3 and C5 from blood through fluid-phase activation,[79] was diluted in PBS and administered at 50 μg i.p. daily on days –2 through 2 relative to treatment, with administration 30 minutes prior to treatment on days 0 and 2. SC57461A (Cayman Chemical, Ann Arbor, MI) was dissolved in DMSO at 150 mg/ml, diluted in PBS, and administered i.p. at 75 mg/kg twice per day on days –1 through 3 relative to treatment, with administration 1 hour prior and 4 hours after treatment on days 0 and 2. CP-105696 (Sigma) was dissolved in DMSO at 400 mg/ml, diluted in 25% 2-hydroxypropyl-β-cyclodextrin (Cayman Chemical), and administered i.p. at 100 mg/kg twice per day on days 0 through 3 relative to treatment, with administration 1 hour prior and 4 hours after treatment on days 0 and 2. Topiroxostat (MedChemExpress) was dissolved in 0.2N NaOH in PBS, the pH was adjusted with HCl, and it was administered i.p. at 150 mg/kg on days 0 and 2, 3 hours prior to treatment.

Metastasis studies

For B16 experimental metastasis studies, mice were implanted with $2.5x10^5$ B16 cells expressing tdTomato s.c. in the flank. Seven days after implantation, $2x10^5$ B16 cells expressing tdTomato were injected i.v. by the tail vein. Ten hours after tail vein injection, the s.c. tumors were treated with PBS or TNF + anti-CD40 + anti-gp75, and the primary tumors were treated again two days later according to the standard treatment protocol. Nine days after tail vein injection, the mice were euthanized, the lungs harvested, and fluorescence images were acquired under a stereomicroscope with fluorescence attachment (Nikon). Discrete fluorescent metastases visible on the exterior of the lungs were counted to obtain metastasis counts. The average nodule area for metastases was determined using ImageJ by thresholding the image to remove background, using the analyze particles function to obtain the total area of the metastases, and dividing this area by the number of metastases.

For 4T1 metastasis studies, $1x10^5$ 4T1 tumor cells were implanted orthotopically in the mammary fat pad. One week post-implantation, when the primary tumor had reached a size of 16-30mm^2, the primary tumor was treated by intratumoral injection of neutrophil-activating therapy or PBS mock treatment, with two injections two days apart, according to the standard protocol. The mice were euthanized 30 days post-implantation and pulmonary metastases were enumerated as previously described[80] by intra-tracheal injection of India ink (15% India Ink, 85% PBS, 0.1% NaOH). India ink-injected lungs were washed in 3mL Fekete's solution (50% ethanol, 6% formaldehyde, and 3% glacial acetic acid) and then placed 5 mL fresh Fekete's solution overnight. White tumor nodules against a black lung background were counted manually.

Knockout of TNFR1 in B16 using CRISPR-Cas9

pSpCas9(BB)-2A-GFP (PX458) was a gift from Feng Zhang (Addgene plasmid # 48138; http://n2t.net/addgene:48138; RRID: Addgene_48138).[76] Two sgRNA target sequences for mouse *Tnfrsf1a* were chosen from the Brie library[81]: AGACCTAG CAAGATAACCAG and GATGGGGATACATCCATCAG, referred to in the text as *Tnfrsf1a* sgRNA1 and *Tnfrsf1a* sgRNA2, respectively. An sgRNA targeting the irrelevant *E. coli* β-galactosidase gene (*LacZ*) was also included as a control. Oligos for these sgRNA target sequences were synthesized by the Stanford Protein and Nucleic Acid facility, with end overhangs to enable cloning into the BbsI site of the PX458 backbone. Oligos were phosphorylated with T4 PNK (NEB) and annealed in a thermocycler at 37°C for 30 minutes, followed by 95°C for 5 minutes, and ramping down to 25°C at 5°C/minute. PX458 was digested with BbsI (NEB) and gel purified using the QIAquick Gel Extraction Kit (Qiagen). Phosphorylated and annealed oligos were ligated into BbsI-cut PX458 with T4 DNA ligase (NEB) and transformed into Stellar Electrocompetent Cells (Clontech) by electroporation with the GenePulser Xcell (BioRad). Plasmids were prepared with the Plasmid Plus Maxi Kit (Qiagen) and transfected into B16 cells using Lipofectamine 2000 (Thermo Fisher Scientific). Successfully transfected cells positive for expression of GFP were sorted on the FACSAria II (BD), followed by three successive rounds of sorting for cells negative for both GFP and TNFR1 staining using APC anti-TNFR1 (clone 55R-286, BioLegend), to achieve a population of cells lacking expression of TNFR1 with the transient expression of GFP and CRISPR machinery removed.

B16-EGFP

To generate B16 cells expressing EGFP on their surface, DNA encoding a fusion of mouse Igκ signal peptide, EGFP, and the transmembrane domain of mouse PDGFR was synthesized using GeneArt Gene Synthesis (Invitrogen). The synthesized gene was digested with BamHI and EcoRI (NEB) and gel purified using the QIAquick Gel Extraction Kit (Qiagen). This was ligated into pLVX-EF1α-IRES-Puro (Clontech) with T4 DNA ligase (NEB) and transformed into Stellar Electrocompetent Cells (Clontech) by electroporation with the GenePulser Xcell (BioRad). Plasmids were prepared with the Plasmid Plus Maxi Kit (Qiagen) and transfected into 293T cells together with the psPax2 and pCMV-VSV-G plasmids using Lipofectamine 2000 (Thermo Fisher Scientific). Virus was collected and used to transduce B16 cells, and successful transductants were selected using 1 μg/ml puromycin (ThermoFisher Scientific).

Flow cytometry

Tumors were digested with collagenase IV and DNase I as described above. Following digestion, tissue was mashed through a 70 μm cell strainer (Falcon), washed, red blood cells were lysed with ACK buffer for 1 minute, and cells were washed again prior to antibody staining. Blood was harvested into PBS plus 20 mM EDTA by cardiac puncture or retro-orbital bleed, lysed in ACK buffer for 5 minutes, and washed prior to antibody staining. Bone marrow was harvested by grinding the femur and tibia in a mortar and pestle and mashing through a 70 μm strainer (Falcon), or by flushing femurs with a syringe and needle, then lysed in ACK buffer for 5 minutes and washed prior to antibody staining. Spleens were harvested by mashing through a 70 μm cell strainer (Falcon), then lysed in ACK buffer for 5 minutes and washed prior to antibody staining.

Live cells were stained with antibodies on ice for 20 minutes in FACS buffer (HBSS 1% BSA 5mM EDTA) with Brilliant Stain Buffer Plus (BD). Following staining, cells were washed twice in FACS buffer and resuspended in 1 μg/ml DAPI plus AccuCount Fluorescent Particles (Spherotech) for absolute count determination. In some experiments, live cells were stained with Live/Dead Fixable Blue Stain (Invitrogen) in HBSS on ice for 20 minutes prior to antibody staining, and DAPI was not used. Cells for the HSC/progenitor experiment were viability stained with 800CW NHS Ester (Li-Cor #929-70020) at a 1:4000 dilution of a 1 mg/ml DMSO stock, for 20 minutes in PBS on ice prior to antibody staining. For assessment of neutrophil depletion efficiency and experiments analyzing Foxp3 and Ki67, cells were stained with Live/Dead Fixable Blue Stain (Invitrogen) in HBSS on ice for 20 minutes, cells were fixed and permeabilized prior to antibody staining using the Foxp3/Transcription Factor Staining Kit (eBioscience) or the True-Nuclear Transcription Factor Set (BioLegend) according to the manufacturer's instructions, and DAPI was not used. This staining following fixation/permeabilization allows identification of neutrophils with depleting antibody-bound extracellular Ly6G by staining intracellular Ly6G. Samples were acquired on an LSRFortessa (BD), except for the HSC/progenitor data, which was acquired on a Cytek Aurora using SpectroFlo V2.2.0.3. The following antibodies were used: BUV395 anti-CD45 (clone 30-F11, BD), BV421 anti-ICAM-1 (clone YN1/1.7.4, BioLegend), BV480 anti-MHC II (clone M5/114.15.2, BD), BV650 anti-CD11b (clone M1/70, BioLegend), PE-Cy7 or BUV737 anti-Ly6G (clone 1A8, BD/BioLegend), PE or AF647 anti-C3 (clone 11H9, Novus Biologicals), APC-R700 anti-CD11c (clone N418, BD), APC-Cy7 or BV785 anti-Ly6C (clone HK1.4, BioLegend), CD177 AF647 (clone Y127, BD Biosciences), SIRPα FITC (clone P84, BioLegend), Siglec F BV480 (clone E50-2440, BD Biosciences), CD101 PE-Cy7 (clone Moushi101, ThermoFisher Scientific), CD14 APC-Cy7 (clone Sa14-2, BioLegend), PD-L1 BV421 or BV711 or PE-Cy7 (clone 10F.9G2, BioLegend), XCR1 APC (clone ZET, BioLegend), F4/80 APC-Cy7 (clone BM8, BioLegend), CD206 FITC (clone C068C2, BioLegend), CD80 PerCP-eF710 (clone 16-10A1, ThermoFisher Scientific), CD86 BUV737 (clone GL1), B220 BV711 (clone RA3-6B2, BioLegend), TCRβ BV421 (clone H57-597, BioLegend), NK1.1 PE-Cy7 (clone PK136, BioLegend), CD8α BV510 (clone 53-6.7, BioLegend), CD4 BV711 (clone RM4-5, BioLegend), Foxp3 AF488 (clone MF23, BD Biosciences), CD25 BV650 (clone PC61, BioLegend), CD62L PerCP-Cy5.5 (clone MEL-14, BioLegend), CD44 APC-eF780 (clone IM7, ThermoFisher Scientific), KLRG1 PE (clone 2F1/KLRG1, BioLegend), PD-1 BV785 (clone 29F.1A12, BioLegend), CD69 APC (clone H1.2F3, BD Biosciences), Ki67 AF700 (clone SolA15, ThermoFisher Scientific), CD34 eF450 or AF700 (clone RAM34, ThermoFisher Scientific), IL-7Rα AF700 (clone A7R34, ThermoFisher Scientific), Sca-1 BV711 (clone D7, BioLegend), Sca-1 PE-Cy7 (clone E13-161/7, BioLegend), cKit FITC (clone 2B8, ThermoFisher Scientific), CD16/32 PE (clone S17011E, BioLegend), CD3ε PE-Cy7 (clone 17A2, ThermoFisher Scientific), CD4 PE-Cy7 (clone GK1.5, ThermoFisher Scientific), CD8α PE-Cy7 (clone 53-6.7, ThermoFisher Scientific), CD11b PE-Cy7 (clone M1/70, ThermoFisher Scientific), B220 PE-Cy7 (clone RA3-6B2, ThermoFisher Scientific), NK1.1 PE-Cy7 (clone PK136, ThermoFisher Scientific), Flt3 APC (clone A2F10, BioLegend), CD106 Pacific Blue (clone 429 (MVCAM.A), BioLegend), CD115 BV605 (clone AFS98, BioLegend), Ly6G PE-Cy5 (clone 1A8, ThermoFisher Scientific), CD81 PerCP-Cy5.5 (clone Eat-2, BioLegend), H-2K^b PE (clone AF6-88.5, BD Biosciences), H-2D^b APC (clone KH95, BioLegend), fluorescein anti-gp75 (clone TA99, Bio X Cell, labeled using NHS-Fluorescein (Thermo Scientific)), MPO FITC (clone 2D4, Abcam), citrullinated Histone H3 (Abcam ab5103), donkey anti-rabbit IgG PE (BioLegend Poly4064), and unconjugated anti-CD16/CD32 (clone 2.4G2, Bio X Cell) to block Fc receptors. For dihydrorhodamine-123 (DHR-123) staining of tumor samples, 5mM DHR-123 in DMSO (Invitrogen) was added to the collagenase mixture at a dilution of 1:4000 and allowed to stain for the duration of the 20-minute collagenase digestion. Flow cytometry data was analyzed using FlowJo software (BD). Staining levels were quantified using the median fluorescence intensity (MFI).

May-Grünwald-Giemsa staining

Tumors were harvested, processed, and stained for flow cytometry as described above, 24 hours after treatment or mock treatment. Cells were stained with FITC anti-CD45 (clone 30-F11, BioLegend), APC-Cy7 anti-CD11b (clone M1/70, BioLegend), and PE anti-Ly6G (clone 1A8, BioLegend), and CD45$^+$CD11b$^+$Ly6G$^+$ neutrophils were sorted on a FACSAria II (BD). Sorted neutrophils were resuspended at 5x10^5 cells/ml in FACS buffer, and 200 μl was spun onto a slide using the StatSpin CytoFuge 2 at 850 rpm for 10 minutes. Slides were dried and then stained for 4 minutes in May-Grünwald stain solution (Electron Microscopy), transferred directly into 4% Giemsa stain solution (Electron Microscopy) for 4 minutes, and washed twice with water for 30 seconds each. Slides were dried and coverslips were mounted using Cytoseal 60 (Richard Allen Scientific). Stained cells were imaged on a Keyence BZ-X810 microscope (Keyence) with the 20X objective and a resolution of 1920 x 1440 pixels.

Immunofluorescence

Tumors were dissected away from surrounding fat, fixed in 2% paraformaldehyde for 2 hours at 4°C, equilibrated in a 30% sucrose solution at 4°C, and embedded and frozen in O.C.T. Compound (Tissue-Tek). Slides were cut to 6 μm and blocked with 1% BSA and 10% serum matched to the secondary antibody species. The following antibodies were used for immunofluorescence: PE anti-Ly6G

(clone 1A8, BioLegend), DyLight 650 anti-gp75 (clone TA99, Bio X Cell, labeled using DyLight 650 NHS Ester (Thermo Scientific)), fluorescein anti-gp75 (clone TA99, Bio X Cell, labeled using NHS-Fluorescein (Thermo Scientific)), FITC anti-DNA/RNA damage (clone 15A3, recognizing 8-hydroxy-2'-deoxyguanosine/8-oxo-7,8-dihydroguanine/8-oxo-7,8-dihydroguanosine, Abcam), and AF647 anti-C3 (clone 11H9, Novus Biologicals). DAPI (Invitrogen) was stained at 1 μg/ml. FITC/fluorescein signal was amplified using AF488 anti-FITC (ThermoFisher Scientific), and PE was amplified using biotin anti-PE (clone PE001, BioLegend) followed by DyLight 594 streptavidin (BioLegend) or DyLight 649 streptavidin (BioLegend). Prior to use of biotinylated antibodies, endogenous biotin was blocked using the Avidin/Biotin Blocking Kit (Vector Laboratories). Prior to DNA/RNA damage staining, sections were permeabilized with 0.1% Triton X-100 in 0.1% sodium citrate. TUNEL (Terminal deoxynucleotidyl transferase dUTP nick end labeling) staining was performed using the *In Situ* Cell Death Detection Kit, TMR Red (Roche) according to the manufacturer's instructions. Briefly, tissue sections were fixed with 4% paraformaldehyde for 20 minutes on ice prior to treatment with 0.1% Triton X-100 in 0.1% sodium citrate for permeabilization. Sections were washed in PBS before incubation for 60 minutes at 37°C with antibodies and TdT enzyme, followed by washing. Images were acquired by tile scanning using a Zeiss LSM 700 confocal laser scanning microscope (Carl Zeiss Microscopy) or a Keyence BZ-X810 microscope (Keyence) using the 20X objective and a resolution of 960 x 720 pixels per tile. Tumor immunostainings were repeated independently at least 2 times in at least biological triplicate and whole tissue section images were acquired. Stitching of images acquired with the LSM 700 was performed using ZEN software, and stitching of images acquired with the BZ-X810 was performed using BZ-X800 Analyzer software. Multiple tumors from the same experiment were embedded together in the same block, stained together in the same section, and acquired together in a tile scan across the entire section. Individual tumors were then cropped from the full tile scan image for display in figures. Images were overlaid and color channel levels were adjusted in Photoshop (Adobe), with individual color channels receiving individual level adjustments based on the staining intensity. All parameters that were quantified were acquired with identical microscope settings and adjusted identically in Photoshop, and all adjustments were applied equally across the entire tumor. Quantification was performed in ImageJ, using the wand tool on the overlaid multichannel image to draw a border around the tumor and then measuring the percent area within that border with signal for the channel of the marker quantified.

LTB_4 ELISA

Tumors were dissected away from surrounding fat 24 hours post-treatment and lysed in PBS using 3 mm zirconium beads (Benchmark Scientific) in the BeadBug Microtube Homogenizer (Benchmark Scientific) for 2 cycles of 45 seconds at 3000 rpm. Crude lysate was centrifuged for 15 minutes at 16000 x *g* at 4°C to obtain clarified lysate. Clarified lysate was deproteinized by ethanol precipitation by adding 4 volumes of 100% ethanol, incubating on ice for 5 minutes, and centrifuging for 10 minutes at 3000 x *g* at 4°C. Deproteinized supernatant was transferred to a new tube, ethanol was removed by evaporation at room temperature, and samples were brought to the appropriate volume in ELISA assay buffer. LTB_4 content was determined with the Leukotriene B_4 ELISA kit (Cayman Chemical 520111) according to the manufacturer's instructions and read with a Victor X4 fluorescence microplate reader (PerkinElmer).

Ex vivo neutrophil LTB_4 assay

B16 tumors were harvested from mice 12 hours after treatment with TNF + anti-CD40 + anti-gp75 and digested with collagenase IV and DNase I as described above. Tumor samples were then split into two halves, with one half undergoing selection with the MojoSort Mouse Ly6G Selection Kit (BioLegend) to generate $Ly6G^+$ and Ly6G-depleted tumor samples and the other half undergoing depletion with an isotype control antibody and streptavidin nanobeads (BioLegend) to generate the "all cells" condition. These selected samples were then plated in 200μl of Opti-MEM (Gibco) and incubated for 30 minutes at 37°C. Following the incubation, the supernatant was collected, centrifuged to remove cells and debris, and analyzed for LTB_4 using the Leukotriene B_4 ELISA kit (Cayman Chemical 520111) as described above.

Mouse *in vitro* neutrophil stimulations

Bone marrow was harvested by grinding bones in a mortar and pestle and mashing through a 70 μm strainer (Falcon). Neutrophils were isolated by negative selection with the MojoSort Mouse Neutrophil Isolation Kit (BioLegend). Following isolation, neutrophils were plated in Opti-MEM (Gibco) at $1x10^5$ cells in 100 μl and stimulated with 10 ng/ml TNF, 1 μg/ml anti-CD40, 1 μg/ml anti-gp75, and/or 50 nM recombinant mouse C5a (R&D Systems) for 30 minutes at 37°C. After 30 minutes, the supernatant was collected, centrifuged to remove cells and debris, and analyzed for LTB_4 using the Leukotriene B_4 ELISA kit (Cayman Chemical 520111) as described above. Additionally, stimulated neutrophils were stained for activation markers and analyzed by flow cytometry as described above.

Determination of oxidized glutathione content

Tumors were dissected away from surrounding fat 24 hours post-treatment and lysed in mammalian lysis buffer (Abcam ab179835) using 3 mm zirconium beads (Benchmark Scientific) in the BeadBug Microtube Homogenizer (Benchmark Scientific) for 2 cycles of 45 seconds at 3000 rpm. Crude lysate was centrifuged for 15min at 16000 x *g* at 4°C, and clarified lysate was deproteinized using the Deproteinizing Sample Preparation Kit – TCA (Abcam ab204708) according to the manufacturer's instructions. Glutathione was detected using the GSH/GSSG Ratio Detection Assay Kit II (Abcam ab205811) according to the manufacturer's instructions, reading the

resulting signal with a Victor X4 fluorescence microplate reader. The percentage of oxidized glutathione was calculated from the reduced glutathione and total glutathione values determined by the kit.

XO assay

Tumors were dissected away from surrounding fat 24 hours post-treatment and lysed in XO assay buffer (Abcam) using 3 mm zirconium beads (Benchmark Scientific) in the BeadBug Microtube Homogenizer (Benchmark Scientific) for 2 cycles of 45 seconds at 3000 rpm. Crude lysate was centrifuged for 10 minutes at 16000 x *g* at 4°C to obtain clarified lysate. XO activity of the lysate was determined using the Xanthine Oxidase Activity Assay kit (Abcam), setting up the fluorometric assay and performing calculations according to the manufacturer's instructions, and reading fluorescence with a Victor X4 fluorescence microplate reader.

ROS assays

For the luminol assay, B16-bearing mice were anesthetized 4 hours post-treatment, and 50 μL luminol sodium salt (Sigma-Aldrich) at 20 mg/mL in PBS was administered intratumorally. Mice were immediately imaged using the IVIS Lumina system (Xenogen). Signal intensity was quantified as photons/second (p/s) over a one-minute exposure in equally sized regions of interest placed over the tumor, using Living Image software (Caliper Life Sciences).

For the OxyBurst assay, neutrophils were isolated from naïve bone marrow or treated tumors, and $1x10^5$ neutrophils were plated in a 96-well plate together with $5x10^3$ B16 tumor cells. The cells were stimulated as in the cytotoxicity studies and cultured for 4 hours at 37°C in the presence of 10 μg/ml OxyBurst Green H_2HFF BSA. After co-culture, the plate was read on a Victor X4 fluorescence microplate reader (PerkinElmer) with 485 nm excitation and 535 nm emission.

Human neutrophil studies

Human neutrophils were isolated from whole blood obtained from de-identified blood donors using the EasySep Direct Human Neutrophil Isolation Kit (StemCell Technologies) according to the manufacturer's instructions. For activation marker studies, neutrophils were plated at $1x10^6$ cells/ml in Opti-MEM (Gibco) and stimulated for 30 minutes at 37°C with human TNF (50 ng/ml, BioLegend), anti-human CD40 (1 μg/ml, clone G28.5, Bio X Cell), anti-human EGFR (1 μg/ml, Cetuximab biosimilar, Bio X Cell), or human C5a (50 nM, R&D Systems), as indicated in the figures. In some experiments, 5mM DHR-123 in DMSO (Invitrogen) was added to the stimulation well at a dilution of 1:4000. Following stimulation, the cells were stained with antibodies on ice for 20 minutes in FACS buffer (HBSS 1% BSA 5mM EDTA) with Brilliant Stain Buffer Plus (BD). Following staining, cells were washed twice in FACS buffer and resuspended in 1 μg/ml DAPI. Samples were acquired on an LSRFortessa (BD). The following antibodies were used: APC-Fire 750 anti-CD11b (clone M1/70, BioLegend), ICAM-1 FITC (clone HA58, BioLegend), CD16 BV711 (BioLegend, clone 3G8), CD32 BV786 (clone FLI8.26, BD Biosciences), CD66b AF647 (clone G10F5, BioLegend), CD63 BV510 (clone H5C6, BD Biosciences), and anti-C5AR1 PE (clone S5/1, BioLegend).

Cytotoxicity assays were performed with the EuTDA assay from the DELFIA TRF cytotoxicity kit (PerkinElmer) according to the manufacturer's instructions. A549 cells were labeled for 30 minutes with BATDA, and $1x10^4$ labeled cells were added per well to a 96 well V-bottom plate in RPMI-1640. Neutrophils were added at a ratio of 50:1 unless specified otherwise. All co-cultures were conducted in the presence of TNF (10 ng/ml), anti-CD40 (1 μg/ml), anti-gp75 (1 μg/ml), and 10% pooled human complement serum (Innovative Research) for 1 hour, except where indicated otherwise.

QUANTIFICATION AND STATISTICAL ANALYSIS

Statistics

Statistical tests were performed in Prism (GraphPad Software, Inc.). Statistical tests used are listed in the figure legends. In cases where conditions were compared across multiple time points or cell types, statistical significance was determined by two-way ANOVA with Tukey's multiple comparisons test, comparing only the conditions within each time point or cell type. For *in vitro* cytotoxicity studies with multiple conditions and groups, statistical significance was determined by two-way ANOVA with Tukey's multiple comparisons test, comparing all conditions and groups with all other conditions and groups. Plots display individual biological replicates obtained from distinct mice, with a line at the mean. For all figures, * denotes $p < 0.05$, ** denotes $p < 0.01$, *** denotes $p < 0.001$, **** denotes $p < 0.0001$, and n.s. indicates not significant, with the exception of Kaplan Meier plots with multiple comparisons, in which case the asterisks are assigned based on Bonferroni-corrected p values. For all experiments, *n* represents the number of mice or the number of samples. Exact *n* values and the number of independent experiments are provided in the figure legends.

Cancer Cell, Volume *41*

Supplemental information

Neutrophil-activating therapy for the treatment of cancer

Ian L. Linde, Tyler R. Prestwood, Jingtao Qiu, Genay Pilarowski, Miles H. Linde, Xiangyue Zhang, Lei Shen, Nathan E. Reticker-Flynn, David Kung-Chun Chiu, Lauren Y. Sheu, Simon Van Deursen, Lorna L. Tolentino, Wen-Chao Song, and Edgar G. Engleman

Supplemental Figures

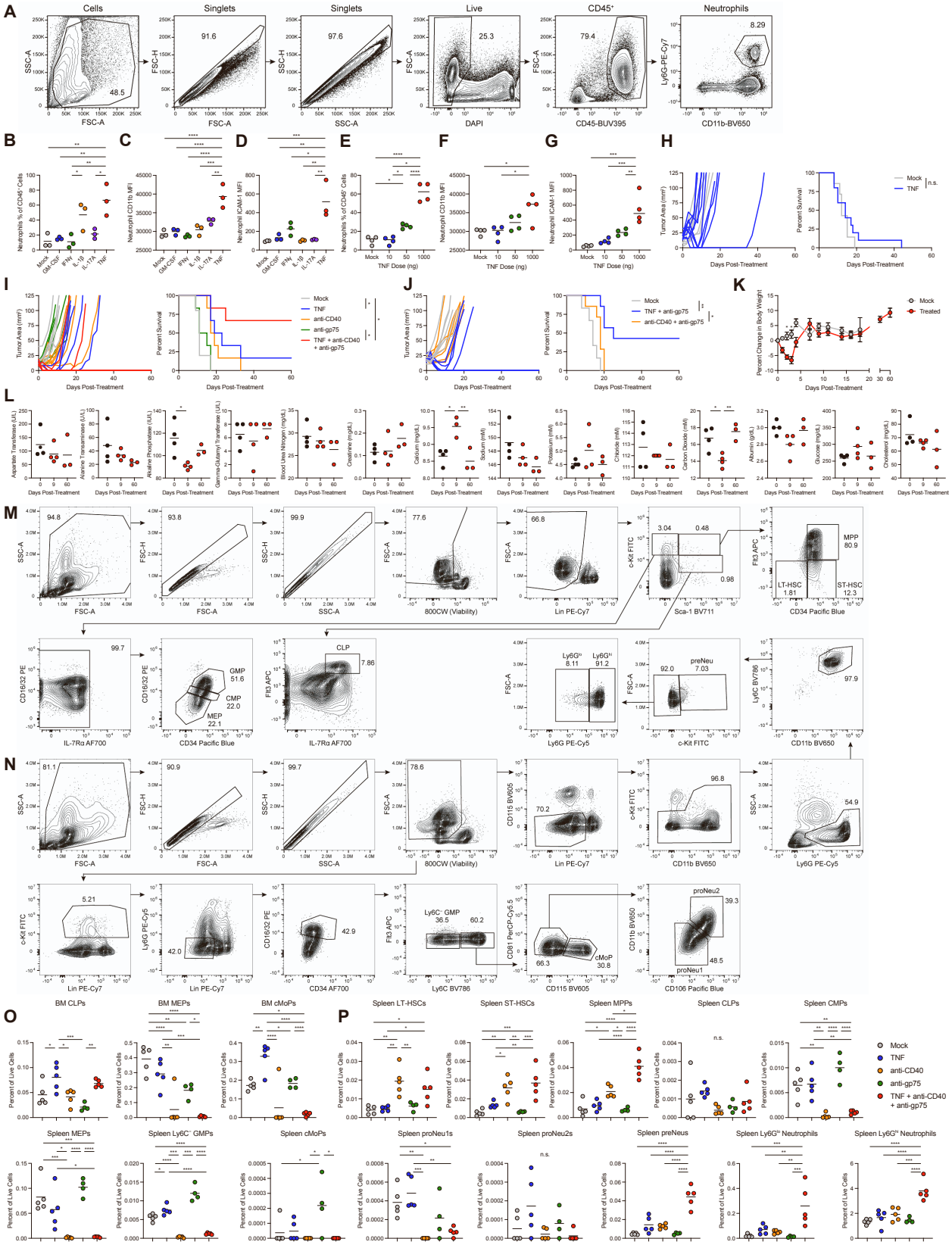

Figure S1: Neutrophil-activating therapy induces neutrophil expansion and recruitment to tumors. Related to Figure 1.

(**A**) Flow cytometry gating strategy for neutrophils. (**B**) Neutrophil infiltration of B16 tumors 24 hours after treatment with the indicated cytokines (n=3). (**C-D**) Expression of CD11b (C) and ICAM-1 (D) on tumor-infiltrating neutrophils 24 hours after administration of the indicated cytokines (n=3). (**E**) Neutrophil infiltration of B16 tumors 24 hours after treatment with the indicated dose of TNF (n=4). (**F-G**) Expression of CD11b (F) and ICAM-1 (G) on tumor-infiltrating neutrophils 24 hours after administration of the indicated dose of TNF (n=4). (**H**) Survival of B16-bearing mice following treatment with 1 μg TNF (mock n=7, TNF n=10). (**I-J**) Survival of B16-bearing mice treated with the indicated factors (I: mock n=5, others n=6; J: mock n=6, others n=7). (**K**) Percent change in mouse body weight following treatment of B16 tumors (n=5, mean +/- SEM shown). (**L**) Mouse blood chemistry values obtained on the indicated days after treatment of B16 tumors with neutrophil-activating therapy (d60 n=3, others n=4). (**M-N**) Flow cytometry gating strategies to identify hematopoietic stem cells, progenitors, and neutrophil precursors. (**O-P**) Frequencies of hematopoietic stem cells, progenitors, and precursor populations in the bone marrow (O) and spleen (P) 24 hours after treatment of B16 with neutrophil-activating therapy (anti-gp75 n=4, others n=5). Statistics: One-way ANOVA with Tukey's multiple comparisons test (B-G, L, O-P), Log-rank test (H), Log-rank test with Bonferroni correction (I-J), Two-way ANOVA with Sidak's multiple comparisons test (K). For all dot plots, the line indicates the mean. Data are representative of 2 (B-G, I-J, O-P) or 1 (K-L) independent experiments or pooled from 4 experiments (H).

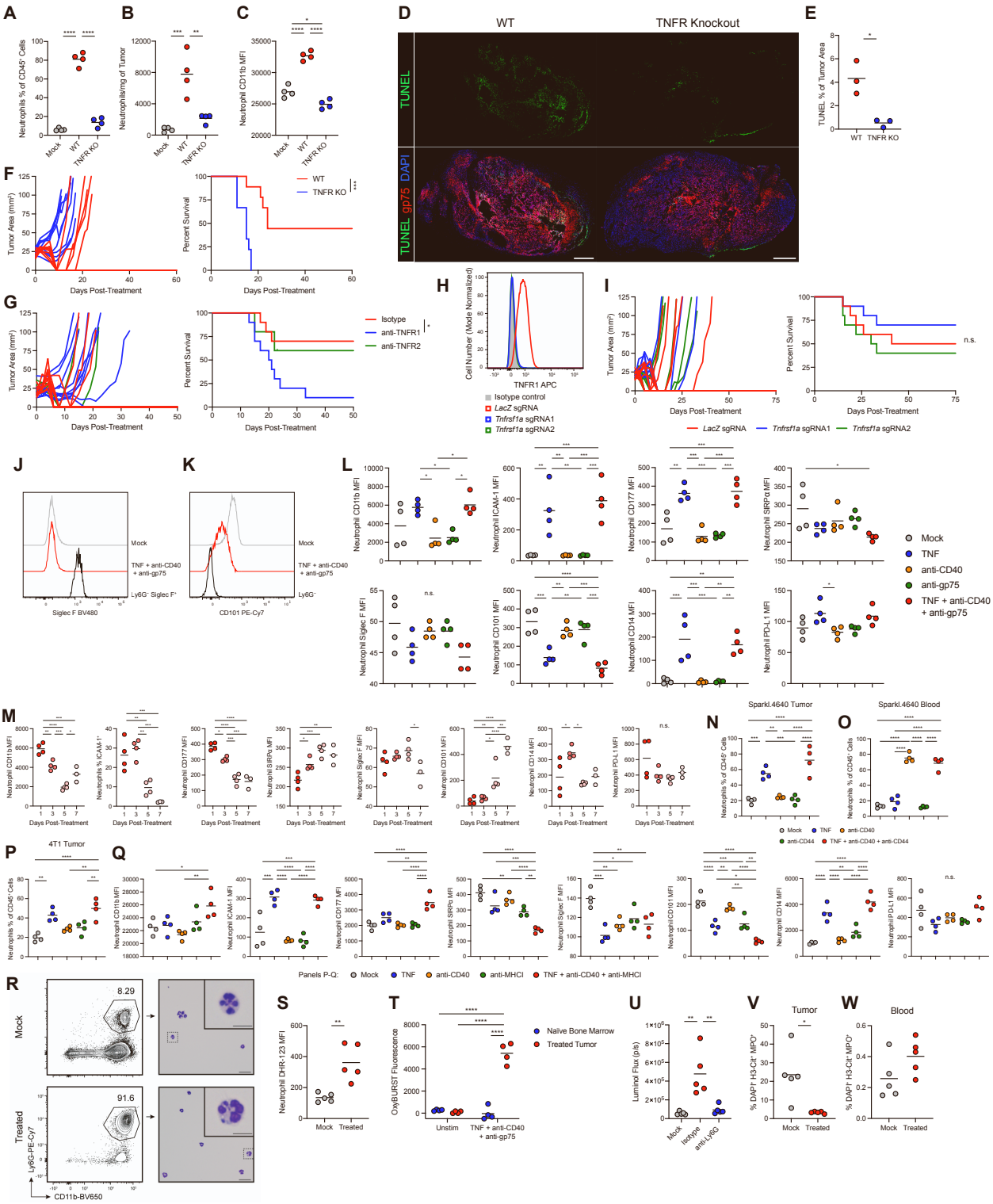

Figure S2: Therapy induces neutrophil activation. Related to Figure 1.

(**A-B**) Tumor-infiltrating neutrophil frequency of CD45$^+$ cells (A) and numbers/mg of tumor (B) 24 hours after treatment of B16 tumors with neutrophil-activating therapy in wild-type (WT) or TNF receptor knockout (TNFR KO) mice (n=4). (**C**) CD11b expression on tumor-infiltrating

neutrophils 4 hours after treatment of B16 tumors with neutrophil-activating therapy in WT or TNFR KO mice (n=4). (**D-E**) Representative immunofluorescence (D) and quantification (E) of TUNEL staining in B16 tumors in WT or TNFR KO mice 24 hours after treatment with neutrophil-activating therapy. Scale bars = 500 μm. (n=3) (**F**) Survival of B16-bearing WT or TNFR KO mice treated with neutrophil-activating therapy (n=9). (**G**) Survival of B16-bearing mice treated with neutrophil-activating therapy following administration of TNFR blocking antibodies (TNFR2 n=5, others n=10). (**H**) TNFR1 staining of B16 cells following knockout of TNFR1 with CRISPR-Cas9 sgRNA targeting *Tnfrsf1a* or the irrelevant *LacZ*. (**I**) Survival of mice bearing TNFR1-knockout B16 following treatment with neutrophil-activating therapy (n=10). (**J**) Representative histograms comparing Siglec F expression in mock or treated tumor-infiltrating neutrophils to Siglec F expression in a $Ly6G^-$ Siglec F^+ cell population in the tumor of mock-treated mice, 4 hours after treatment. (**K**) Representative histograms comparing the expression level of CD101 in mock or treated tumor-infiltrating neutrophils to that of $Ly6G^-$ cells in the tumor of mock-treated mice, 4 hours after treatment. (**L**) Surface marker expression on neutrophils in the blood 4 hours after treatment of B16 tumors with the indicated components (n=4). (**M**) Surface marker expression on neutrophils in the blood at the indicated times post-treatment with the full neutrophil-activating therapy (d7 n=3, others n=4). (**N-O**) Neutrophil frequency in the tumor (N) and blood (O) 24 hours after treatment of Sparkl.4640 with neutrophil-activating therapy (n=4). (**P**) Neutrophil frequency in 4T1 tumors 24 hours after treatment with the indicated components (n=4). (**Q**) Surface marker expression on neutrophils in 4T1 tumors 4 hours after treatment with the indicated components (n=4). (**R**) Representative flow cytometry staining of $CD11b^+Ly6G^+$ cells, gated on single/live/$CD45^+$ cells (left panels), and May-Grünwald-Giemsa staining of sorted $CD45^+CD11b^+Ly6G^+$ cells (right panels), in B16 tumors 24 hours after treatment with neutrophil-activating therapy. Image scale bars = 30 μm. Inset scale bars = 10 μm. (**S**) Tumor-infiltrating neutrophil MFI of the ROS-sensing dye dihydrorhodamine-123 (DHR-123) 4 hours after treatment with neutrophil-activating therapy (n=5). (**T**) Fluorescence of OxyBURST Green H_2HFF BSA following *in vitro* stimulation of neutrophils isolated from treated tumors or naïve bone marrow with neutrophil-activating therapy (n=4). (**U**) Bioluminescence in the tumor emitted from the ROS-sensing molecule luminol during *in vivo* imaging 4 hours after treatment of B16 with neutrophil-activating therapy (n=5). (**V-W**) Percentage of neutrophils staining triple positive for DAPI, citrullinated histone H3 (H3-Cit), and myeloperoxidase (MPO) in the tumor (V) and blood (W) of mice treated with neutrophil-activating therapy (n=5). Statistics: One-way ANOVA with Tukey's multiple comparisons test (A-E, L-Q, U), Log-rank test (F), Log-rank test with Bonferroni correction (G, I), Unpaired two-tailed

t test (S, V-W), Two-way ANOVA with Tukey’s multiple comparisons test (T). For all dot plots, the line indicates the mean. Data are representative of 3 (F, S), 2 (A-E, H, J-P, R, T, U-W) or 1 (Q) independent experiments or pooled from 2 experiments (G, I).

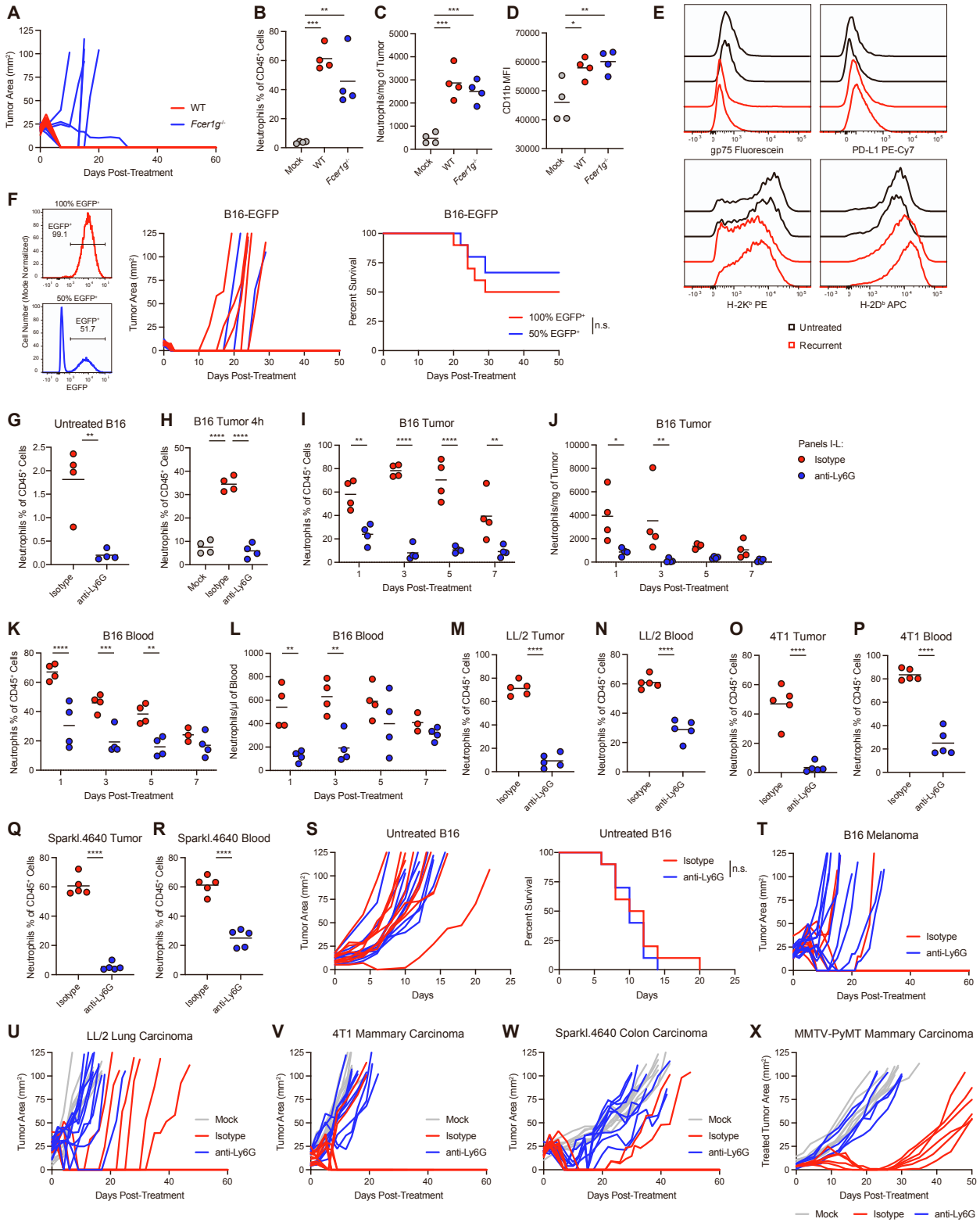

Figure S3: Neutrophil depletion prevents tumor clearance. Related to Figure 2.

(**A**) Tumor growth in WT and *Fcer1g*$^{-/-}$ B16-bearing mice after treatment with neutrophil-activating therapy (n=10). (**B-D**) Neutrophil frequency (B), numbers (C), and CD11b expression (D) in WT versus *Fcer1g*$^{-/-}$ mice, 24 hours after treatment (n=4). (**E**) Expression of gp75, PD-L1, and MHCI molecules on B16 tumor cells from day 0 untreated tumors or tumors that recurred following neutrophil-activating therapy. (**F**) Tumor growth and survival of mice implanted with B16 tumors, in which either 50% or 100% of the B16 cells expressed EGFP on the surface, following treatment with TNF + anti-CD40 + anti-EGFP (n=10). (**G**) Neutrophil frequency in untreated B16 tumors in mice administered anti-Ly6G or isotype control (n=4). (**H**) Neutrophil frequency in B16 tumors 4 hours after treatment with neutrophil-activating therapy in mice administered anti-Ly6G or isotype control (n=4). (**I-L**) Neutrophil frequencies (I, K) and numbers (J, L) in the tumor (I-J) and blood (K-L) of B16-bearing mice at multiple time points after the Ly6G depletion plus neutrophil-activating therapy protocol (n=4). (**M-R**) Neutrophil frequency in the tumor (M, O, Q) and blood (N, P, R) 24 hours after neutrophil-activating treatment of Ly6G-depleted mice bearing LL/2 (M-N), 4T1 (O-P), and Sparkl.4640 (Q-R) tumors. (n=5) (**S**) B16 tumor growth and survival of mice receiving anti-Ly6G or isotype control in the absence of neutrophil-activating therapy (n=10). (**T-W**) Tumor growth in mice bearing B16 (T) (n=10), LL/2 (U) (mock n=8, others n=10), 4T1 (V) (n=10), or Sparkl.4640 (W) (mock n=8, isotype n=10, anti-Ly6G n=9) tumors that received anti-Ly6G or isotype control prior to neutrophil-activating therapy or mock treatment. (**X**) Growth of the treated tumor in MMTV-PyMT mice administered anti-Ly6G or isotype control prior to neutrophil-activating therapy. Isotype control mice were euthanized at day 50 due to tumor burden in distant untreated breasts. (mock n=8, others n=6) Statistics: One-way ANOVA with Tukey's multiple comparisons test (B-D, H), Log-rank test (F, S), Unpaired two-tailed t test (G, M-R), Two-way ANOVA with Tukey's multiple comparisons test (I-L). For all dot plots, the line indicates the mean. Data are representative of 3 (T), 2 (A-D), or 1 (E-S) independent experiments or pooled from 3 (U-W) or 6 (X) experiments.

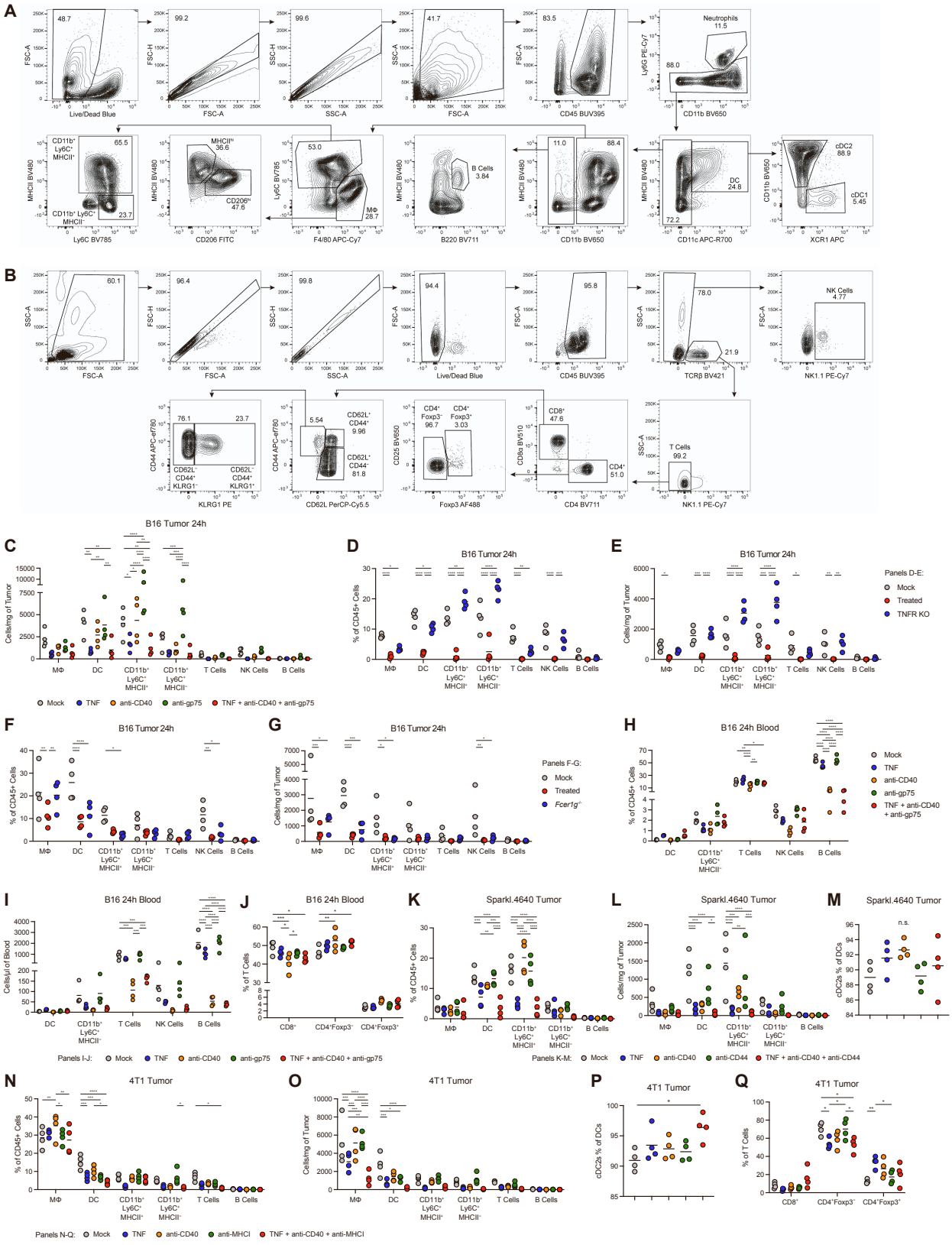
A
B
C
D
E
F
G
H
I
J
K
L
M
N
O
P
Q
B16 Tumor 24h
B16 24h Blood
Sparkl.4640 Tumor
4T1 Tumor
Panels D-E: Mock Treated TNFR KO
Panels F-G: Mock Treated Fcer1g-/-
Panels I-J: Mock TNF anti-CD40 anti-gp75 TNF + anti-CD40 + anti-gp75
Panels K-M: Mock TNF anti-CD40 anti-CD44 TNF + anti-CD40 + anti-CD44
Panels N-Q: Mock TNF anti-CD40 anti-MHCI TNF + anti-CD40 + anti-MHCI

Figure S4: Impact of neutrophil-activating therapy on the numbers and frequencies of other immune cells. Related to Figure 3.

(**A-B**) Flow cytometry gating strategy for identifying myeloid and lymphoid subsets. $CD4^+Foxp3^-$ T cells were gated for memory and effector phenotype in the same manner as the $CD8^+$ T cells shown. (**C**) Numbers of other immune cells in B16 tumors 24 hours after treatment with the indicated components (n=4). (**D-E**) Frequencies (D) and numbers (E) of immune cells in B16 tumors 24 hours after treatment of WT or TNFR KO mice with the full neutrophil-activating therapy (n=4). (**F-G**) Frequencies (F) and numbers (G) of immune cells in B16 tumors 24 hours after treatment of WT or *Fcer1g*$^{-/-}$ mice with the full neutrophil-activating therapy (n=4). (**H-I**) Frequencies (H) and numbers (I) of immune cells in the blood of B16-bearing mice 24 hours after treatment with the indicated components (n=4). (**J**) Frequencies of T cell subsets as a percentage of total T cells in the blood 24 hours after treatment of B16 tumors with the indicated components (n=4). (**K-L**) Frequencies (K) and numbers (L) of immune cells in Sparkl.4640 tumors 24 hours after treatment with the indicated components (n=4). (**M**) Percent of $CD11b^+$ cDC2s out of total DCs in Sparkl.4640 tumors 24 hours after treatment (n=4). (**N-O**) Frequencies (N) and numbers (O) of immune cells in 4T1 tumors 24 hours after treatment with the indicated components (n=4). (**P**) Percent of $CD11b^+$ cDC2s out of total DCs in 4T1 tumors 24 hours after treatment (n=4). (**Q**) Percent of T cell subsets out of total T cells in 4T1 tumors 24 hours after treatment (n=4). Statistics: Two-way ANOVA with Tukey's multiple comparisons test (C-L, N-O, Q), One-way ANOVA with Tukey's multiple comparisons test (M, P). For all dot plots, the line indicates the mean. Data are representative of 2 (C-J) or 1 (K-Q) independent experiments.

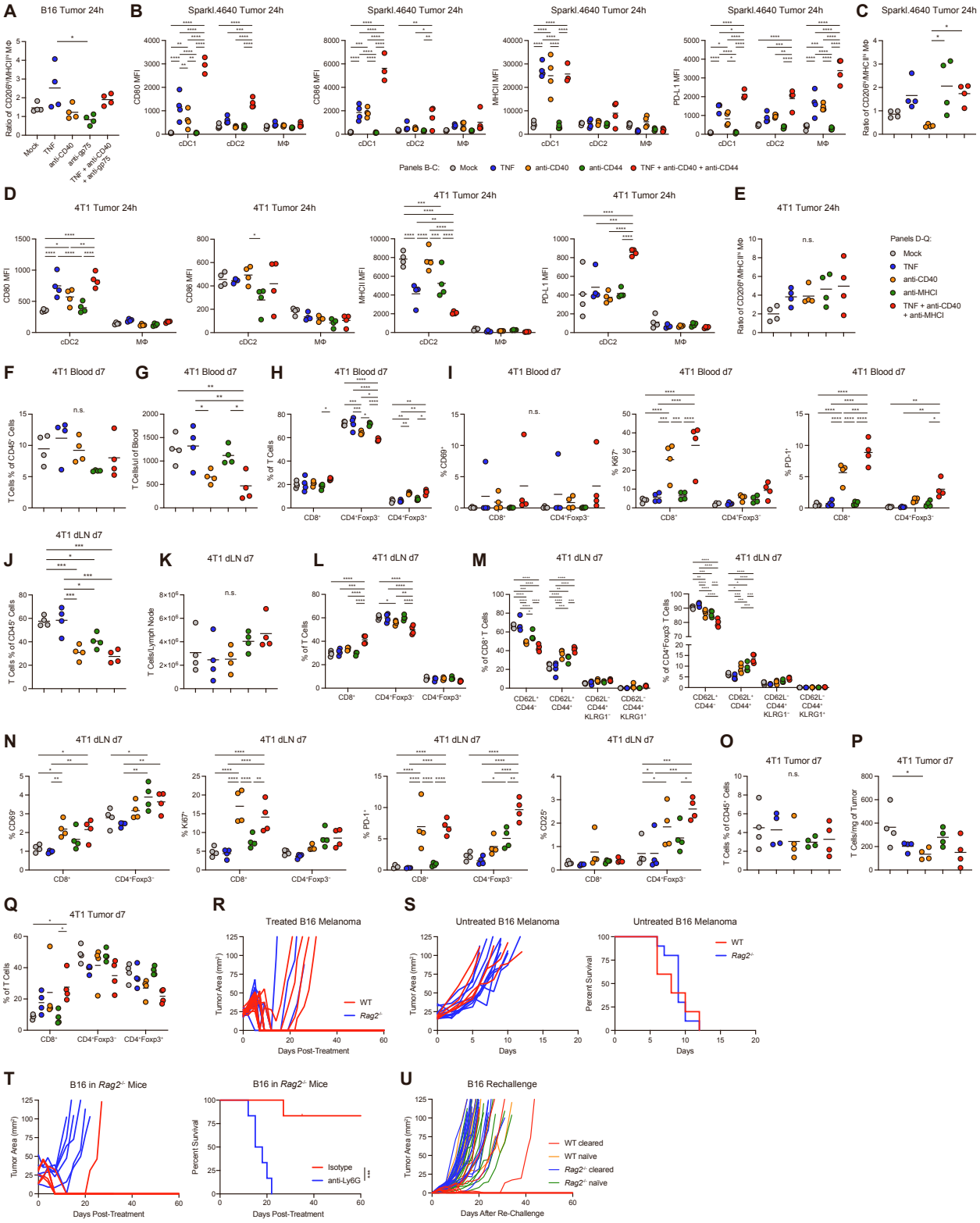

Figure S5: Activation and priming of immune cells induced by neutrophil-activating therapy. Related to Figure 3.

(**A**) Ratio of CD206^{hi} to MHCII^{hi} macrophages in B16 tumors 24 hours after treatment with the indicated components (n=4). (**B**) Expression of activation markers on APC populations in SparkI.4640 tumors 24 hours after treatment with the indicated components (n=4). (**C**) Ratio of CD206^{hi} to MHCII^{hi} macrophages in SparkI.4640 tumors 24 hours after treatment with the indicated components (n=4). (**D**) Expression of activation markers on APC populations in 4T1 tumors 24 hours after treatment with the indicated components (n=4). (**E**) Ratio of CD206^{hi} to MHCII^{hi} macrophages in 4T1 tumors 24 hours after treatment with the indicated components (n=4). (**F-G**) Frequencies (F) and numbers (G) of total T cells in the blood 7 days after treatment of 4T1 (n=4). (**H**) Percent of T cell subsets out of total T cells in the blood 7 days after treatment of 4T1 (n=4). (**I**) Expression of markers on T cell subsets in the blood 7 days after treatment of 4T1 (n=4). (**J-K**) Frequencies (J) and numbers (K) of total T cells in the tumor-draining lymph node (dLN) 7 days after treatment of 4T1 (n=4). (**L**) Percent of T cell subsets out of total T cells in the dLN 7 days after treatment of 4T1 (n=4). (**M**) Memory and effector phenotypes of T cell subsets in the dLN 7 days after treatment of 4T1 (n=4). (**N**) Expression of markers on T cell subsets in the dLN 7 days after treatment of 4T1 (n=4). (**O-P**) Frequencies (O) and numbers (P) of total T cells in the tumor 7 days after treatment of 4T1 (n=4). (**Q**) Percent of T cell subsets out of total T cells in the tumor 7 days after treatment of 4T1 (n=4). (**R**) Growth of B16 in WT or *Rag2*$^{-/-}$ mice following treatment with neutrophil-activating therapy (n=15). (**S**) Growth of B16 in untreated WT or *Rag2*$^{-/-}$ mice (WT n=5, *Rag2*$^{-/-}$ n=10). (**T**) Tumor growth and survival of B16-bearing *Rag2*$^{-/-}$ mice treated with neutrophil-activating therapy after administration of anti-Ly6G or isotype control (n=6). (**U**) Growth of B16 implanted in tumor-naïve or B16-cleared WT or *Rag2*$^{-/-}$ mice 50 days after initial treatment with neutrophil-activating therapy (WT cleared n=14, *Rag2*$^{-/-}$ cleared n=18, WT naïve n=10, *Rag2*$^{-/-}$ naïve n=15). Statistics: One-way ANOVA with Tukey's multiple comparisons test (A, C, E-G, J-K, O-P), Two-way ANOVA with Tukey's multiple comparisons test (B, D, H-I, L-N, Q), Log-rank test (S-T). For all dot plots, the line indicates the mean. Data are representative of 3 (R), 2 (A, U), or 1 (B-Q, T) independent experiments or pooled from 2 experiments (S).

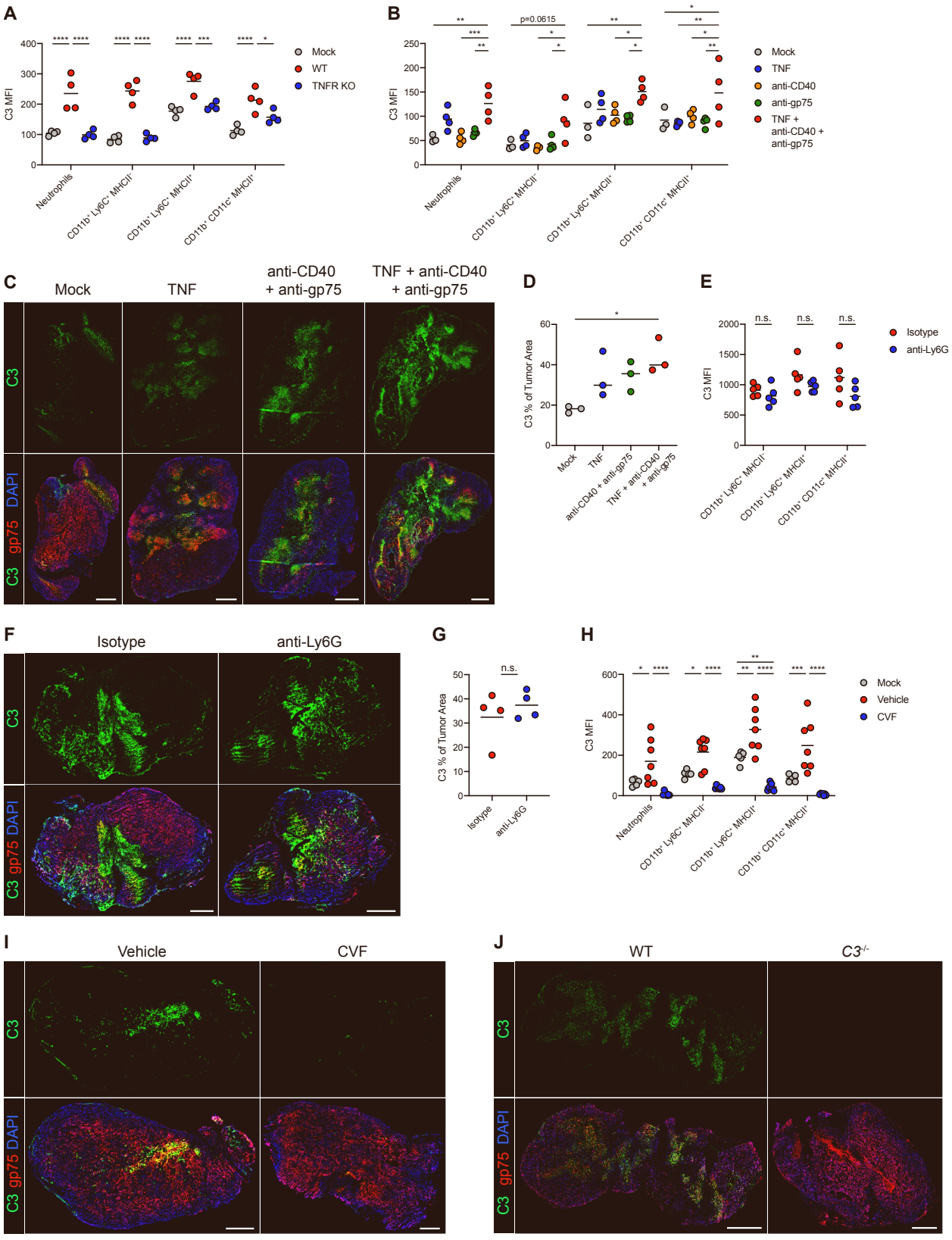
A
C3 MFI
Mock
WT
TNFR KO
Neutrophils
CD11b+ Ly6C+ MHCII+
CD11b+ Ly6C+ MHCII+
CD11b+ CD11c+ MHCII+
B
C3 MFI
p=0.0615
Mock
TNF
anti-CD40
anti-gp75
TNF + anti-CD40 + anti-gp75
C
Mock
TNF
anti-CD40 + anti-gp75
TNF + anti-CD40 + anti-gp75
C3
C3 gp75 DAPI
D
C3 % of Tumor Area
Mock
TNF
anti-CD40 + anti-gp75
TNF + anti-CD40 + anti-gp75
E
C3 MFI
n.s.
Isotype
anti-Ly6G
F
Isotype
anti-Ly6G
C3
C3 gp75 DAPI
G
C3 % of Tumor Area
n.s.
H
C3 MFI
Mock
Vehicle
CVF
I
Vehicle
CVF
C3
C3 gp75 DAPI
J
WT
C3-/-
C3
C3 gp75 DAPI

Figure S6: Complement activation is induced by neutrophil-activating therapy. Related to Figure 4.

(**A**) MFI of C3 deposition on myeloid cell populations in B16 tumors 4 hours after treatment of WT or TNFR KO mice with neutrophil-activating therapy (n=4). (**B**) MFI of C3 deposition on myeloid cell populations in B16 tumors 4 hours after treatment with the indicated components (n=4). (**C-D**) Representative immunofluorescence (C) and quantification (D) of C3 staining in B16 tumors 4 hours after treatment with the indicated components. Scale bars = 500 μm. (n=3) (**E**) MFI of C3 deposition on myeloid cell populations in B16 tumors 4 hours after treatment of Ly6G-depleted mice with neutrophil-activating therapy (n=5). (**F-G**) Representative immunofluorescence (F) and quantification (G) of C3 staining in B16 tumors 4 hours after treatment following Ly6G depletion. Scale bars = 500 μm. (n=4) (**H**) MFI of C3 deposition on myeloid cell populations in B16 tumors 4 hours after neutrophil-activating therapy following complement depletion by CVF (mock n=5, others n=7). (**I**) Representative immunofluorescence of C3 staining in B16 tumors 4 hours after neutrophil-activating therapy following administration of CVF. Scale bars = 500 μm. (**J**) Representative immunofluorescence of C3 staining in B16 tumors 4 hours after treatment of WT or *C3*$^{-/-}$ mice. Scale bars = 500 μm. Statistics: Two-way ANOVA with Tukey's multiple comparisons test (A-B, E, H), One-way ANOVA with Tukey's multiple comparisons test (D, G). For all dot plots, the line indicates the mean. Data are representative of 3 (I), 2 (B, E-G), or 1 (A, C-D, J) independent experiments or pooled from 2 experiments (H).

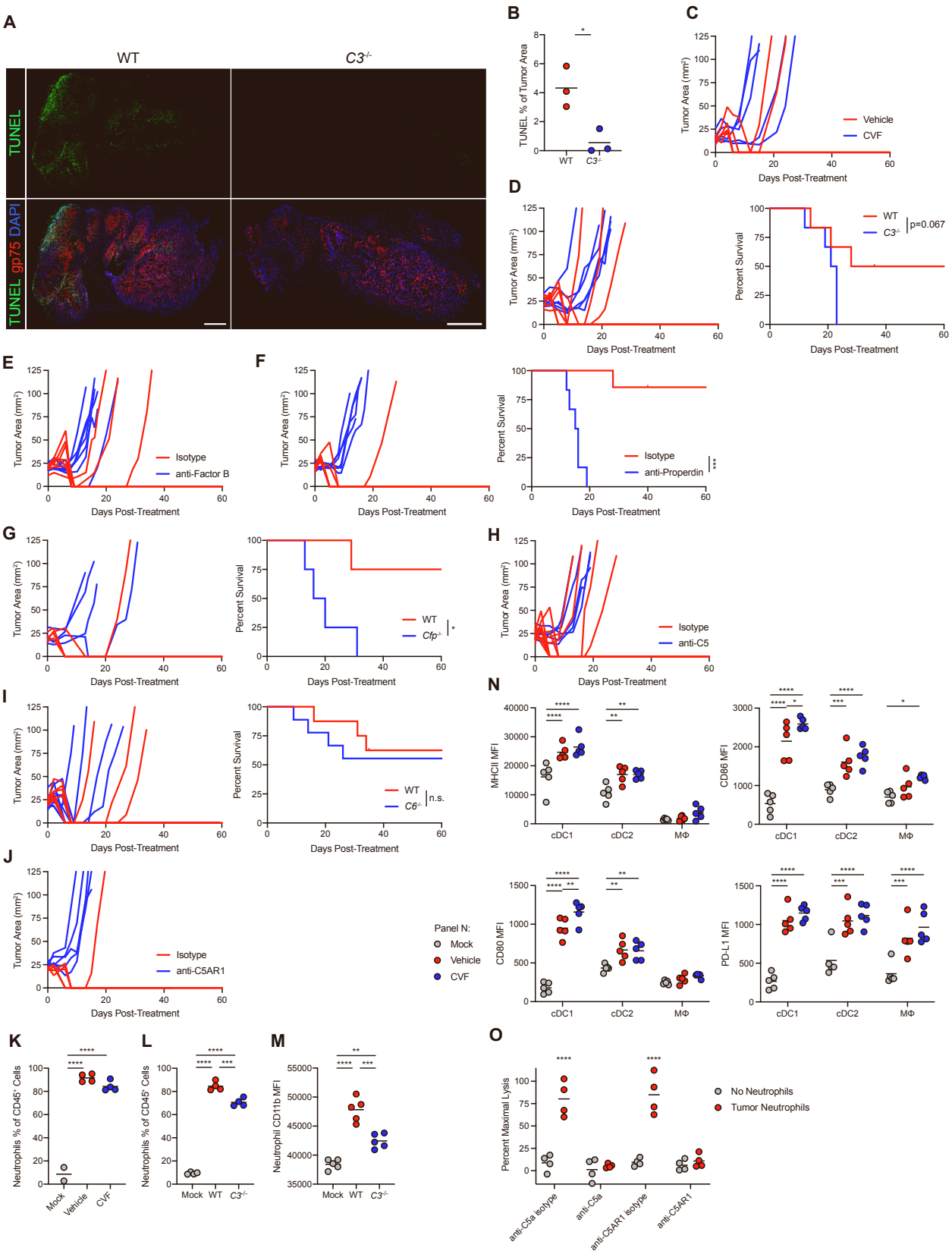
A
WT
C3-/-
TUNEL
TUNEL gp75 DAPI
B
TUNEL % of Tumor Area
WT
C3-/-
C
Tumor Area (mm2)
Vehicle
CVF
Days Post-Treatment
D
Tumor Area (mm2)
Days Post-Treatment
Percent Survival
WT
C3-/-
p=0.067
Days Post-Treatment
E
Tumor Area (mm2)
Isotype
anti-Factor B
Days Post-Treatment
F
Tumor Area (mm2)
Days Post-Treatment
Percent Survival
Isotype
anti-Properdin
***
Days Post-Treatment
G
Tumor Area (mm2)
Days Post-Treatment
Percent Survival
WT
Cfp-/-
*
Days Post-Treatment
H
Tumor Area (mm2)
Isotype
anti-C5
Days Post-Treatment
I
Tumor Area (mm2)
Days Post-Treatment
Percent Survival
WT
C6-/-
n.s.
Days Post-Treatment
J
Tumor Area (mm2)
Isotype
anti-C5AR1
Days Post-Treatment
Panel N:
Mock
Vehicle
CVF
N
MHCII MFI
CD86 MFI
CD80 MFI
PD-L1 MFI
cDC1
cDC2
MΦ
K
Neutrophils % of CD45+ Cells
Mock
Vehicle
CVF
L
Neutrophils % of CD45+ Cells
Mock
WT
C3-/-
M
Neutrophil CD11b MFI
Mock
WT
C3-/-
O
Percent Maximal Lysis
No Neutrophils
Tumor Neutrophils
anti-C5a isotype
anti-C5a
anti-C5AR1 isotype
anti-C5AR1

Figure S7: The alternative complement pathway induces neutrophil activation through C5a. Related to Figure 4.

(**A-B**) Representative immunofluorescence (A) and quantification (B) of TUNEL staining in B16 tumors 24 hours after treatment of WT or *C3*$^{-/-}$ mice. Scale bars = 500 μm. (n=3) (**C**) Growth of B16 tumors in mice depleted of complement with Cobra Venom Factor (CVF) prior to treatment with neutrophil-activating therapy (n=5). (**D**) Tumor growth and survival of B16-bearing WT or *C3*$^{-/-}$ mice following treatment with neutrophil-activating therapy (n=6). (**E**) Growth of B16 in mice treated following administration of anti-Factor B (n=7). (**F**) Tumor growth and survival of B16-bearing mice treated with neutrophil-activating therapy following administration of a blocking antibody targeting properdin (isotype n=7, anti-properdin n=6). (**G**) Tumor growth and survival of B16-bearing WT or *Cfp*$^{-/-}$ mice following treatment with neutrophil-activating therapy (n=4). (**H**) Growth of B16 in mice treated with neutrophil-activating therapy following administration of anti-C5 (mock n=12, anti-C5 n=5). (**I**) Tumor growth and survival of B16-bearing WT or *C6*$^{-/-}$ mice following neutrophil-activating therapy (WT n=8, C6$^{-/-}$ n=9). (**J**) Growth of B16 in mice treated following administration of anti-C5AR1 (n=5). (**K**) Frequency of B16 tumor-infiltrating neutrophils 24 hours after treatment with neutrophil-activating therapy following CVF administration (mock n=2, others n=4). (**L**) Frequency of B16 tumor-infiltrating neutrophils 24 hours after treatment of WT or *C3*$^{-/-}$ mice with neutrophil-activating therapy (n=4). (**M**) MFI of CD11b on B16 tumor-infiltrating neutrophils in *C3*$^{-/-}$ mice 4 hours after neutrophil-activating therapy (n=4). (**N**) Activation marker expression on tumor APCs 4 hours after treatment of complement-depleted mice with neutrophil-activating therapy (n=5). (**O**) Percent lysis of B16 cells co-cultured with neutrophils isolated from treated tumors, stimulated *in vitro* with TNF + anti-CD40 + anti-gp75 in active serum in the presence of blocking antibodies targeting C5a, C5AR1, or isotype controls. Asterisks indicate significance relative to the six samples without elevated levels of lysis (n=4). Statistics: One-way ANOVA with Tukey's multiple comparisons test (B, K-M), Log-rank test (D, F-G, I), Two-way ANOVA with Tukey's multiple comparisons test (N-O). For all dot plots, the line indicates the mean. Data are representative of 2 (C-E, J-O) or 1 (A-B, G) independent experiments or pooled from 2 experiments (F, H-I).

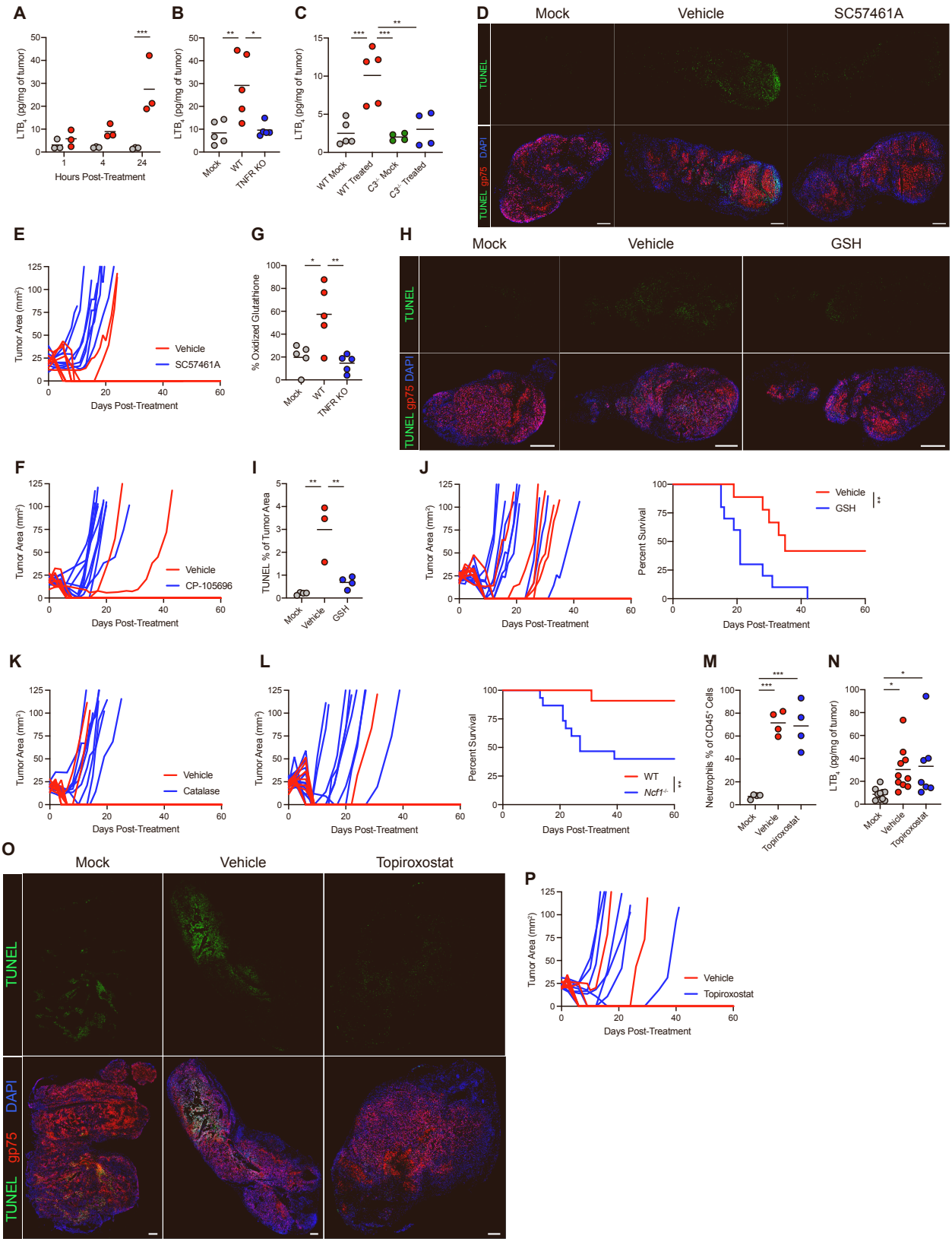

Figure S8: Xanthine oxidase induces cell death downstream of neutrophil infiltration and secretion of LTB_4. Related to Figures 5 and 6.

(**A**) LTB_4 levels in B16 tumors following treatment with neutrophil-activating therapy (n=3). (**B**) LTB_4 levels in B16 tumors 24 hours after treatment of WT or TNFR KO mice with neutrophil-activating therapy (n=5). (**C**) LTB_4 levels in B16 tumors 24 hours after treatment of WT or *C3*$^{-/-}$ mice with neutrophil-activating therapy (WT n=5, *C3*$^{-/-}$ n=4). (**D**) Representative TUNEL immunofluorescence in B16 tumors 24 hours after treatment following administration of the LTA_4H inhibitor SC57461A. Scale bars = 500 μm. (**E-F**) Growth of B16 in mice administered SC57461A (E) (vehicle n=9, SC57461A n=8) or the BLT1 antagonist CP-105696 (F) (vehicle n=9, CP-105696 n=10) prior to treatment with neutrophil-activating therapy. (**G**) Oxidized glutathione percentage of total glutathione in B16 lysates 24 hours after neutrophil-activating therapy in WT or TNFR KO mice (n=5). **(H-I**) Representative immunofluorescence (H) and quantification (I) of TUNEL staining in B16 tumors 24 hours after treatment following GSH administration. Scale bars = 500 μm. (vehicle n=3, others n=4) (**J**) Tumor growth and survival of B16-bearing mice treated following administration of GSH (vehicle n=9, GSH n=10). (**K**) Growth of B16 in mice administered catalase during treatment with neutrophil-activating therapy (n=9). (**L**) Tumor growth and survival of B16-bearing WT or *Ncf1*$^{-/-}$ mice following treatment with neutrophil-activating therapy (WT n=11, *Ncf1*$^{-/-}$ n=15). (**M**) Frequency of neutrophils in B16 tumors 24 hours after treatment with neutrophil-activating therapy following topiroxostat administration (n=4). (**N**) LTB_4 levels in B16 tumors 24 hours after neutrophil-activating therapy following topiroxostat administration (topiroxostat n=7, others n=10). (**O**) Representative TUNEL immunofluorescence in B16 tumors 24 hours after treatment with neutrophil-activating therapy following administration of topiroxostat. Scale bars = 500 μm. (**P**) Growth of B16 in mice administered topiroxostat during treatment with neutrophil-activating therapy (vehicle n=9, topiroxostat n=8). Statistics: Two-way ANOVA with Tukey's multiple comparisons test (A), One-way ANOVA with Tukey's multiple comparisons test (B-C, G, I, M-N), Log-rank test (J, L). For all dot plots, the line indicates the mean. Data are representative of 2 (B, G, J, M, P) or 1 (A, C-D, H-I, O) independent experiments or pooled from 2 experiments (E-F, K-L, N).

Supplemental Table

Table S1: Oligonucleotide sequences, Related to STAR Methods

Name	Sequence	Source	Identifier
Tnfrsf1a sgRNA1	AGACCTAGCAAGATAACCAG	Doench et al., 2016	N/A
Tnfrsf1a sgRNA2	GATGGGGATACATCCATCAG	Doench et al., 2016	N/A
Surface EGFP	ATAGCAGGATCCGCCGCCACCATGGAGACCGAT ACCCTCCTGCTGTGGGTTCTCCTGCTGTGGGT GCCTGGCTCCACCGGTGATATGGTTAGCAAGG GCGAAGAGCTCTTTACTGGCGTCGTGCCAATAC TCGTCGAGCTGGATGGGGACGTTAATGGCCATA AATTCAGCGTGAGCGGCGAGGGGGAGGGGGA CGCCACCTACGGAAAGCTTACTTTGAAGTTTATT TGCACTACAGGCAAGTTGCCTGTGCCTTGGCCT ACACTCGTGACCACACTCACTTACGGGGTGCAG TGTTTTTCTAGGTATCCTGATCACATGAAACAGC ACGACTTTTTCAAGAGCGCAATGCCTGAAGGCTA CGTCCAGGAGAGAACCATATTTTTCAAGGATGAT GGTAACTACAAAACTAGAGCTGAAGTCAAGTTTG AGGGGGACACCCTCGTGAACAGAATTGAATTGA AAGGCATTGATTTCAAGGAGGACGGAAACATTCT CGGACACAAACTGGAATATAATTACAATAGTCATA ACGTCTATATCATGGCAGATAAGCAGAAGAACGG GATTAAAGTCAATTTCAAAATCAGACACAATATCG AGGATGGCTCCGTTCAACTGGCTGATCATTATCA ACAGAACACCCCTATCGGCGACGGACCTGTTTT GCTCCCTGACAATCACTACTTGTCTACCCAGTCC GCTCTCAGCAAAGACCCCAACGAAAAGCGCGAT CACATGGTTCTGCTGGAGTTCGTGACAGCCGCA GGCATAACACTGGGGATGGACGAGCTTTACAAG AATTCTATGGGAGGAGATAGTCAGGAGGTGACC GTCGTGCCTCACTCCCTGCCCTTTAAGGTGGTC GTTATCTCAGCTATACTTGCCCTTGTGGTTTTGA CTGTTATATCCCTGATTATCCTCATCATGCTGTG GCAGAAAAAGCCCCGGTAATCTAGAACTCGT	Synthesized by GeneArt, ThermoFisher Scientific	N/A